Studies of suppression using monoclonal regulatory T cells

and

the importance of co-receptor Lck coupling ratios for negative selection

Inauguraldissertation

zur Erlangung der Würde eines Doktors der Philosophie

vorgelegt der

Philosophisch-Naturwissenschaftlichen Fakultät

der Universität Basel

von

Céline Gubser

aus Basel-Stadt

Basel, März 2016

Genehmigt von der Philosophisch-Naturwissenschaftlichen Fakultät auf Antrag von:

Prof. E. Palmer

Prof. D. Finke

Basel, den 10.11.2015

Prof. Dr. Jörg Schibler

Namensnennung-Keine kommerzielle Nutzung-Keine Bearbeitung 3.0 Schweiz
(CC BY-NC-ND 3.0 CH)

Sie dürfen: **Teilen** — den Inhalt kopieren, verbreiten und zugänglich machen

Unter den folgenden Bedingungen:

Namensnennung — Sie müssen den Namen des Autors/Rechteinhabers in der von ihm festgelegten Weise nennen.

Keine kommerzielle Nutzung — Sie dürfen diesen Inhalt nicht für kommerzielle Zwecke nutzen.

Keine Bearbeitung erlaubt — Sie dürfen diesen Inhalt nicht bearbeiten, abwandeln oder in anderer Weise verändern.

Wobei gilt:

- **Verzichtserklärung —** Jede der vorgenannten Bedingungen kann **aufgehoben** werden, sofern Sie die ausdrückliche Einwilligung des Rechteinhabers dazu erhalten.
- **Public Domain (gemeinfreie oder nicht-schützbare Inhalte) —** Soweit das Werk, der Inhalt oder irgendein Teil davon zur Public Domain der jeweiligen Rechtsordnung gehört, wird dieser Status von der Lizenz in keiner Weise berührt.
- **Sonstige Rechte —** Die Lizenz hat keinerlei Einfluss auf die folgenden Rechte:
    - Die Rechte, die jedermann wegen der Schranken des Urheberrechts oder aufgrund gesetzlicher Erlaubnisse zustehen (in einigen Ländern als grundsätzliche Doktrin des **fair use** bekannt);
    - Die **Persönlichkeitsrechte** des Urhebers;
    - Rechte anderer Personen, entweder am Lizenzgegenstand selber oder bezüglich seiner Verwendung, zum Beispiel für **Werbung** oder Privatsphärenschutz.
- **Hinweis —** Bei jeder Nutzung oder Verbreitung müssen Sie anderen alle Lizenzbedingungen mitteilen, die für diesen Inhalt gelten. Am einfachsten ist es, an entsprechender Stelle einen Link auf diese Seite einzubinden.

Quelle: http://creativecommons.org/licenses/by-nc-nd/3.0/ch/ Datum: 12.11.2013

Table of contents

Table of Figures

1 Summary

Normal physiology is not given without immunological tolerance. Depending on the origin of induction, tolerance can be divided into central and peripheral tolerance. Central tolerance comprises depletion of autoreactive T cells in the thymus (i.e. negative selection), and with this prevents autoimmunity. Peripheral tolerance critically depends on regulatory T cells (Tregs) maintaining lymphocyte homeostasis. Hallmark features of $CD4^+$ Tregs are the expression of high surface IL-2-Rα (CD25) and the transcription factor Forkhead box protein P3 (Foxp3). Expression of non-functional Foxp3 results in lethal multi-organ lymphocytic infiltrations and cytokine secretions. Numerous data agree on an indispensable role for Tregs enabling physiological immunity. Yet an understanding of how Tregs function at a cellular and molecular level has not been fully elucidated.

In the first part of the thesis we made use of a Rag^{KO} TCR transgenic mouse expressing a Foxp3 transgene. This mouse provides a source of monoclonal $CD4^+$, $Foxp3^+$ T cells with a defined specificity. We show that monoclonal B3K506 Tregs are fully functional in vitro and in vivo and clearly require cognate antigen to be suppressive. We further show that the strength of Treg stimulation determines the strength of Treg mediated suppression. Finally we analysed various suppressive mechanisms used by monoclonal Tregs and found that Treg-Tconv proximity is an important parameter, which correlates with effective suppression.

In the second part of the thesis we aimed to understand the molecular mechanism underlying the affinity threshold for negative selection. We quantified the amount of Lck coupled to CD8 or CD4 coreceptors. We found that CD4 co-receptors have higher Lck coupling ratios than do CD8 co-receptors. In addition we determined the absolute numbers of surface molecules (i.e. CD8α, CD4 and CD3ε) on double positive (DP) thymocytes in B6 and MHC-class I restricted, TCR Tg mouse strains. A model, explaining how the TCR measures antigen affinity to initiate a negative selection signal, was generated. Here we show that the affinity threshold for different co-receptors depends on the probability that a peptide-MHC-TCR complex will collide with a co-receptor carrying Lck during the time pMCH binds to the TCR (Stepanek, O. et al. Cell, 2014)

2 Introduction

2.1 Tolerance, resistance and immunity

The every day challenge of our immune system is to fight unwanted pathogen invasion while maintaining tolerance to self and important commensals. Immunity is the balanced state between tolerance and resistance, which every healthy individual critically depends on. Affected immunity results in infections, autoimmune diseases and malignant conditions, which can ultimately lead to death.

The gut represents an ideal example to illustrate immunity. Here, digestion and nutrient up take critically depend on immune tolerance promoting commensalism. Resistance to gut microbiota has devastating consequences for the host. Lymphocyte invasion and tissue damage by inflammatory mediators cause a breakdown of the gut mucosal barrier, leading to nutrient malabsorption and dangerous microbial invasion of former sterile tissues. Unless adequately treated, septic colitis usually kills the host.

However, tolerating virulent pathogens also provokes severe damages. Exponential pathogen growth and loss of important resources or toxin secretion harms the host. Elimination of virulent pathogen induces short-term pain and swelling in the affected tissue. The benefit of resisting pathogen invasion and preventing parasitism results in survival. Nevertheless, establishing immune resistance fighting foreign antigens/pathogens can be a trigger for unwanted immune reactions toward self. Failed discrimination between self and foreign antigens, or breakdown of tolerance inducing mechanisms, can lead to allergic reactions and autoimmune diseases.

2.2 Central tolerance

Long-lasting protective immunity is provided through our adaptive immune system and mediated by specific B and T lymphocyte responses against antigens. T lymphocytes derive from a multi-potent hematopoietic stem cell in the bone marrow. T cell precursors migrate to the thymus where they further develop and differentiate into T cell receptor expressing, mature single positive CD8 or CD4 thymocytes. The T cell receptor (TCR) is a heterodimer of two protein chains. Most TCRs consist of an α and β chain, however

there is a small fraction (≈5%) of γ:δ chain TCRs. Each α:β T cell expresses a single TCR with unique antigen specificity. The generation of TCRs relies on a random rearrangement of antigen receptor genes (V, D, J) resulting in a broad TCR repertoire. This repertoire comprises a major part of TCRs incapable of binding to antigen and a small fraction of dangerous TCRs recognizing self-antigens from tissues of the body. These self-reactive T lymphocytes can cause autoimmunity and need to carefully be prevented from entering the pool of mature T cells in the periphery.

Burnet first postulated the mechanism of central tolerance in the 1960's[1]. Each developing thymocyte undergoes a selection process in the thymus. Double positive (DP) $CD4^+CD8^+$ thymocytes binding weakly to self-antigen MHC complexes presented by cortical thymic epithelial cells (cTEC), get positively selected and survive. They cease to express one of the co-receptors, becoming single positive (SP) $CD8^+$ or $CD4^+$ thymocytes, ready to leave the thymus and form the peripheral T cell repertoire.

However, thymocytes binding strongly to self-antigen MHC complexes, presented by medullary thymic epithelial cells (mTECs), get negatively selected and die. MTECs express the autoimmune regulator gene (AIRE) which has an important role in the process of negative selection[2]: via the induction of peripheral-tissue antigen presentation on the surfaces of mTECs, AIRE contributes to clonal deletion, i.e. apoptotic cell death of auto-reactive thymocytes, and thus controls autoimmunity[3].

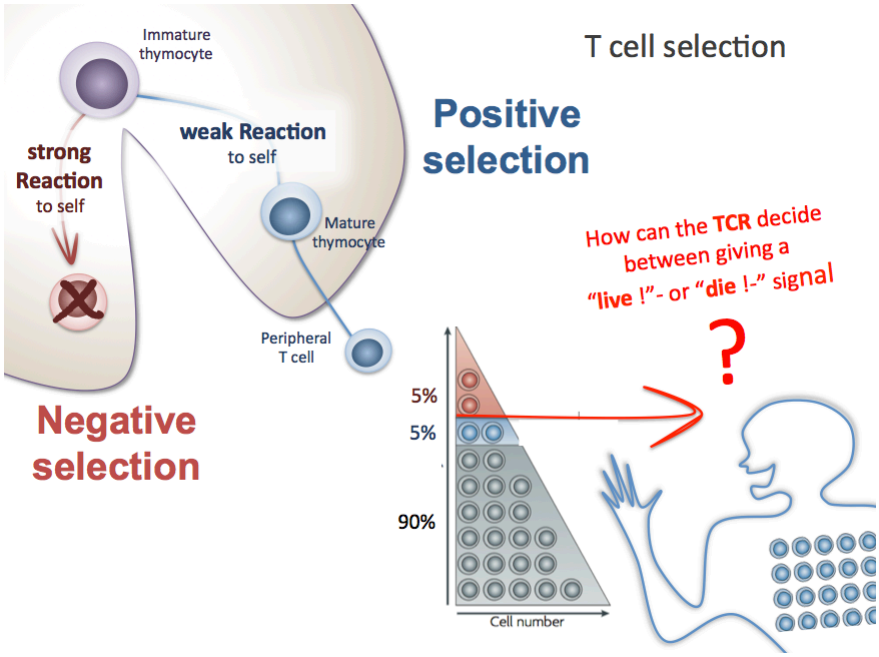

Figure 2.2.1 Graphical abstract of thymic T cells selection

In the thymus, 90% of thymocytes never interact with antigen and die by neglect (grey). 5% of all thymocytes get negatively selected (red) and only a fraction get positively selected and home to the periphery where they homeostatically expand (blue)

2.2.1 Negative selection

Thymic negative selection results in the depletion of autoimmune T cells expressing TCRs with high affinity for self-antigens. It is therefore considered a key mechanism in the induction of tolerance. To negatively select a thymocyte, peptide affinity needs to generate a strong enough TCR signal to initiate thymocyte apoptosis[4,5]. The TCR can measure antigen affinity by the duration of TCR peptide-MHC complex interaction (antigen dwell-time)[6-8]. A ligand dissociation constant (K_D) of 6uM and a half-life of ≈ 2 seconds was proposed to define the affinity threshold for a MHC class I restricted double positive (DP) thymocyte to succumb to negative selection in the thymus[6,8]. Recent data from our lab measured that an antigen dwell time of ≈ 0.9 seconds defines the affinity threshold for MHC class I restricted, double positive thymocytes to succumb to negative selection in the thymus. For MHC class II restricted TCRs this threshold is lower (antigen dwell time of ≈ 0.2 seconds) and as a consequences leads to negative selection in response to weaker self-antigens[9].

Peptide-MHC driven TCR signaling initiates with co-receptor bound Lck, phosphorylating ITAMs within the TCR/CD3 complex. Not every co-receptor carries Lck

indicating that only some collisions between a TCR and a co-receptor are capable of triggering a TCR signaling (see results 5.2). Therefore not all co-receptor TCR collisions are productive. CD4 co-receptors carry more TCR-signal-inducing-kinase Lck than do CD8 co-receptors. A shorter antigen dwell time for MHC class II restricted thymocytes can elicit a strong enough TCR signal to initiate negative selection[9].

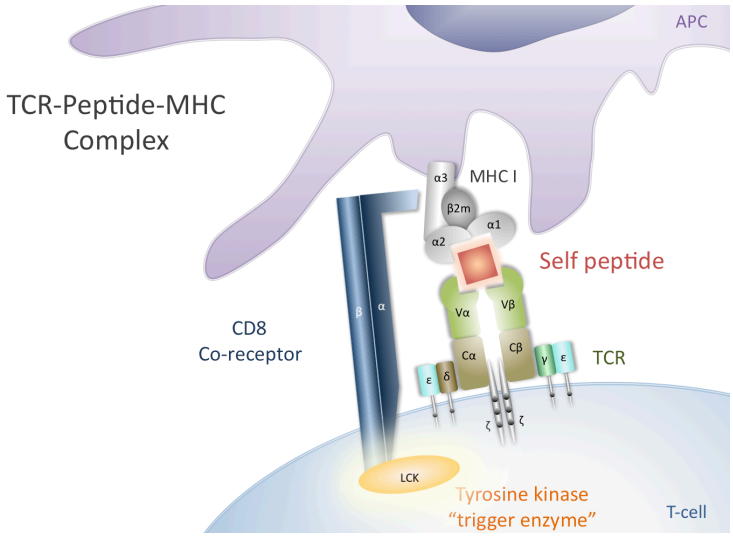

Figure 2.2.2 Co-receptor coupled Lck initiates TCR signalling

2.3 Peripheral tolerance and Tregs

Elimination of potentially self-reactive T cell clones in the thymus is an important process enabling immunological tolerance. However despite its efficiency, negative selection is not 100% complete. A small number of T cells, with potential to cause autoimmune diseases, escape negative selection. The periphery established additional control mechanism to prevent mature self-reactive T cells from unwanted responses toward self. Recessive peripheral tolerance or clonal T cell anergy, was described in the 1980 when mature T cells were rendered unresponsive to antigen recall responses in the absence of co-stimulation[10,11].

The idea of a "suppressor T lymphocyte" controlling peripheral tolerance was first postulated in the 1960's. Mice, thymectomized at day 3 of life, suffered from sever autoimmune ovary inflammation and autoimmune gastritis. It was suggested that "suppressor T lymphocytes" emerge from the thymus after day 3 of life to prevent immune responses against self-antigens[12-14].

In 1995 Sakaguchi and colleagues described a small population (5-10%) of $CD4^+CD25^+$ T cells that appear in the periphery only after day 3 of life and upon depletion lead to lethal multiple autoimmune diseases in mice[15,16]. An x-linked syndrome of diarrhea, polyendocrinopathy and fatal infection in infancy (IPEX) has long been described in humans[17]. Male patients suffer from severe colitis, autoimmune endocrinopathies, food allergies, dermatitis and scarcely reach the age of 6 years. The equivalent phenotype in mice termed "scurfy" arose as a spontaneous mutation in radiation-exposed animals and was described by Godfrey and colleagues in 1991[18,19]. In 2001 Brunkow and others[20] mapped the Forkhead box protein P3 (Foxp3) gene mutation and evidence was supplied that the scurfy disease in mice and the IPEX syndrome in humans resulted from a defective expression of the transcription factor Foxp3[21].

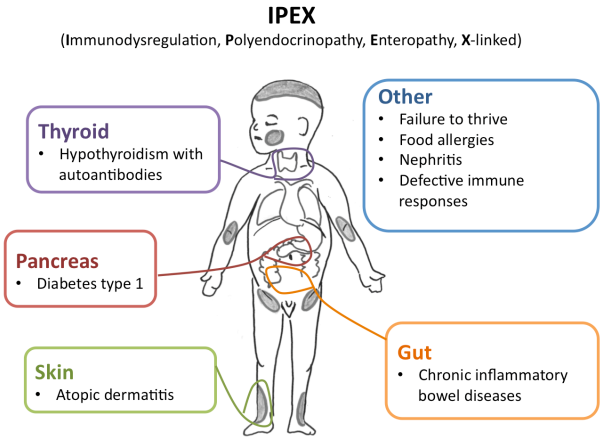

Figure 2.3.1 Diagram of IPEX symptoms

Work of Schubert et al. showing that Foxp3 acts as a repressor of transcription and regulator of T cell activity accounts for a major Treg breakthrough[22]. In subsequent steps diverse independent teams could identify Foxp3 as the master controller for the development and function of $CD4^+CD25^+$ regulatory T cells[23-25].

Today dominant peripheral tolerance refers to this population of $Foxp3^+CD4^+CD25^+$ T cells. Regulatory T cells are believed to form a TCR repertoire skewed toward self-recognition and exert key regulatory functions in the maintenance of peripheral T cell homeostasis.

2.4 Treg origins and nomenclature

Tregs can be divided into two main subgroups based on their place of origin: **t**hymic Tregs (tTregs) emerge from the **t**hymus and **p**eripheral Treg (pTregs) from the **p**eriphery. However du to the lack of defining selection markers, this classification has been revised (see 2.4.3-5)[26]

2.4.1 Thymic Tregs

Thymic Tregs (tTregs) are thought to arise during thymic selection and to be survivors of negative selection[27-29]. As mentioned above, negative selection is not a hundred percent complete. Along with the danger of high affinity self-reactive Tconvs escaping, there is the beneficial effect of generating Tregs expressing a TCR repertoire skewed towards self-recognition. TTregs are estimated to account for seventy to ninety percent of the Treg population[26,30]. Data suggest that tTregs express the transcription factor Helios (also known as IKZF2) and respond to high affinity self-peptides presented in the context of MHC class II molecules[31]. Expression of the surface marker neuropilin 1 was also associated with tTregs[32]. Up to date these markers provide the best tool to distinguish between thymic derived and peripherally induced Foxp3$^+$ regulatory T cells[30].
Emerging tTregs are maintained in secondary lymphoid organs as a result of homeostatic proliferation due to self-peptide encounter in the periphery. They are critically involved in the prevention of autoimmune diseases and represent a key mechanism for induction and maintenance of peripheral tolerance.

2.4.2 Peripheral Tregs

It is well accepted that approximately ten to thirty percent of Treg cells are generated by conversion of T conventional cells (pTregs) in the periphery[33]. In vitro conversion of T conventional cells occurs in a milieu where TCR stimulation, IL-2 and the presence of tTregs, expressing surface coupled TGF-β, is provided[34,35]. In vivo experiments could show the emergence of pTregs as a subsequent wave of T effector differentiation during inflammation, resulting in resolution of the disease[36]. Importantly, a non-redundant role for peripherally generated Tregs could be shown, enabling TCR diversity for suppression of chronic inflammation and autoimmunity in Foxp3 deficient mice[33] .

While pTregs express a big part of Treg signature genes, it is reasonable to assume that thymic and pTreg populations exhibit different TCR repertoires and functional profiles. However, owing to the lack of validated markers, a Treg nomenclature based on defining markers and functional properties rather than origin (i.e. **t**hymic and **p**eripheral Tregs) was proposed[26] (i.e. central, effector and tissue-resident Tregs).

2.4.3 Central Tregs

Central Tregs mark the biggest population of Tregs. After Tregs emerge from their origin they circulate through secondary lymphoid organs. They highly express homing markers like CD62L and CCR7 and are low on activation markers like CD44 and CD25. Their phenotype resembles one of naïve or memory T conventional cells[26].

However upon TCR and co-stimulatory activation signals, they up regulate CD25 and exert suppressive functions. Central Tregs depend on IL-2. This allows homeostasis of the Treg and Tconv populations, since IL-2 production by Tconvs inversely correlates with Tconvs suppression [26,37]. Their high basal proliferation rate is counterbalanced by a high apoptosis rate due to Foxp3 mediated phosphorylation of the pro-apoptotic marker Bim[38]. Bim on the other hand is antagonized by the pro-survival factor Mcl-1 that is up regulated in Tregs upon IL-2 signaling[39].

If the high turnover of central Tregs is due to constant TCR triggering or is a direct consequence of the Foxp3 transcriptional program (or both) needs yet to be examined. Importantly growing evidence suggests that Treg suppression and homeostasis in secondary lymphoid organs alone, cannot guarantee immunological tolerance.

2.4.4 Effector Tregs

Effector Tregs or “activated” Tregs mark a minor but important population of the Treg pool. Due to recent antigen encounter, their phenotype resembles one of activated conventional T cells. They are high on CD44, CD25, KLRG1, CD103 and low on CD62L and CCR7[40]. This profile allows migration through non-lymphoid tissues in order to locate the site of need[40].

Effector Treg differentiation from central Tregs requires the transcription factor IRF4 and involves Blimp-1 up regulation[41]. Further polarization of effector Tregs takes place upon unknown stimuli and depends on the place of recruitment. Up regulation of transcription

factors like Tbet, STAT3, BCL-6 or PPARγ act together with Foxp3, inducing expression of required surface chemokine and homing receptors[42].

IL-2 is a minor player in the maintenance of polarized effector Tregs, leaving essential cues to cytokines like IL-7, IL-27, IL-10, IL-6 and IL-1. This observation implies that effector Tregs are tailored to match the type of T conventional cells, i.e. Th1, Th2 or Th17 that needs to be suppressed[43]. It is still unclear whether the change of phenotype from central to effector Treg is reversible or terminal.

2.4.5 Tissue-resident Tregs

Non-lymphoid tissues, that have been reported to harbor a substantial number of Treg, include gut, skin, lung, liver, adipose tissue, placenta, inflammatory tissues and tumors[44]. Tools for discrimination between residential tissue Tregs and migrating effector Tregs are still limited. However, new insights from the gut and adipose tissue lead to improved understanding of tissue resident Treg populations. The gut harbors the largest pool of tissue-resident Tregs. Especially in the colon, where bacterial colonization has a non-redundant role in maintaining gastrointestinal physiology, it is of utter importance to control inflammatory immune responses at the intestinal barrier. Colonic tissue resident Treg cells are induced by indigenous clostridium species and respond to homeostatic mediators of microbial metabolites called SCAFs (short-chain fatty acids)[45,46].

Another important site of tissue-resident Tregs is the visceral adipose tissue (VAT). IL-33 signaling via the ST-2 receptor represents an essential environmental cue for VAT Treg differentiation[47]. VAT Tregs express the transcription factor PPAR-γ and are critically involved in regulating metabolism related processes, i.e. prevention of obesity-associated inflammation, preservation of insulin sensitivity and glucose tolerance[48,49].

$CCR4^+CD103^+$ Tregs are found in the skin and after resolution of inflammatory responses, survive as memory Tregs with enhanced functional activity[50,51]. Regulation of humeral immunity relies on $CXCR5^+BCL\text{-}6^+$ T follicular regulatory cells (TFR), which are found in germinal centers of secondary lymphoid organs and limit the numbers of T follicular helper (TFH) and germinal B cells[52,53]. In mice a distinct $Helios^+NRP\text{-}1^+$ growth factor amphiregulin expressing Treg population is critically involved in the repair of dystrophic muscles[54]. Finally, pregnancy imprints protective memory by generating maternal Tregs with fetal specificity, persisting at elevated levels, and rapidly re-accumulating in subsequent pregnancies[55].

2.5 Tregs and Foxp3

The transcription factor Foxp3 represents the master regulator and controller of Tregs[56,57]. Expression of a non-functional Foxp3 leads to lethal massive multi-organ lymphocytic infiltration and cytokine secretion, a condition termed “scurfy” in the mouse and IPEX in the human.

2.5.1 Structure

The transcription factor Foxp3 belongs to the forkhead/winged–helix family of transcriptional regulators. The protein consist of 431 aa encoded by 11 exons[20].
It contains a Forkhead domain at its carboxyl-terminal which is responsible for DNA binding and nuclear localization[58]. The proline rich N-terminal contains the repressor domain. Here epigenetic regulation via binding of histone acetyltransferases (HATs) and deacetylases (HDACs) is mediated. Also the transcription factors ROR-α and ROR-γt bind to this region of Foxp3. The leucine zipper in the middle allows Foxp3 dimerization. Runx1 binds to a region between the zipper and the Forkhead domain. Finally the Forkhead domain, besides mediating DNA binding and nuclear localization, binds the transcription factor NFAT (nuclear factor of activated Tcells) which inhibits the promoter of IL-2[59]

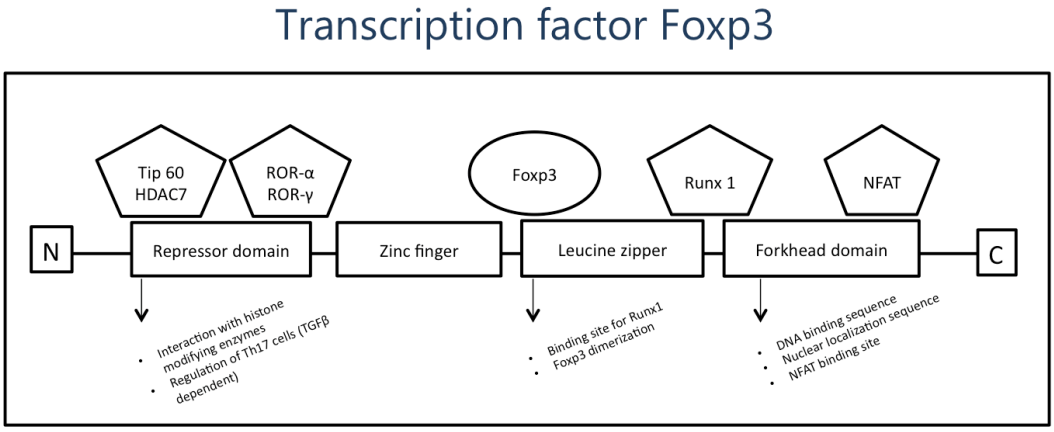

Figure 2.5.1 Diagram of the transcription factor Foxp3

2.5.2 Function

Depending on its interaction partners, Foxp3 either acts as a transcriptional repressor or a transcriptional activator. The typical Treg phenotype results from transcriptional repression of the IL-2, IL-4 and INFγ genes and transcriptional activation of suppressor molecules like CTLA-4, GITR and CD25.

Foxp3 competes against AP-1 (a dimer of c-FOS and c-JUN) for a cooperative binding with NFAT. The Foxp3/NFAT complex inhibits the IL-2 promoter. In Tconv (i.e. Foxp3 negative) cells the AP-1/NFAT complex activates the IL-2 promoter. Foxp3 and RUNX1, RUNX2 and RUNX3 interactions inhibit the production of the cytokines Il-2 and INFγ.

Depending on environmental TGF-β levels Foxp3 regulates Th17 deviation through interactions with ROR-γt. High levels of TGF-β lead to repression of ROR-γt mediated activities and keep Th17 cell numbers low. This allows for optimal Treg expansion.

Epigenetic modifications are changes to chromatin packing and thus the accessibility of transcription factors to genes. An active role of Foxp3 in epigenetic chromatin remodeling of target genes is well established. Foxp3 accesses genes critical for Treg development and phenotype, i.e. IL-2, INFγ, CD25, GITR, CTLA-4, Foxp3. Modifications at histone levels involve methylation (inhibition) or acetylation (activation) of DNA. These processes are mediated through HAD7/9 and Tip60 bound to the Foxp3 repressor domain. Sustained Foxp3 expression allows the de-methylation of the Treg-specific-de-methylated region (TSDR), creating a positive-feedback pathway to further enhance Foxp3 expression and maintain stable Treg lineage[60].

2.5.3 Regulation of *Foxp3*

Foxp3 has three highly conserved non-coding sequence (CNS1-3) regions. These are important regarding the regulation of Foxp3 expression[61].

Their role has been described as follows: CNS1, containing a TGF-β–NFAT response element, is essential for the generation of peripheral Tregs involved in maternal-fetal tolerance of placental animals[62]. CNS1 deficient females suffer form peripheral Treg cell paucity and have increased spontaneous abortions[62]. CNS2 seems to be dispensable for *Foxp3* induction but is important for maintaining its expression in dividing Treg cells. Via a CBFβ-RUNX1-*Foxp3* complex, DNA is demethylated and induces the heritability of the activated *Foxp3* locus and with this Treg lineage stability[61]. C-rel, a member of the NF-κB family, can directly bind to CNS3 and open the enhancer/promoter region of *Foxp3*[63,64]. In c-rel deficient mice, thymic Treg cell numbers are markedly reduced.

It could be shown that *Foxp3* makes use of a pre-existent enhancer landscape established during T cell differentiation. Treg lineage specification emerges form a late-acting opportunistic transcriptional modification of T cell specific enhancers present in precursors from Foxp3$^-$ T cells[65]. Numerous transcription factors like Foxo-1, Helios, Eos, IRF4, Tbet, BLIMP-1 and GATA-1 help maintain a stable epigenetic landscape within a Treg cell[66]. Thus the epigenetic signature of a Treg seems to be set in a mostly *Foxp3* independent manner.

2.5.4 Differences in Mouse and human Foxp3

Foxp3 is transiently induced upon TCR stimulation in human conventional CD4 T cells[67]. The functional consequences regarding pathogen-specific or autoimmune reactions are under investigation.

However, this phenomenon is not seen in mouse CD4$^+$ T conventional cells. Human Foxp3 has multiple isoforms generated by alternative splicing, i.e. FOXP3ΔEx2, FOXP3ΔEx7, FOXP3ΔEx2Ex7[68]. In mice there is only a single Foxp3 isoform. Since exon 2 and 7 partially encode the proline rich and the leucine zipper domain, it is assumed that the lack leads to failure of Foxp3 dimerization and binding of ROR-γt and ROR-α. However the functional implications of these human isoforms and which Foxp3 is expressed in which Treg cell population is still unclear.

Finally, a new binding partner of human Foxp3 was identified which is not seen in the mouse. The Foxp3-interacting KRAB domain-containing protein (FIK) can bind to the

human Foxp3 splice variant of the zinc finger protein 90 and interact with TIF1β to form a repressive chromatin-remodeling complex[69].

2.6 Tregs and IL-2

Interleukin 2 (IL-2) plays an important role as dominant regulator of homeostasis and growth of regulatory T cells[70]. Tregs continuously express the high affinity IL-2 receptor alpha chain (CD25) but are incapable of producing IL-2 them selves. Thus their survival is dependent on a consistent source of paracrine IL-2.

2.6.1 Ligand

IL-2 is a 15kDa small protein with T-cell stimulatory capacity. IL-2 has a short half live of 15-30 minutes[71,72] and is cleared from the circulation via the kidneys. Under steady state conditions, CD4 conventional T cells are the main source of IL-2. CD8, NK, NKT and DC cells additionally produce low amounts of IL-2.

Upon TCR and CD28 stimulation transcriptional induction of the IL-2 gene is induced and activated T cells rapidly secret IL-2. TCR signaling induces and activates transcription factors like AP-1, NFAT and NF-κB promoting their nuclear localization where they bind and transcribe the IL-2 gene[73].

IL-2 can inhibit its own production via an auto-regulatory negative feedback loop: upon IL-2 uptake, STAT5 (Signal transducer and activator of transcription) activation leads to Blimp-1 induction and ultimate repression of the IL-2 gene[74,75].

2.6.2 Receptor and signaling

The trimeric IL-2 receptor expressed on activated T cells consists of CD25, CD122 and CD132 (or IL-2Rα, IL-2RB and the common γ chain). With a dissociation constant (K_d) of 10e-11 M it has a high affinity for IL-2. CD25 has no part in signaling but initially binds IL-2 on its own which leads to the assembly of CD122 and CD132. The dimeric IL-2 receptor consisting of CD122 and CD132 has a lower affinity for IL-2 (K_d≈10e-9) and is only detectably expressed on CD8 and memory T cells.

Upon IL-2 binding the receptor-ligand complex is rapidly internalized ($t_{1/2}$ 10-20min)[73]. The signaling subunits CD122 and CD132 are degraded. CD25 gets recycled and reappears on the cell surface[76]. Binding of the IL-2 ligand by its receptor leads to phosphorylation of the Janus activated kinase 1 and 3 (JAK1, 3)[77] associated with CD122 and CD132. This in term leads to the activation and dimerization of STAT5. pSTAT5 trans locates to the nucleus where it activates a number of genes involved in cell survival, growth and transcriptional regulation[78].

PSTAT5 also binds to the *Foxp3* promoter amplifying the Treg's suppressive capacity by maintaining high Foxp3 levels[79]. Together with Foxp3, STAT5 acts on CD25 to maintain high CD25 surface expression in Tregs.

IL-2 signal transduction differs between $CD4^+Foxp3^+$ regulatory and $CD4^+$ conventional T cells: apart form the JAK-STAT signaling pathway, phosphorylation of the IL-2 receptor also leads to activation of the PI3K-mTOR and MAPK signaling pathways in CD4 T conventional cells. However $Foxp3^+$ regulatory T cells express high levels of the negative regulator PTEN resulting in inhibition of the Akt-mTOR pathway[80].

2.6.3 Role in development and homeostasis

It has been shown that IL-2, CD25 or CD122 deficient mice show rapid and lethal autoimmune syndromes[81-83]. These results suggest a non-redundant role for IL-2 in the development, maintenance and regulation of the immune system[84,85]. IL-2 influences terminal differentiation, effector responses or memory recall responses of CD8 and CD4 T cells. Importantly, IL-2 plays an essential part in thymic development, homeostasis and function of regulatory T cells[38,70].

CD122 deficient mice suffer form sever autoimmune diseases due to the lack of development and survival of regulatory T cells. In these mice, thymic-targeted expression of CD122 restored Treg numbers and prevented disease[85] emphasizing an important role for IL-2 signaling in developing Tregs.

$Foxp3^+$ T cells are not detected until after the stage of positive selection. The thymus contains very few IL-2 producing cells that are mainly located in the cortical medullary junction. IL-2 is believed to induce a terminal developmental and survival signal, promoting maturation of precursor ($Foxp3^{low}$, $CD25^{low}$, Bim^{low}, $Bcl\text{-}2^{high}$) Tregs into mature ($Foxp3^{high}$, $CD25^{high}$) Tregs. Deprivation of this niche-dependent and limiting γc signal results in a unique pro-apoptotic protein signature ($PUMA^{++}$, $p\text{-}BIM^{++}$, $p\text{-}JNK^{++}$

DUSP6$^-$) that represses Bcl-2 survival signals and leads to Foxp3 induced cell death of Treg precursors[38].

Once CD4$^+$CD25$^+$Foxp3$^+$ Tregs emerge from the thymus, in a first step they home to secondary lymphoid tissues (lymph nodes and spleen), where their homeostasis again relies on IL-2. Due to direct repression of the IL-2 promoter via Foxp3, Tregs cannot produce their own IL-2 and rely on a constant source of paracrine IL-2. Since IL-2 secretion form T cells activated by foreign antigen may happen at a great distance to the Treg and is unpredictable, it seems unlikely that this is their main source of paracrine IL-2. A more reliable source is a naïve CD4$^+$ T cell encountering ubiquitously present self-peptide in the periphery. Constant and high expression of surface CD25 on Tregs allows for uptake of excess paracrine IL-2 with beneficial effects for all players: consuming IL-2 gives the Treg a survival signal; due to low amounts of paracrine IL-2 the Tconv is stopped from further activation and will not proliferate; physiological levels of IL-2 are restored in the system and homeostasis is preserved.

That peripheral tolerance solely relies on the suppressive mechanism of passive IL-2 consumption by Tregs seems unlikely. However tolerance may profit from IL-2 clearance by Tregs since potentially dangerous terminal effector development or memory generation gets interfered with[72,73].

2.6.4 IL-2 complexes

Due to its potent immune regulatory function, IL-2 is a promising therapeutic candidate in clinical settings. However when used at high doses IL-2 toxicity causes dangerous vascular leak syndrome. Rapid renal clearance and a short half live poses yet another serious problem for IL-2 immunotherapy. Still, high-dose IL-2 applications induced activation of antitumor-lymphocytes and achieved positive results regarding the survival of patients suffering from metastatic renal or skin cancer[86,87]. Importantly low dose IL-2 applications were shown to correlate with Treg expansion. First clinical trials administering low dose IL-2 in patients with autoimmune diseases like diabetes type 1 or graft-versus-host-disease (GVHD) describe beneficial effects on the induction of Treg numbers and/or function[88].

Apart from the serious adverse effects described above, an additional problem of injecting soluble IL-2 is the stimulation of both cytotoxic T and regulatory T cells. Coupling IL-2 to IL-2-specific, neutralizing, monoclonal antibodies like JES6-1A12 or S4B6 is a method to overcome this problem. Directing IL-2 to distinct T cell subsets

results in either enhanced or suppressed immune responses. While injection of IL-2-S4B6 complexes in mice lead to increased CD8 memory T and NK cell populations, injection of IL-2-JES6-1 complexes selectively expands $CD25^{+}Foxp3^{+}$ regulatory T cells. Similar effects were observed using human IL-2 coupled with the human IL-2 to the specific monoclonal antibody 5344[89-93].

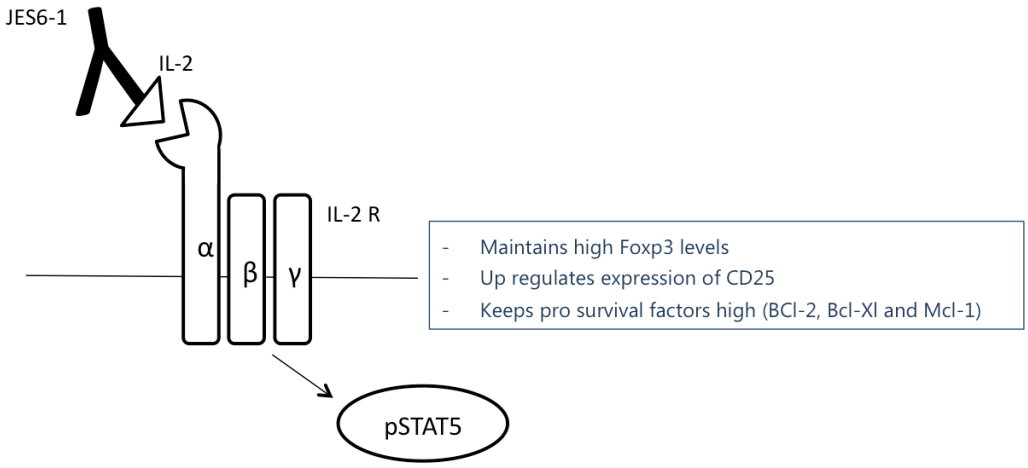

Figure 2.6.1 Effects of IL-2/JES6-1 mAb complex administration

2.7 Tregs and TCR signalling

The Treg TCR repertoire is described to be enriched in self-reactive cells specific for tissue-restricted antigens and TCRs expressed by Tregs are thought to be of higher affinity for self-antigens than conventional T cells[94].

The RAS/MAPK, NFκB as well as mTor signaling pathways are considered the driving pathways in controlling proliferation and activation of a conventional T cell. They are major components of TCR signaling, tightly regulating the transcription of the IL-2 gene via NFAT/AP-1 and thus controlling proliferation, activation and survival of the T cell[59]. How intracellular signaling events differ between Tregs and T effectors is still incompletely understood.

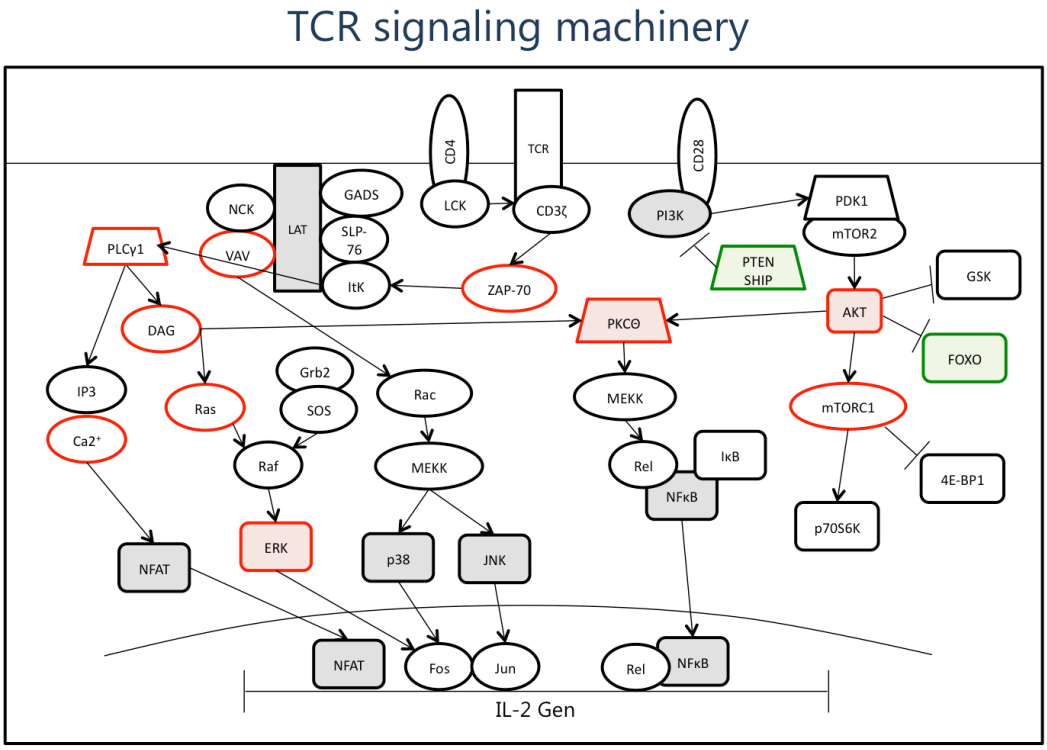

Figure 2.7.1 Diagram of TCR signalling pathways in CD4$^+$ Tcell

In green: Signalling intermediates that were described to be increased in Tregs

In red: Signalling intermediates that were described to be decreased in Tregs

TCR signaling initiates with co-receptor coupled Lck, phosphorylating the immune-receptor tyrosine-based activation motives (ITAMS) within the CD3 complex[95]. Subsequent recruitment and phosphorylation of Zap-70 follows. Zap-70 phosphorylates the adaptor protein LAT, which then recruits SLP76, Grb2 and SOS to activate the MAP kinase ERK either via Raf-1 or via PLCγ and RAS[8]. Co-stimulatory signals are also important for T cell activation. CD28 recruits PKCθ to the synapse leading to activation of the NFκB signaling pathway[96,97]. CD28 signal transduction activates PI3 kinase, which activates Akt to induce signaling through the mTor pathway[98].

Despite the self-reactivity of Tregs, the role of TCR signalling in Treg biology has been controversial and is still not fully understood. Numerous reports support the idea that TCR signalling in Tregs is uncoupled from the signalling pathways described in conventional T cells[99-101]. Mechanisms that inhibit the onset of TCR signaling have been proposed. Among them is a negative feedback loop involving Dok-1 and 2. These proteins recruit the C-terminal Src kinase (Csk) to the plasma membrane[102,103] and negatively regulate Lck, resulting in reduced phosphorylation of CD3ζ and of Zap-70[104].

Recently it was demonstrated that the catalytic activation of Zap-70 is not required for the suppressive activity of Tregs[100]. It's been proposed that ZAP-70 has a scaffolding function, which is independent of its catalytic function, and contributes to the lymphocyte function-associated antigen 1 (LFA-1) mediated adhesion[100]. In terms of the RAS/MAPK pathway, Tregs have been shown to have decreased levels of PLCγ, DAG, RAS and ERK[99]. Furthermore many signaling intermediates are not activated by TCR signaling. For example Ca^{2+} mobilization seems to be impaired upon TCR engagement[101]. Decreased levels of PKCθ and thus hampered activity of NFκB have also been described[105]. Taken together the idea that TCR signaling in Tregs is blunted or deviated to maintain an anergic, suppressive Treg phenotype has received experimental support.

However, recent data indicate that continuous expression and signalling of the TCR is required for effective suppression to occur in vivo[106]. Deletion of the TCR in peripheral Treg cells from $Foxp3^{eGFP\text{-}Cre\text{-}ERT2}$ x $TCR\alpha^{FL/FL}$ mice resulted in a marked loss of effector Tregs. These mice developed sever autoimmunity and died by day 13 of life. Interestingly loss of the TCR did not alter the amount of Foxp3, CD25 or GITR expression in these "Tregs"[106]. The role of downstream TCR signaling, together with its influence on Treg suppressive functions, was further addressed by Schmidt et al[107]. Their work revealed that TCR signals through SLP-76 and PLCγ1 (resulting in downstream signaling of DAG) play an essential role in Treg suppression but that Tregs lacking molecules involved in TCR-mediated integrin activation, displayed normal suppressive functions[107].

Overall these data suggest that proximal and distal TCR signals are required in Tregs (also see results), but that TCR mediated integrin activation has a non-essential role for effective Treg suppressive functions.

2.8 Tregs and suppressive mechanisms

Numerous work characterized Tregs and described their suppressive mechanisms. These mechanisms can be divided into two main groups, i.e. those that are dependent on cell-to-cell contact and those that are not.

2.8.1 Cell-contact dependent mechanisms

In regard of contact dependent mechanisms, studies using transwell suppression assays, where a semipermeable membrane prevents Treg and Tconv contact, suggested a

predominate role for cell contact dependent suppressive mechanisms[108,109]. However, a failure to observe suppression in these experiments could be explained by the inability of diffusible suppressive molecules to function in the relatively large volume of the in vitro culture. Theoretically, suppression might utilize Treg secreted molecules but additionally require proximity between Tregs and Tconv cells[110].

The cytotoxic T-lymphocyte-associated Protein 4 (CTLA-4) is constitutively expressed on Tregs[111]. Mice with Treg specific CTLA-4 deficiency suffer from spontaneous development of systemic lymphoproliferation and fatal T cell autoimmunity[112]. It was proposed that Tregs initiate the catabolism of tryptophan in dendritic cells through a CD80/86-CTLA-4 dependent mechanism, generating metabolites, which convert naïve CD4 Tconv into tolerogenic Foxp3$^+$ Tregs[113-115]. CTLA-4 has an additional function that down regulates co-stimulatory molecules CD80 and CD86 on antigen presenting cells (APCs) via trans-endocytosis[116-118]. By diminishing the APC's capacity to efficiently present antigen, Tregs likely prevent priming of Tconvs[119,120].

High LFA-1 expression on Tregs was proposed to augment the physical interaction between Tregs and APCs[121]. In this way Tregs can out compete Tconv for space on the APC. Tregs expressing LAG-3 were shown to bind MHC-2 and block DC maturation[122]. Since LAG-3 deficient mice do not show autoimmune disorders the relevance of LAG-3 for suppression remains to be established[123].

2.8.2 Cell-contact independent mechanisms

Cell-contact independent mechanisms depend on the action of cytokines and chemokines. Tregs produce immunosuppressive cytokines like transforming growth factor β (TGFβ) and IL-10, which have been shown to control Tconv proliferation[124,125]. Treg cell-derived TGFβ was shown to convert naïve T cell precursors into suppressive Foxp3$^+$ T cells[34]. However, the role of TGFβ in Treg suppression remains controversial since Tregs mediate suppression of Tconvs from TGFβRII KO and Smad3$^{-/-}$ mice[126]. In addition Tregs from neonatal TGFβ^{KO} mice retained their suppressive capacity[126]. Gut Tregs were shown to secrete IL-10, which was required for mucosal immune homeostasis and the control of colitis[127-129]. However, Treg-specific IL-10 deficient mice did not suffer from systemic autoimmunity per se but failed to control immune responses at mucosal, environmental interfaces (i.e. gut, lung)[130]. Further more, blockade of either IL-10 or TGF-β failed to abrogate Treg mediated suppression in vitro[131].

Another possible suppressive mechanism is the Treg mediated release of granzymes A or B[132-134]. Tregs have been shown to disrupt Tconv metabolism through cyclic adenosine monophosphate (cAMP)[135,136,] or by scavenging cytokines[137]. Tregs constitutively express high levels of CD25, which could steal IL-2 from Tconvs preventing their full activation[70]. However two observations question the idea that Tregs function by consuming Tconv generated IL-2: (i) Tregs from CD25 KO mice are suppressive, in vitro and (ii) mice with specific peripheral abrogation of Treg CD122 (IL-2RB) expression don't suffer from autoimmune disorders[85]. However more recent work mitigated these interpretations. CD122 deficient Tregs can still respond, albeit to a diminished extent[138], to IL-2 signaling and CD25 deficient Tregs were proposed to display compensatory up regulation of CD122 and CD132[110,139], which renders them capable of responding to, and consuming IL-2. Finally another line of evidence for IL-2 consumption as a suppressive mechanism lies in the fact that addition of exogenous, IL-2 abrogates suppression (in vitro)[108,109].

2.9 Tregs and clinic

Disruption of Treg homeostasis leads to dysfunctional immunity and devastating conditions in the host. Autoimmune diseases, chronic infections and tumorous illnesses[140] are the consequences. Although we lack a full understanding of how Tregs function at a cellular and molecular level, Tregs are being used in clinical trials. Three main approaches of Treg treatment are pursued;

(i) Treg induction: i.e. increase and maintenance of Tregs in patients with autoimmune diseases like diabetes type 1[141] via IL-2 complex treatment[89], rapamycin administration[142] or monoclonal antibody treatment (i.e. anti-CD3, anti-thymocyte globulin, anti-CD52)[143]. After global T cell depletion, these antibodies possibly induce a shift in the Treg/non-Treg re-population of the periphery, resulting in a functional enrichment of Tregs. Another approach of Treg induction therapy is the generation of antigen specific Tregs in the host. Nexvax2[144-146] is a vaccine, comprising a dominant peptide epitope of the gluten protein. Upon oral gluten consummation, allergic T cell mediated reactions in the gut mucosa of celiac patients are suppressed by gluten-antigen specific Tregs[144].

(ii) Treg cell therapy includes in vitro expansion and autologous transfusion or over-expression of Foxp3 in T cells using a vector system, which ensures continuous high expression levels of Foxp3[147]. In vitro expansion and transfusion of autologous Tregs was

shown to reduce the risk of GVHD after hematopoietic stem cell transplantation[148-151]. Recently this approach was also shown to suppress autoreactive T cells in Morbus Crohn patients[152].

(iii) Treg-depletion, i.e. depletion of Tregs using specific monoclonal anti-CTLA-4 or anti-PD1 antibodies in cancer patients[153,154]. Upon Treg depletion, cytotoxic, tumor-reactive T cells can attack and clear the tumor without being suppressed.

Using Tregs as cellular therapies entails safety concerns including the expansion/transfusion of un-pure Treg populations and the instability of Treg lineage commitment. A better understanding of Treg biology is still required, so Treg cell treatment can be administered safely and with a predictable outcome.

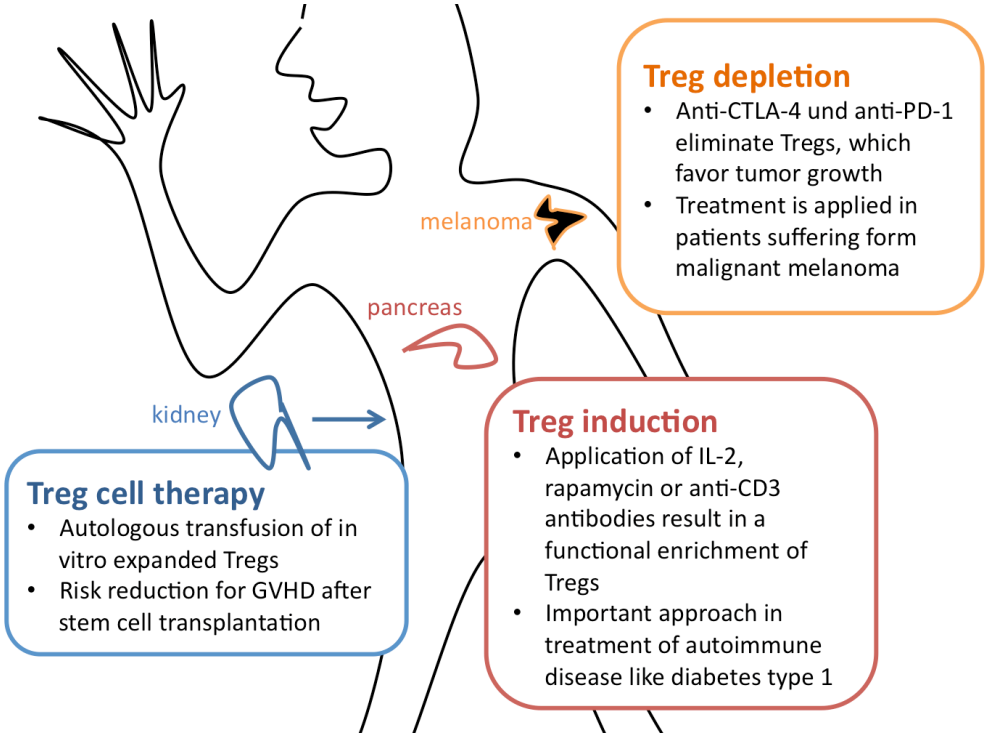

Figure 2.9.1 Diagram of three main approaches in Treg cell therapy

Examples of diseases where Treg-cell therapy is applied

3 Hypothesis

3.1 Part A: Studies of suppression using monoclonal regulatory T cells

In the first part of the thesis, we re-assessed the mechanisms of Treg mediated suppression and the TCRs contribution, making use of mice expressing a population of monoclonal, TCR transgenic Tregs (B3K506 Tregs).

3.2 Part B: The importance of co-receptor Lck coupling ratios for negative selection

In the second part of the thesis, we examined if the TCR affinity threshold is defined by the time it takes a TCR to collide with a co-receptor carrying Lck and if a difference in the co-receptor Lck coupling ratios of CD8 and CD4 coreceptors explains the decrease in antigen affinity needed to initiated negative selection in class II restricted DP thymocytes.

4 Material/methods

4.1 Part A

4.1.1 Mice

Foxp3 Tg mice on a C57BL/6 background were described previously[57] and kindly provided by S. F. Ziegler. B3K506 TCR Tg Rag$^{-/-}$ mice on a C57BL/6 background were described previously[155] and kindly provided by J. W. Kappler. B3K506 TCR Tg Foxp3 Tg mice were generated in our lab by crossing B3K506 TCR Tg Rag$^{-/-}$ to Foxp3 Tg animals. Foxp3-^{EGFP} reporter mice on a C57BL/6 background were described previously[156] and kindly provided by B. Malissen. ABM (anti-bm12) TCR Tg mice on a C57BL/6 background were described previously[157] and generated by E. Palmer. IL-2-^{EGFP} Reporter mice on a C57BL/6 background were described previously[158] and kindly provided by A. A. Freitas. OT-II TCR Tg Rag$^{-/-}$ IL-2-^{EGFP} Reporter mice were generated in our lab by crossing OT-II TCR Tg Rag$^{-/-}$ to IL-2-^{EGFP} Reporter animals. OT-II TCR Tg mice on a C57BL/6 background, C57BL/6 Ly5.1, C57BL/6 Ly5.2, H2-Abm12 and BALB/c mice were purchased from The Jackson Laboratory (Bar Harbor, Maine, USA). CD3$^{-/-}$ mice on a C57BL/6 background were described previously[159] and kindly provided by P. Marrack. HA TCR Tg mice on a BALB/c Ly5.1 background were previously[160] described and kindly provided by A. Rolink. All adult mice were 6–12 weeks old and bred in our colony (University Hospital Basel) in accordance with the Cantonal and Federal laws of Switzerland. The Cantonal Veterinary Office of Basel-Stadt, Switzerland, approved the animal protocols.

4.1.2 Media, antibodies and reagents

All cells were grown in RPMI 1640 (Gibco /Lifetechnologies) supplemented with 10% heat-inactivated FCS. Biotin-conjugated anti-CD3 (145-2C11), Biotin-conjugated anti-CD4 (RM4-5), Biotin-conjugated anti-CD8 (53-6.7), PE-conjugated anti-CD45.2 (104), Alexa700-conjugated anti-IFNγ (XMG1.2), PerCP-conjugated anti-CD45.1 (A20), FITC-conjugated anti-CD69 (H1.2F3), FITC-conjugated anti-CD44 (IM7), APC-conjugated anti-CD19 (1D3), PE-conjugated anti-CD62L (Mel-14), PE-conjugated anti-CD5 (53-7.3), PerCP-conjugated anti-CD3 (145-2C11), Alexa700-conjugated anti-CD4 (RM4-5), APC-conjugated anti-CD11a (M17/4), PE-conjugated anti-TCRValpha 2 (B20.1), PE-conjugated

anti-TCRVbeta 5 (MR9-4), PE-conjugated anti-p4G10, PE-conjugated anti-pCD3zeta, PE-conjugated anti-pZap-70 and APC-conjugated anti-TCRVbeta 8 (MR5-2) were purchased from BD Pharmigen (www.bdbioscience.com). PerCP-conjugated anti-NRP-1 was purchased from R&D Systems Inc. (www.RnDSystems.com). PE-Cy7-conjugated anti-GITR (DTA-1), PE-conjugated anti-TBET (4B10), PE-Cy7-conjugated anti-Foxp3 (FJK-16a) and APC-conjugated anti-Helios (22F6) were purchased from eBioscience (www.eBioscience.com). Pacific blue-conjugated anti-CD4 (RM4-4), Alexa700-conjugated anti-CD86 (GL-1), APC-conjugated anti-LAP (TW7-16B4), Alexa700-conjugated anti-CD25 (PC61) and APC-conjugated anti-CTLA-4 (UC10-4B9) were purchased from BioLegend (San Diego, CA, USA). Anti-pERK and anti-pc-JUN were purchased from Cell Signalling. EasySep Mouse CD4+ T cell Isolation Kit and EasySep Mouse B cell Isolation Kit, were purchased from Stemcell Technologies (www.stemcell.com). Recombinant Mouse IL-2 was purchased from BioLegend (San Diego, CA, USA). Cell Proliferation dye eFluor 670 was purchased from eBioscience (www.eBioscience.com). BD Cytofix/Cytoperm Plus Fixation/Permeabilization Kit with GolgiStop and BD Cytometric Bead Array Mouse Th1/Th2/Th17 CBA Kit was purchased from BD Pharmigen (www.bdbioscience.com). Anti–IL-2 (JES6-1) and anti-CD3 (145-2C11) were produced in our lab. Protein G Sepharose 4 Fast Flow, was purchased from (www.gelifescience.com). Peptides 3K (FEA QKA KAN KAV), P8G (FEA QKA KAN GAV), P2A (FEA AKA KAN KAV), and OVA (323-339) (ISQ AVH AAH AEI NEA GR), were purchase from AnaSpec (Fremont, CA, USA). HA-Peptide (YPY DVP DYA) was kindly provided by L. Klein (LMU, Germany). Dynabeads Biotin Binder, Cell trace CFSE and LIVE/DEAD fixable Near-IR were purchased from Invitrogen (Eugene, Oregon, USA). PMA, Ionomycin, methanol, PFA and glycine were purchased from Sigma-Aldrich (www.sigmaaldrich.com). Streptavidin was purchased form Jackson Immunoresearch. I-A^b 3K monomers were kindly provided by Prof. E. Huseby.

4.1.3 Generation of JES6-1 monoclonal Antibody

JES6-1 hybridoma cells were grown at a density of 10e6/ml in RPMI media completed with 2% low IgG FCS. FCS was carefully run over a Potein G column twice to reduce the amount of IgG protein. IgG protein levels were controlled for by western blot. Hybridoma cells were cultured in roller bottles at 37°C for 21 days until >80% of cells were dead. Culture media was centrifuged and decanted into fresh container to get rid of cell debris. In addition culture media was filtered through a 0,2 µm pore filter and 0.02% of sodium azide was added for

storage at 4°C until further processed. Culture supernatant was run over a 5ml protein G column at a speed of 60-120ml/hour. IgG was eluted with 0.1M gycine (pH 2.8) into 50µl of 1M Tris (pH 9.0). High concentrated elution fractions were dialyzed against endotoxin free PBS for 48 hours. Antibody fractions were sterile filtered and concentration was determined by absorbance at 280 nm with a nanodrop system.

4.1.4 IL-2 complex treatment

B3K506 TCR Tg Foxp3 Tg $Rag^{-/-}$ and B3K506 TCR Tg $Rag^{-/-}$ (ctrl) mice were injected intra peritoneal (i.p.) with 7.5µg anti-IL-2 antibody (JES6-1) complexed to 2.5µg mouse recombinant IL-2 in 200µl PBS on three subsequent days. Complex formation was achieved by adding IL-2 and JES6-1 to PBS and letting it incubate for 30 min at 37°C.

4.1.5 Preparation and sorting of lymphocytes

LNs (axillary, inguinal, superficial cervical, mandibular, and mesenteric) were harvested from 6-12 week old mice. For single cell preparation they were mashed through a mesh into RPMI/10% FCS. B3K506 TCR Tg Foxp3 Tg cell suspensions were then incubated with Pacific Blue conjugated anti-CD4 and PE-Cy7 conjugated anti-GITR antibodies for 10 min at 4°C, washed, and then sorted for $CD4^{+}GITR^{high}$ cells on a BD INFLUX Cell Sorter (purity ≥96%) into RPMI/10%FCS. B6 $Foxp3^{EGFP}$ cell suspensions were sorted for GFP^{+} cells on a BD INFLUX Cell Sorter (purity ≥98%) into RPMI/10%FCS. Spleens were harvested from 6-12 week old mice. For single cell preparation they were mashed through a mesh into Erytrocyte lysis buffer and incubated for 1 min. The cells were washed in RPMI/10% FCS. After incubating the cell suspension for 10 min with biotin-conjugated anti-CD4, biotin-conjugated anti-CD8, biotin-conjugated anti-CD3 antibodies, T cell depletion was preformed with the EasySep Mouse B cell Isolation Kit from Stemcell technologies (according to manufacture's protocol) or with Dynabeads Biotin Binder Kit (according to manufacture's protocol, Invitrogen).

4.1.6 In vitro suppression culture

10e5 B3K506 Tregs, 10e5 B6 $Foxp3^{-EGFP}$ Tregs or 10e5 B3K506 Tconv (ctrl) were cultured in 96-well plates (0.2 ml) with 2.5x10e4 OT-II Tconv and 10e5 T cell–depleted splenocytes,

0.1 µg/ml anti-CD3 or 3K, P8G or P2A (at various concentrations, see figures). T cell depleted splenocytes were preloaded with 10e-7 M OVA (323-339) peptide for 4.5h at 37°C and carefully washed. OT-II Tconv were labelled with 5µM CFSE or 5µM eFlour 670 according to manufacture's protocols. Flow cytometric analysis of suppressive cultures was preformed after 24, 48 or 72h.

4.1.7 Staining and flow cytometry

Surface staining was preformed in PBS/3% FCS at 4°C for 10 min with various antibodies. For intracellular staining cells were fixed and permeabilized (according to manufacture's protocol) using the Cytofix/Cytoperm Plus Fixation/Permeabilization Kit from BD. Intracellular Foxp3 staining was preformed at 4°C for 1h. For intracellular cytokine staining cultured cells were re-stimulated with 100ng/ml PMA, 1.5µM Ionomycin and 1.5µl/ml Monensin (BD Pharmigen) and left for 5h at 37°C. Flow cytometry was preformed with a FACSCanto II from BD Pharmigen (www.bdbioscience.com).

4.1.8 In vivo graft transplantation

Tail skin from B6.bm12 $Rag^{-/-}$ mice was isolated and transplanted onto the back of B6 $Rag^{-/-}$ mice and allowed to heal in for 7 days. The following day mice were injected with 2x10e4 ABM (I-Abm12 specific) Tconvs along with 2x10e5 $Foxp3^{-EGFP}$ Tregs or 2x10e5 B3K506 Tregs. In one group mice received 30µg 3K peptide/200µl PBS IP. injections every 2nd day until day 15. A control group was injected with 2x10e4 ABM Tconvs alone. Graft rejection was checked for every 2nd day.

4.1.9 Cytokine assay

Culture supernatants were stored at -80°C and thawed. The BD Cytometric bead array (CBA) system using antibody-coated capture beads was used to quantitate various cytokines in the culture supernatants (see manufacture's protocol). Analysis was preformed with Excel software (version 14.4.3) calculating the unknown sample concentrations from a standard curve.

4.1.10 EC50 determination of B3K506 TCR APLs

10e5 T cell depleted splenic B cells were isolated and loaded with varying amounts of peptide for 4.5 h at 37°C before addition of 2.5x10e4 B3K506 Tconvs or 2.5x10e4 OT-II Tconvs. Cells were cultured in 96-well plates (0.2ml) with RPMI/10% FCS for 24h at 37°C. T cells were then surface stained (described above) for CD3, CD4 and CD69 and flow cytometry was preformed. The EC50 values for CD69 up regulation were calculated using a nonlinear regression curve (log (agonist) vs. response (three parameters), Prism, version 6.0b).

4.1.11 Signalling assays

For short time point stimulation assays (I.e. 30, 60, 90 and 150 seconds) 3K tetramers were used. T cells were rested at a concentration of 40x10e6 in RPMI/10% FCS for 20 minutes on a shaker at 37°C. Tetramers were added at a 2X concentration (i.e. 200nM). At time point, the tetramer-cell mix was re-suspended in 8% PFA. In addition cells were spun at 1000G for 2 minutes and re-suspended in ice-cold methanol. After carefully washing with PBS, primary antibody in signaling buffer was applied and left over night at 4°C. After washing secondary antibody diluted in signaling buffer was applied and left for 1 hour on ice.
For longer time point stimulation assays (i.e. 60 and 150 minutes) peptide pulsed splenocytes were used to stimulate T cells. To enhance conjugate formation, cells were spun at 1500 RPM for 3 minutes. To break conjugates at indicated time points, 5mM EDTA in PBS was applied and cell suspension was pipetted up and down for 5 minutes.

4.1.12 Tetramers

Tetramers consist of four I-A^b monomers (30 kDa each) coupled to one molecule of streptavidin (53 kDa). Tetramers were generated by incubating biotinylated monomers with streptavidin at a ratio of 4:1 on ice. Streptavidin was added in two steps. After each streptavidin addition, mix was allowed to incubate for 60 minutes on ice. Tetramer stock was diluted in PBS to a final concentration of 2mM and could be stored for several weeks at 4°C.

4.1.13 Same/separate APC experiments

For same APC cultures, 10e5 B3K506 Tregs (I-A^b restricted), 2.5x10e4 HA Tg Tconvs (I-E^d restricted) and 10e5 splenic B cells from F1 mice (BALB/c x B6, on a I-E^d x I-A^b background) were cultured in a 96-well plate (0.2ml) with RPMI/10%FCS at 37°C. For separate APC cultures, 10e5 B3K506 Tregs (I-A^b restricted), 2.5x10e4 HA Tg Tconvs (I-E^d restricted), 10e5 splenic B cells from B6 (I-A^b background) and 10e5 splenic B cells from BALB/c (I-E^d background) were cultured in a 96-well plate (0.2ml) with RPMI/10%FCS at 37°C. 3K peptide (10e-7M) and HA peptide (10e-5M) was added to same and separate APC cultures. Cultures were analyzed using flow cytometry after 72 h.

4.1.14 Statistics

Cell proliferation Index (PI) was calculated using FlowJo software (version 9.7.7). % Suppression was calculated using the formula (100-(% proliferated Tconv from suppressed culture/% proliferated Tconv)*100). Curve fitting and statistical analysis was performed using Prism version 6.0b and Excel version 14.4.3.

4.2 Part B

4.2.1 Mice

All adult mice were 6-12 weeks old and had a C57Bl/6 genetic background. OTI $Rag^{-/-}$, OT-I $Rag^{-/-}$ $\beta2m^{-/-}$, B3K508 $Rag^{-/-}$ mice were described previously[8,155]. CD8.4 OT-I $Rag^{-/-}$ $\beta2m^{-/-}$ strain was generated by crossing CD8.4 knock-in mouse[161] with OT-I $Rag^{-/-}$ $\beta2m^{-/-}$. B3K508 $Rag^{-/-}$ I-$A^{-/-}$ mice were generated by breeding B3K508 $Rag^{-/-}$ with I-$A^{-/-}$ mice. Crossing the CD8.4 knock-in mouse with B3K508 $Rag^{-/-}$ generated the CD8.4 B3K5008 $Rag^{-/-}$ strain.

4.2.2 Media, antibodies and reagents

All cells suspension were made in RPMI 1640 (Gibco/ Lifetechnologies) supplemented with 10% heat-inactivated FCS. Antibodies to following antigens were used: Lck (clone 3A5), were purchased from Santa Cruz Biotechnology. CD3ε (clone 145-2C11), CD8α (clone 53-6.7), CD8β (clone 53-5.8), CD4 (clones RM4-5 and H129.19) and TCRβ (clone H57-597)

were purchase from BD Pharmingen. For flow cytometry, antibodies were conjugated to various fluorescent dyes by the manufacturers. For western blotting a secondary light-chain-specifc goat-anti-mouse HRPO-conjugated antibody was purchased from Jackson Immunoresearch. Protein G sepharose beads and full-range rainbow molecular weight marker were purchased from GE Healthcare. Acrylamide mix (30%), Trans-blott nitrocellulose membrane, Milk powder, ECL western blotting reagents, ECL Hyperfilm and TEMED were purchased from BIO RAD. CML latex beads were purchased from Invitrogen. Laemmli sample buffer, MES hydrate, Tris Base, Glycine, SDS and EDAC (Ethyl-3-(3-dimethylaminopropyl)carbodiimid) were purchased from Sigma-Aldrich. Halt Protease and Phosphatase Inhibitor Cocktail was purchased from Thermo scientific. RCP-30-5A calibration beads were purchased from Spherotech Inc.

4.2.3 Immunoprecipitation and Western blotting

10e7 thymocytes from OT-1 WT or OT-1 CD8.4 mice were lysed in 50µl lysis buffer and incubated for 15 minutes on ice. Cell lysates were cleared by centrifugation at 14000 rpm for 10 minutes at 4 °C. Immunoprecipitation was preformed in 400µl lysis buffer with 2µg monoclonal antibody and 20µl of 50 % protein G sepharose for 1.5 hours on a rotation wheel at 4°C. Upon washing sample and beads were boiled for 5 miuntes at 95 °C in 20µl Laemmli buffer. SDS-PAGE and western blotting was preformed. After proetein transfer, nitrocellulose membrane was blocked for 1hour in blocking buffer. Primary antibody (anti-LCK clone 3A5) was applied in blocking buffer and incubated over night at 4 °C. Upon washing, HRPO-conjugated light-chain specific goat-anti-mouse antibody was applied for 1 hour at room temperature. Nitrocellulose membrane was developed in 2ml of ECL western blotting detection reagents for 3 minutes at room temperature. The luminescence of HRPO-mediated conversion of the ECL detection reagent was captured by exposing the membrane to ECL hyperfilms for appropriate periods of time and developing the films on a Curix80 developer.

4.2.4 CML bead antibody coating[162]

18x10e6 CML beads were washed twice in MES buffer, and re-suspended in 50µl MES buffer. 20µl of EDAC/MES buffer (50µg/µl) was applied and incubated for 15 minutes at 25 °C. Beads were then washed 3 times in PBS and 50µl of monoclonal antibody (0.2mg/ml) was applied and incubated overnight at room temperature. Beads were carefully washed 3

times in PBS. For quenching, beads were re-suspended at a concentration of 25x10e6/ml in storage buffer and stored at 4°C.

4.2.5 IP-FCM

10e6 cells were lysed in 50 µl lysis buffer for 30 minutes on ice. 75,000 CML beads coupled to anti-CD4 (clone RM4.4), anti-CD8α (clone 53-6.7), or anti-MHCI (clone Y3.8) antibodies, as described above, were added to the lysate and incubated for 3 hours at 4°C. Beads were washed 3x in lysis buffer and stained with different PE-conjugated antibodies to CD4 (clone H129.19), CD8β (clone 53-5.8), or Lck (clone 3A5) at saturating concentrations (40 min, on ice) and analyzed by flow cytometry. The geometric mean fluorescence intensities (gMFI) were taken as the measure of the antibody binding. The CD8, CD8.4 or CD4-Lck coupling ratio was calculated as Lck signal to CD8 or CD4 signal (after subtracting respective background signal calculated from control anti-MHCI beads) and adjusted for the PE/antibody ratio.

4.2.6 Determination of surface molecule numbers

Saturating concentrations of PE–conjugated antibodies were determined (0.04 mg/ml for CD3ε, CD8α and 0.01 mg/ml for CD4). 25,000 cells were stained in 25 µl of staining buffer (PBS/2% FCS) for 40 min on ice, washed, and analyzed along with PE calibration beads by flow cytometry. A calibration curve was generated based on the fluorescence signal from calibration beads to transform the geometric mean of fluorescence intensity (after subtraction of background signal from antibody stained peripheral B cells) into mean equivalent of PE intensity (MEPE) values. The actual number of surface molecules was calculated by adjusting the MEPE values to the PE/antibody ratio (determined by absorbance at 560 nm using soluble PE as a standard). Number of antigens captured by one molecule of antibody (assumed as 2^{163}), except for TCR, where the results were further corrected for the presence of 2 molecules of CD3ε per TCR/CD3 complex.

4.2.7 Buffers and gels

Lysis buffer	1% NP-40, 10 mM Tris pH 7.4, 140 mM NaCl, 2 mM EDTA, Protease Inhibitor Cocktail (Sigma-Aldrich).
IP-FCM staining/washing buffer	50mM Tris ph 7.4, 100mM NaCl, 0.02% NaN3, 5% FBS or 1% BSA, 1% Np-40.
Storage buffer	1% BSA, 0.02% NaN3 in PBS.
SDS resolving gel (12%), 20ml	6.6ml H2O, 8ml 30% acrylamide mix (4°C), 5ml TRIS 1.5 M (pH 8.8), 200ul 10% SDS, 200ul of 10% freshly prepared ammonium persulfate, 8ul TEMED.
SDS stacking gel (5%), 6ml	4.1ml H2O, 1ml 30% acrylamide mix (4°C), 750ul TRIS 1 M (ph 6.8), 60ul 10% SDS, 60ul 10% freshly prepared ammonium persulfate, 6ul TEMED.
SDS Running buffer, 20L	60g Tris Base, 288g Glycine, 20g SDS in 20L H2O.
Transfer buffer, 1L	100ml Towlin (10x), 100ml Methanol, 800ml H2O.
Blocking buffer, 50ml	2.5g milk powder dissolved in 50 ml of 1% Tween.
Washing buffer, 2L	200ml TBS (10x), 1800ml H2O, 2ml Tween.
Tris buffer 1M (pH 6.8), 500ml	60.6 g TRIS in 200ml H2O, adjust pH with 12N HCL.
Tris buffer 1,5M (pH 8.8), 500ml	90.8g TRIS in 400ml H2O, adjust pH with 12N HCL.
Tris-buffered Saline 10x, 1L	24 g Tris base (Formula weight: 121.1 g), 88 g NaCl (Formula weight: 58.4 g) dissolve in 900 ml distilled water, adjust pH to 7.6 with 12N HCL. Add distilled

	water for final volume of 1 liter.
Erythrocyte lysis Buffer (10X)	8,26 g of NH4Cl, 1,19 g of NaHCO3, 200 µL EDTA (0,5 M, pH8) add distilled water until 100 mL. Adjust pH to 7.3 and filter sterile
Signalling buffer	PBS, 3% FCS, 0.3% Triton X , 5% Goat serum

5 Results

5.1 Part A

A Foxp3 transgene was backcrossed to TCR transgenic B3K506 Rag$^{-/-}$ mice to generate B3K506 Tg Foxp3 Tg "Treg" mice. Forty-50 % of T cells in the B3K506 Tg Foxp3 Tg strain are Foxp3^{+}. This contrasts with T cells from B3K506 Rag$^{-/-}$ animals, where almost all T cells are Foxp3^{-} (Tconvs) (Figure 5.1.1)

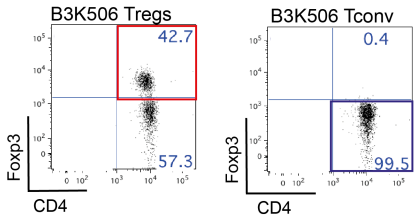

Figure 5.1.1 Foxp3 distribution

Representative flow cytometry plots of live, CD4^{+} LN T cells from B3K506 TCR Tg Foxp3 Tg Rag$^{-/-}$ (B3K506 Treg) and B3K506TCR Tg Rag$^{-/-}$ (B3K506 Tconv) mice are shown. Numbers in plots depict % of cells in the quadrant.

Compared to polyclonal B6 Tregs, monoclonal B3K506 Tregs expressed slightly reduced levels of CD25, GITR and LFA-1 and clearly decreased amounts of CTLA-4. B3K506 Tregs neither expressed Helios nor NRP-1 (Figure 5.1.2).

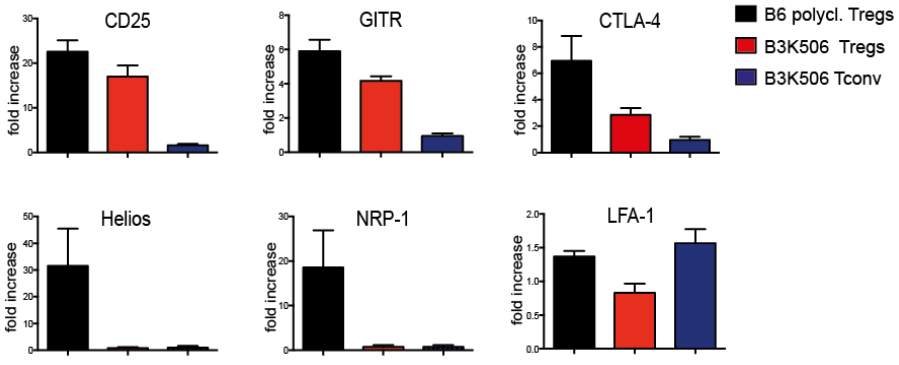

Figure 5.1.2 B3K506 Treg phenotype

Surface marker expression on monoclonal LN B3K506Tregs, polyclonal B6 Foxp3^{EGFP} Tregs and monoclonal LN B3K506 Tconvs. Expression (MFI) for each marker was normalized to that expressed on CD4^{+} B6 Tconvs. Data show fold increase +/- SD, n=4.

B3K506 Tg Foxp3 Tg mice are lymphopenic. IL-2 coupled to JES6-1 monoclonal antibody was reported to specifically enrich Tregs[91,92]. We administered injections of IL-2/JES6-1 mAb complexes (IL-2C) to B3K506 Tg Foxp3 Tg mice on three subsequent days (Figure 5.1.3 A). Total cell numbers in the lymph nodes were increased compared to PBS treatment (Figure 5.1.3 B, C). However a specific enrichment of the Foxp3$^+$ population was not observed (Figure 5.1.3 D).

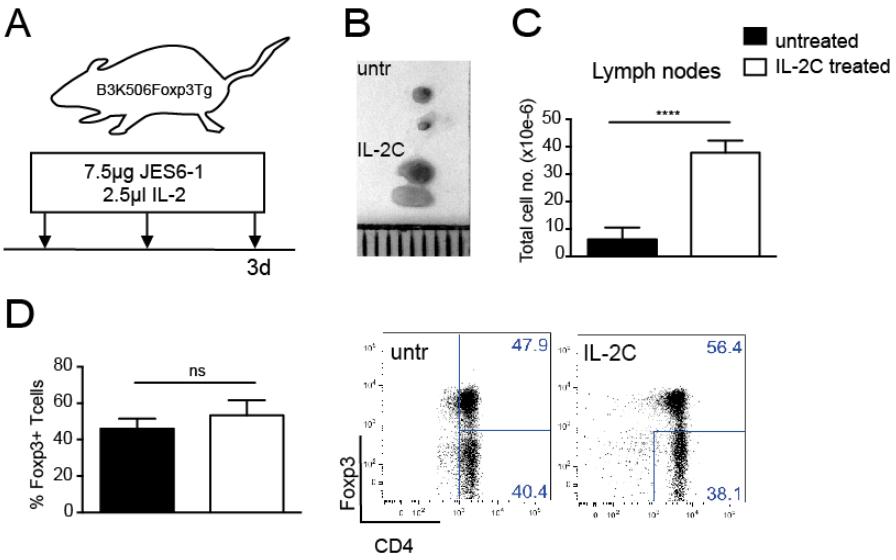

Figure 5.1.3 IL-2/JES6-1 mAb treatment

A) IL-2/mAb injection scheme. B) Inguinal lymph nodes from PBS injected or IL-2 complex injected B3K506TCR Tg, Rag$^{-/-}$ mice. C) Bar graph shows mean number +/- SEM of LN cells isolated from PBS injected (black bar) or IL-2 complex injected (white bar) B3K506TCR Tg, Rag$^{-/-}$, Foxp3 Tg mice, n=3. D) Bar graph and representative flow cytometry plots show mean % +/- SEM of Foxp3$^+$ LN T cells isolated from mice described in A, n=3. Numbers in the plots depict % of cells in gate.

Treatment with IL-2/mAb complexes might have increased the number of NK T cells in B3K506 Treg mice. By staining for NK1.1 and CD49b surface markers one can follow the enrichment of NK Tcells in IL-2/JES6-1 mAb treated B3K506 Tg Rag$^{-/-}$ mice. Comparing Il-2/JES6-1 mAb treated B3K506 Tg Rag$^{-/-}$ to PBS treated B3K506 Tg Rag$^{-/-}$ and B6 mice, there was a slight increase in total number of CD3$^+$ cells. However we did not observe an increase of CD3$^+$NK1.1$^+$ or CD3$^+$CD49b$^+$ cells (Figure 5.1.4 A).

Compared to polyclonal B6 and untreated B3K506 Tg Foxp3 Tg Rag$^{-/-}$ mice, IL-2/JES6-1 mAb treated B3K506 Tg Foxp3 Tg Rag$^{-/-}$ animals showed a significant decrease in CD122

and increase in GITR expression but no differences in CD25, CTLA-4, LFA-1, Helios and NRP-1 expression (Figure 5.1.4 B).

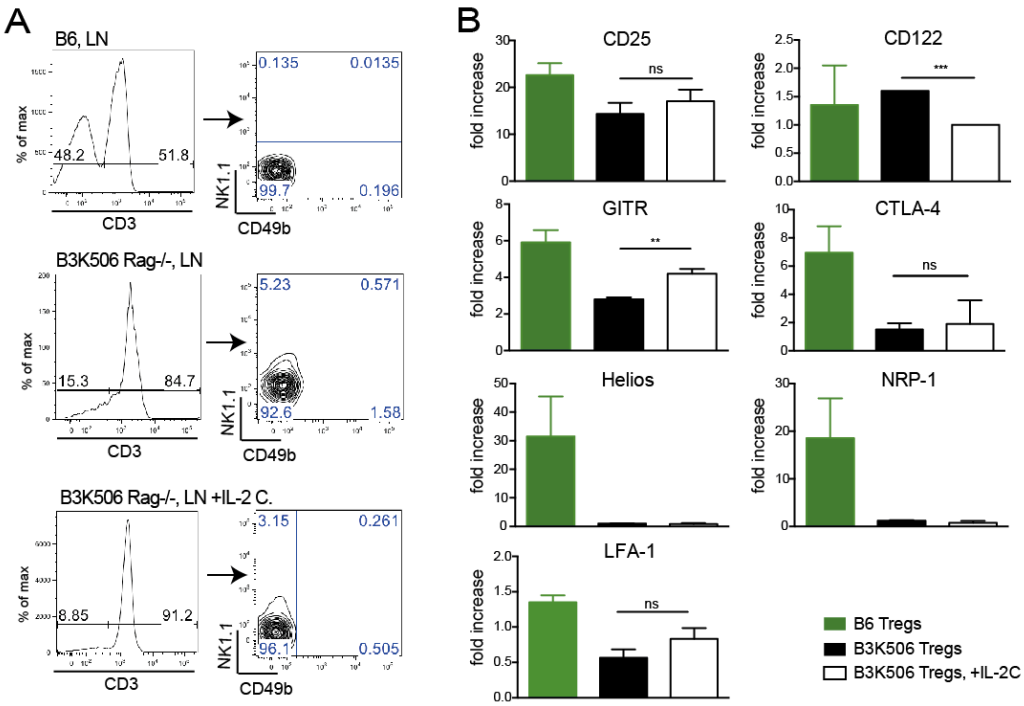

Figure 5.1.4 Effect of IL-2/mAb treatment on CD3$^+$ T cells and B3K506 Treg phenotype

A) IL-2/mAb treated B3K506 Tg Rag$^{-/-}$ compared to PBS treated B3K506 Tg Rag$^{-/-}$ and B6 mice. Histograms of IL-2/mAb treated animals show slightly increased CD3$^+$ cell numbers. Flow cytometry plots show CD3$^+$ LN cells of mice described. Number in the plots depict % of cells in the quadrant. B) Comparison of IL-2/mAb treated B3K506 Tg Foxp3 Tg Rag$^{-/-}$ mice (white bars) to PBS treated B3K506 Tg Foxp3 Tg Rag$^{-/-}$ (black bars) and B6 mice (green bars). Expression (MFI) for each marker was normalized to that expressed on CD4$^+$ B6 Tconvs, Data show mean fold increase +/- SD, n=4. Statistical significance was calculated using a two-tailed t-test. NS=p>0.05, *=p≤0.05, **=p≤0.01, ***=p≤0.001, ****=p≤0.0001

Expression of the glucocorticoid-induced TNFR-related protein (GITR) was significantly increased on IL-2/JES6-1 mAb treated B3K506 Tregs. Of this we made use to optimally sort the Foxp3$^+$ population in the B3K506 Tg Foxp3 Tg mouse. Sorting CD4$^+$ GITR^{high} cells resulted in a >95% pure monoclonal B3K506 Treg population (Figure 5.1.5). We used this approach for all experiments to reduce the amount of mice needed for one experiment.

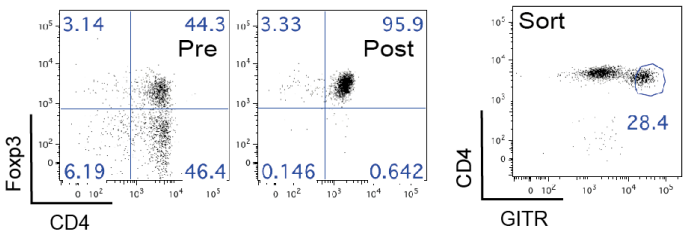

Figure 5.1.5 Sorting strategy

Representative flow cytometry plots of B3K506 Tregs pre- and post-cell sorting, which was carried out based on CD4^{high} and GITR^{high} expression. Numbers in the plots depict % of cells in gate/quadrant.

We examined the suppressive capacity of sorted monoclonal B3K506 Tregs in a conventional suppression assay using soluble anti-CD3ε antibody. No significant difference between the suppressive capacity of monoclonal B3K506 and polyclonal B6 Tregs was observed. As expected B3K506 Tconv cells are not suppressive (Figure 5.1.6).

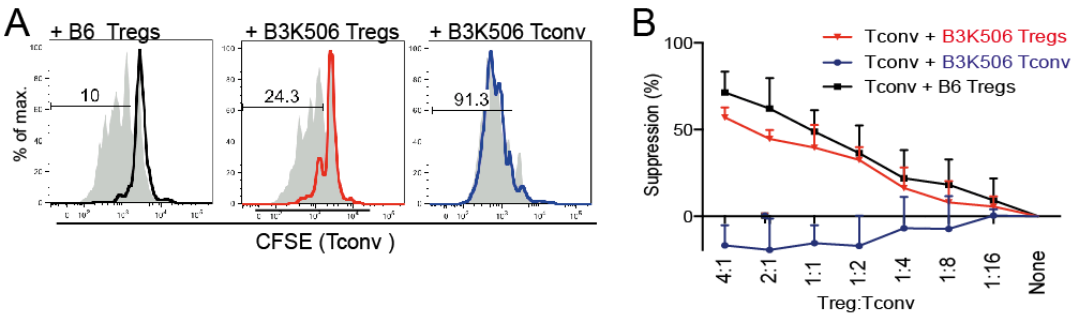

Figure 5.1.6 Conventional anti-CD3 suppression assay

A) Representative proliferation of polyclonal B6 CD4^{+} Tconvs co-cultured with polyclonal B6 Foxp3-^{EGFP} Tregs (black), monoclonal B3K506 Tregs (red) or B3K506 Tconv (blue). Grey histograms indicate proliferation of B6 CD4^{+} Tconvs cultured without Tregs. Number in histograms depict % proliferated cells. Graph shows mean % suppression +/- SD at 72h, n=5. B) In vitro anti-CD3ε suppression assays. Capacity of monoclonal B3K506 Tregs (red), polyclonal B6 Foxp3-EGFP Tregs (black) and monoclonal B3K506 Tconv (negative control; blue) to suppress proliferation of polyclonal B6 CD4^{+} T cells at varying Treg/Tconv ratios. Data show mean % suppression +/- SD, n=3. Statistical significance was calculated using a two-tailed t-test. NS=p>0.05, *=p≤0.05, **=p≤0.01, ***=p≤0.001, ****=p≤0.0001

A peptide specific suppression assay where monoclonal B3K506 Tregs and monoclonal OT-II CD4 Tconvs received specific peptide stimulation (i.e., 3K and OVA peptide, respectively) was established. Tregs needed to be stimulated via their TCR in order to be suppressive. Depriving B3K506 Tregs from their cognate peptide stimulus clearly abrogated suppression (Figure 5.1.7). From these results, we conclude that monoclonal B3K506 Tregs are functional Tregs, which require cognate peptide stimulation for effective suppression, in vitro.

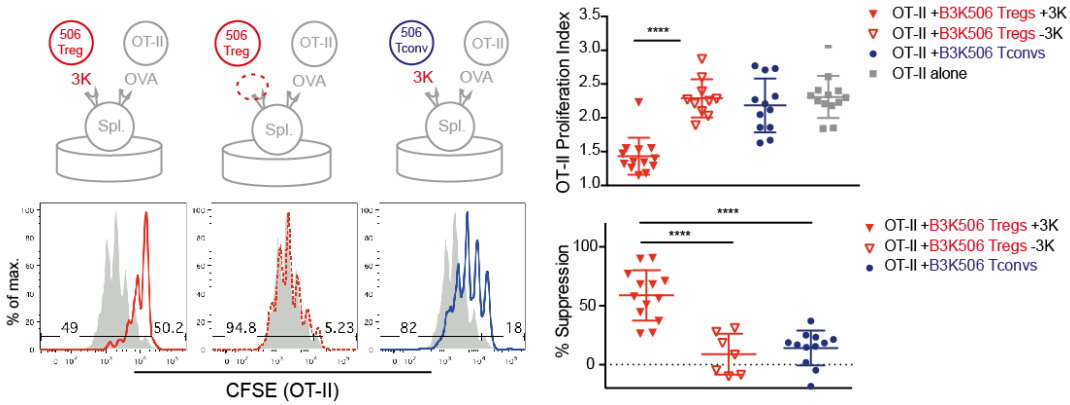

Figure 5.1.7 Peptide specific suppression assay

Monoclonal B3K506 Tregs lacking their cognate peptide antigen are not suppressive. Left: CFSE labelled OT-II Tconvs were co-cultured with B3K506 Tregs with 3K (red histogram) and without 3K (dotted red histogram) peptide or B3K506 Tconvs with 3K peptide (blue histogram). OVA peptide was added to all cultures. OT-II proliferation in the absence of Tregs is shown (grey histograms). Numbers in histograms represent % proliferated cells. Right: OT-II proliferation index and % suppression in co-cultures described in above. Monoclonal B3K506 Tregs + 3K peptide (red triangles); monoclonal B3K506 Tregs -3K peptide (empty red triangles); monoclonal B3K506 Tconv (blue circles); OT-II Tconv alone (grey squares). Data show mean proliferation index and mean % suppression +/- SD, n=7-13. Statistical significance was calculated using an one-way ANOVA and subsequently Bonferroni's multiple comparisons test. NS=p>0.05, *=p≤0.05, **=p≤0.01, ***=p≤0.001, ****=p≤0.0001

B3K506 Tregs require TCR stimulation to be suppressive in vitro. This led us to examine how TCR signalling between B3K506 Tregs and B3K506 Tconvs might differ. Peptide-MHC driven TCR signaling initiates with co-receptor bound Lck phosphorylating ITAMs within the TCR/CD3 complex. First we determined the Lck co-receptor coupling ratios of polyclonal B6 Tregs (red) and Tconvs (blue). No significant difference was detected (Figure 5.1.8 A). Comparing surface expression of CD4 and TCRVβ8 on monoclonal B3K506 Tregs (red) and B3K506 Tconvs (blue) we detected a twofold increase of CD4 co-receptor expression on B3K506 Tconvs. TCR Vβ8 were similar on both cells (Figure 5.1.8 B).

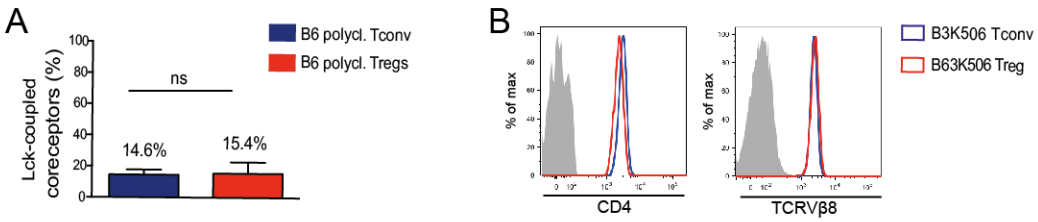

Figure 5.1.8 Lck-coupling ratios and expression levels of CD4 and TCR Vβ8

A) Bar graphs show Lck co-receptor coupling ratio of polyclonal B6 Tregs (red) and Tconv (blue). Data show mean Lck co-receptor coupling ratio (%) +/- SD, n=3. Statistical significance was calculated using a two-tailed t-test. NS=p>0.05, *=p≤0.05, **=p≤0.01, ***=p≤0.001, ****=p≤0.0001. B) Representative histograms of monoclonal B3K506 Tregs (red) and B3K Tconvs are shown. Histograms depict CD4 (left) and TCR Vβ8 (right) overlays of cells described.

Baseline levels of pERK, p4G10, pZAP-70, pCD3ζ and pcJUN in un-stimulated, resting B3K506 Tregs were examined. Expression levels were normalized to resting B3K506 Tconvs (Figure 5.1.9, A). PCD3ζ, accounting as a very proximal TCR signaling molecule, was slightly reduced. At the same time distal mediators of TCR signaling (i.e. pERK and pcJUN) showed a modest increase (Figure 5.1.9 A). Using 3K:I-A^b tetramers we performed short-term stimulation assays with monoclonal B3K506 Tregs (red) and monoclonal B3K506 Tconv (blue) comparing the total phosphorylation status (p4G10) and proximal TCR signaling (pCD3ζ) in these cells (Figure 5.1.9, B). B3K506 Tregs showed decreased levels of proximal TCR signaling (i.e. CD3ζ) and decreased levels of total cell phosphorylation (measured by p4G10, Figure 5.1.9 B).

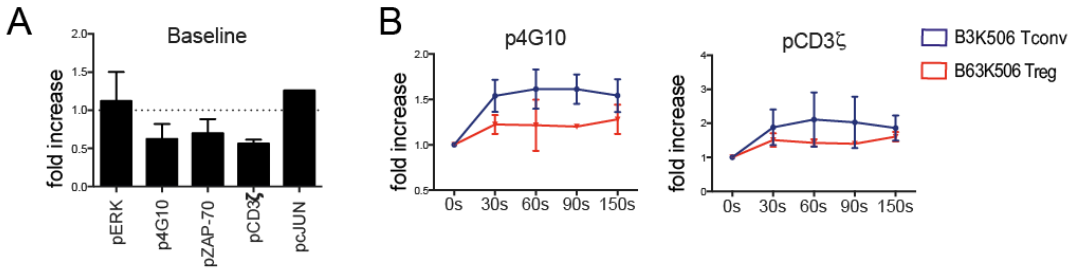

Figure 5.1.9 Signaling molecules; Treg baseline and short-term stimulation

A) Bar graph shows mean expression levels of indicated signaling molecules in resting, monoclonal B3K506 Tregs. Expression level of each signaling molecule was normalized to that of resting monoclonal B3K506 Tregs. Data show mean fold increase, +/- SD, n=3. B) Short-term stimulation (seconds) assays were performed with 3K:I-A^b tetramers. Lines depict increase of p4G10 or pCD3ζ over time (seconds) +/- SD, n=2-5. Blue line; B3K506 Tconvs, red line; B3K506 Tregs.

For longer-term stimulation assay (i.e. 60-150 minutes) we used 3K peptide pulsed splenocytes APCs (Figure 5.1.10). To increase conjugate formation APCs and Tcells were spun down. We detected a slight reduction (≈15%) in B3K506 Treg ERK phosphorylation (Figure 5.1.10, first panel, left and histograms right). However phosphorylation of c-JUN, which is critically involved in cell cycle progression, is regulated in a similar way in B3K506 Tregs and Tconvs (Figure 5.1.10, lower left panel).

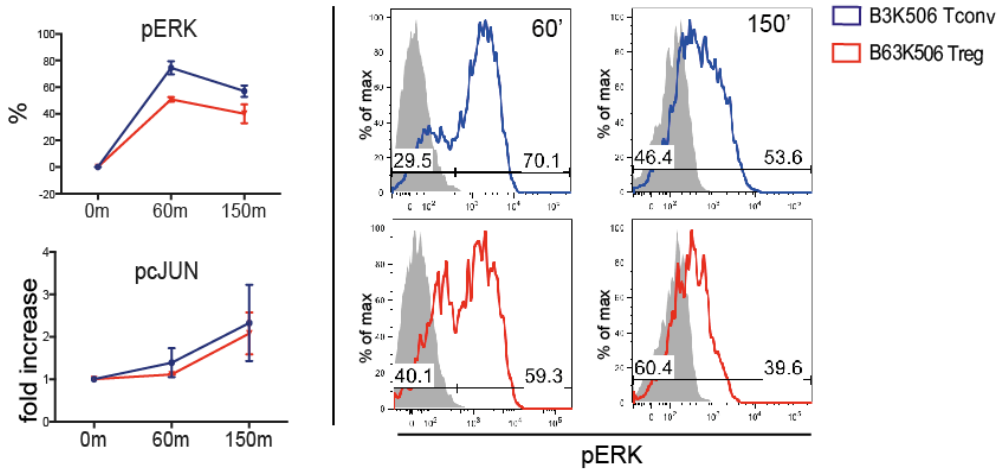

Figure 5.1.10 TCR induced pERK and pc-JUN up-regulation

Monoclonal B3K506 Tregs (red) and monoclonal B3K506 Tconvs (blue) were stimulated with 3K pulsed splenocytes for indicated time (minutes). Left: Lines in top panel show altered up-regulation of pERK in Tregs and Tconv. Data show % pERK positive cells +/-SD, n=3. Lower panel shows similar up-regulation of pc-JUN in Tregs and Tconv. Data show mean fold increase of pc-JUN over time, +/-SD n=2. Expression levels were normalized to unstimulated cells. Right: Histograms depict % positive pERK cells at 60 and 150 minutes in stimulation assay described above. Blue; B3K506 Tconvs, red; B3K506 Tregs and grey; unstimulated ctrl.

B3K506 Tregs require TCR signaling to be suppressive in vitro, however proximal TCR signaling (measured by pCD3ζ) and overall phosphorylation (measured by p4G10) of B3K506 Tregs is reduced compared to B3K506 Tconvs. Similar regulation of TCR induced c-JUN phosphorylation might indicate that the Treg's capacity to proliferate is not diminished compared to that of Tconvs.

Unfortunately we did not have the time to investigate this finding any further. To make a concluding statement, we should have preformed more experiments and examined additional signaling pathways.

Next we wondered whether B3K506 Tregs required antigen stimulation for suppressive activity in vivo. Therefore skin grafts from B6.bm12 Rag$^{-/-}$ donor mice were transplanted on to B6 Rag$^{-/-}$ mice and challenged with a combination of adoptively transferred ABM (I-Abm12 specific) Tconvs and B3K506 Tregs in the presence or absence of cognate 3K peptide (Figure 5.1.11 A, B). By administering 3K peptide until day 15, we could induce 50% graft survival lasting ≥ 75 days.

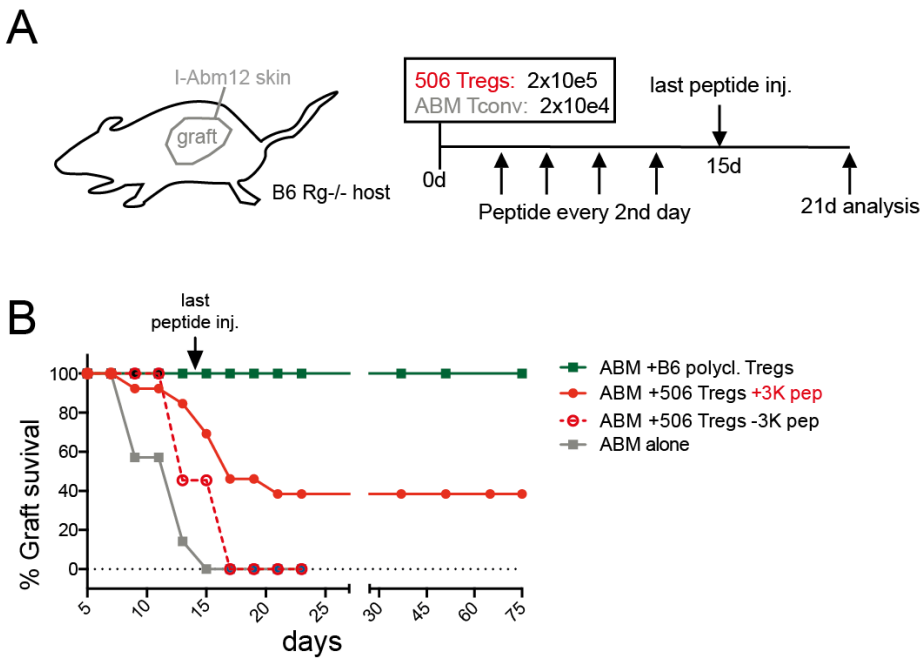

Figure 5.1.11 In vivo suppression assay

A) Experimental design of in vivo suppression assay. B) Skin from B6.bm12 Rag$^{-/-}$ donor mouse was transplanted onto B6 Rag$^{-/-}$ mice and allowed to heal for 7 days. The following day mice were injected with 2x10e4 ABM (I-Abm12 specific) Tconvs along with polyclonal B6 Foxp3^{-EGFP} Tregs (green line) or monoclonal B3K506 Tregs (solid red and dashed lines). An additional group (grey line) was injected with ABM Tconvs alone. One group (solid red line) received 3K (30 µg per mouse, IP every second day until day 15. Graph shows mean % graft survival +/- SD vs. time. Each group contains 5 to 8 mice and results are pooled from 2 individual experiments.

A few animals from both groups (receiving or not receiving 3K peptide) were sacrificed and analysed on day 21 (Figure 5.1.12 A, B). Graft acceptance correlated with extensive B3K506 Treg survival and Foxp3 expression. In mice tolerating their graft, there were >70 % B3K506 Tregs and very few ABM Tconvs remaining in the draining LN (Figure 5.1.12 A).

From these results we conclude that TCR signalling is crucial for Treg suppression both in vitro and in vivo.

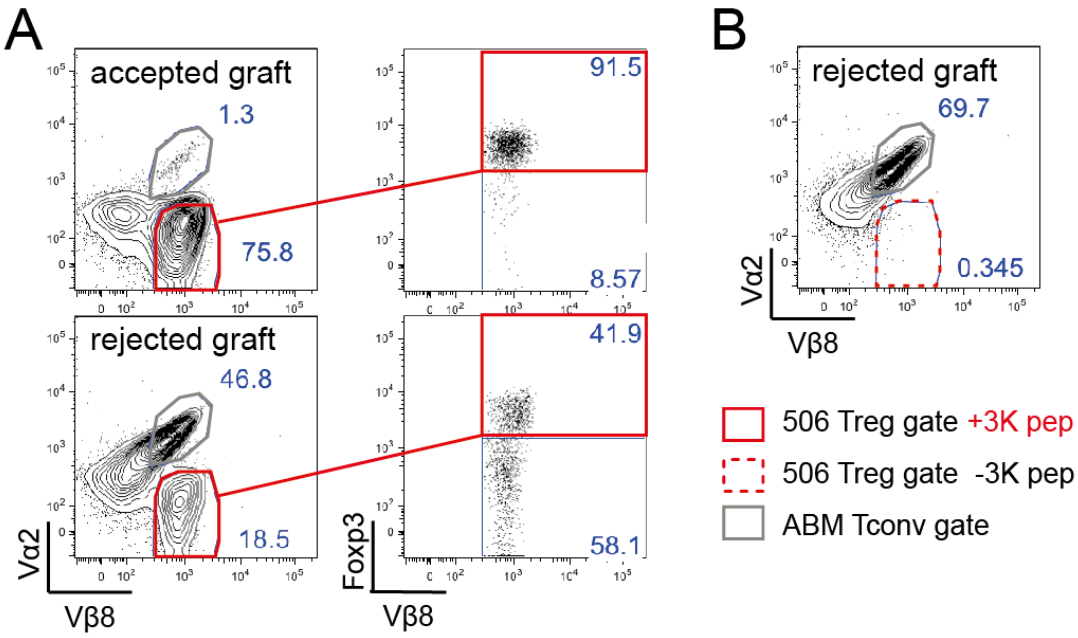

Figure 5.1.12 Draining LN's from grafted mice

A) Representative flow cytometry plots show ABM Tconvs and B3K506 Tregs from the draining LN of skin-grafted mice. Cells in upper plots are from a mouse which received 3K peptide and accepted the skin graft, while cells in the lower plots are from a mouse which rejected it's graft, despite receiving the Treg cognate peptide, 3K. Number in the plots depict % of cells in each gate/quadrant. B) Representative flow cytometry plot showing ABM Tconvs and B3K506 Tregs from the draining LN of skin-grafted mice, which did not receive 3K peptide treatment and rejected their graft. Numbers in the plot depict % of cells in each gate/quadrant.

We wondered how antigen recognition by Tregs influences the survival/expansion and functional profile of co-cultured $CD4^+$ OT-II Tconvs. Therefore live cell numbers of B3K506 Tregs and OT-II Tconvs along with the up-regulation of activation markers and cytokine concentrations in supernatants of suppressive (+3K peptide) and non-suppressive (-3K peptide) cultures were analysed over time (Figure 5.1.13 A, B).

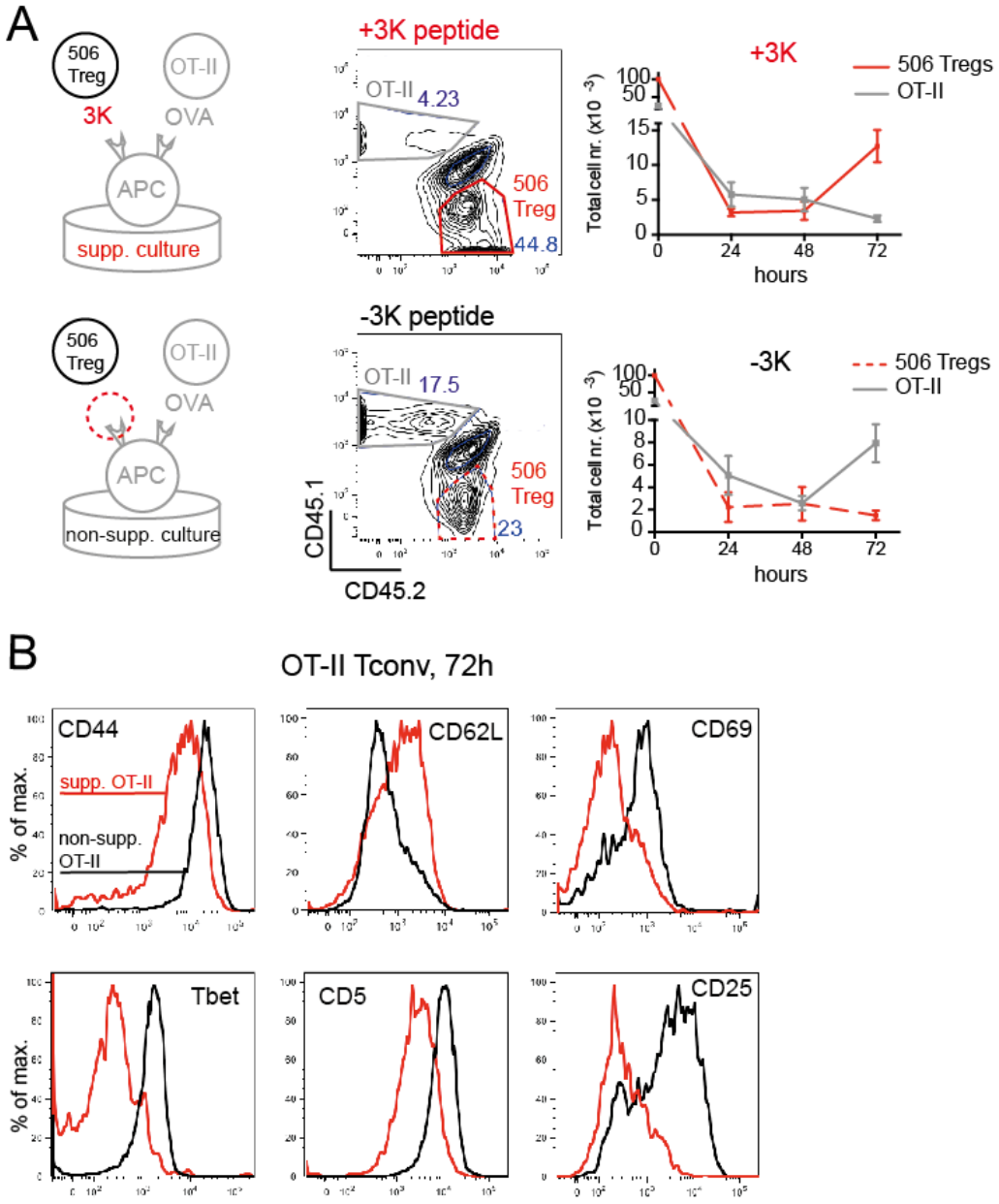

Figure 5.1.13 Functional profile of suppressed OT-II Tconvs

A) B3K506 Tregs outcompete OT-II Tconvs, in vitro. Representative flow cytometry plots show % of OT-II Tconvs and B3K506 Tregs in suppressive (with 3K peptide) and non-suppressive (without 3K peptide) co-cultures at 72h. Numbers in the plots represent % of live cells in gate. Graphs show mean numbers +/- SD of live OT-II Tconvs (grey) and B3K506 Tregs (red) from co-cultures described in A), n=3. B) Representative histograms show CD44, CD62L, CD69, Tbet, CD5 and CD25 expression on OT-II Tconvs in suppressive (with 3K peptide, red) vs. non-suppressive (without 3K peptide, black) co-cultures at 72h.

In suppressive cultures, OT-II Tconvs are not only prevented form proliferating but they also secrete reduced amounts IFNγ and IL-2 (Figure 5.1.14 A, B). This is consistent with the observation that suppressed OT-II Tconvs are less activated and express lower levels of CD25 and CD69 than do non-suppressed OT-II Tconvs (Figure 5.1.14 C, D).

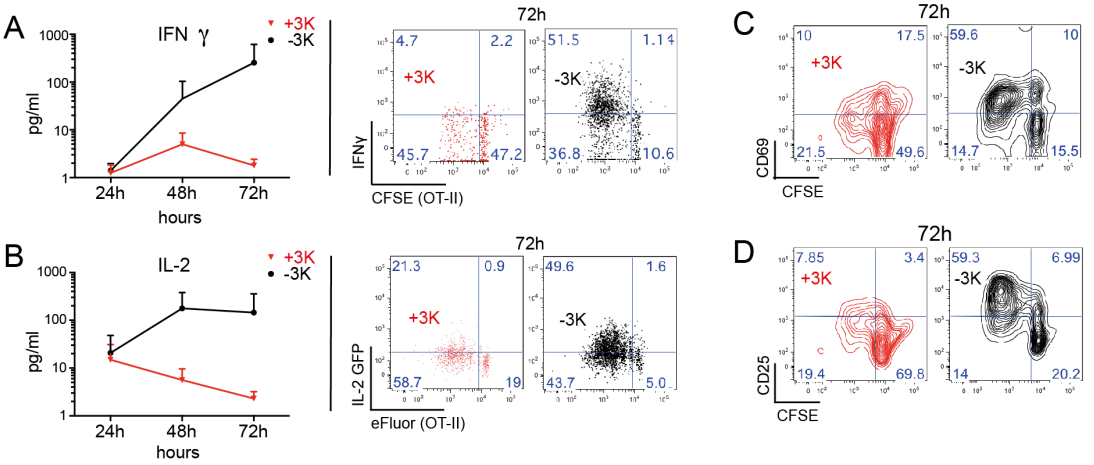

Figure 5.1.14 Cytokine production and activation status of suppressed OT-II Tconvs

A) Left: Graph depicts mean IFNγ (pg/ml) +/- SD in supernatants of suppressive (red) and non-suppressive (black) co-cultures, n=3. Right: Representative flow cytometry plots show intracellular IFNγ staining of OT-II Tconvs in suppressive (red) vs. non-suppressive (black) co-cultures. B) Left: Graph depicts mean IL-2 (pg/ml) +/- SD in supernatants of suppressive (red) and non-suppressive (black) co-cultures, n=3. Right: Representative flow cytometry plots show GFP expression from eFluor labelled OT-II IL-2-GFP reporter Tconvs in suppressive (red) vs. non-suppressive (black) co-cultures. C) Representative flow cytometry plots show CD69 expression on CFSE labelled OT-II Tconvs from suppressive (red) and non-suppressive (black) cultures at 72h, n=3-5. Numbers in the plots represent % of cells in each quadrant. D) Representative flow cytometry plots show CD25 expression on CFSE labelled OT-II Tconvs from suppressive (red) and non-suppressive (black) cultures at 72h, n=3-5. Numbers in the plots represent % of cells in each quadrant.

To further investigate the role of TCR signalling in suppression, we stimulated co-cultures with various altered peptide ligands for B3K506 Tregs at various concentrations and analysed them. All three peptides induced suppression when used at their EC50 concentration for CD69 (Figure 5.1.15).

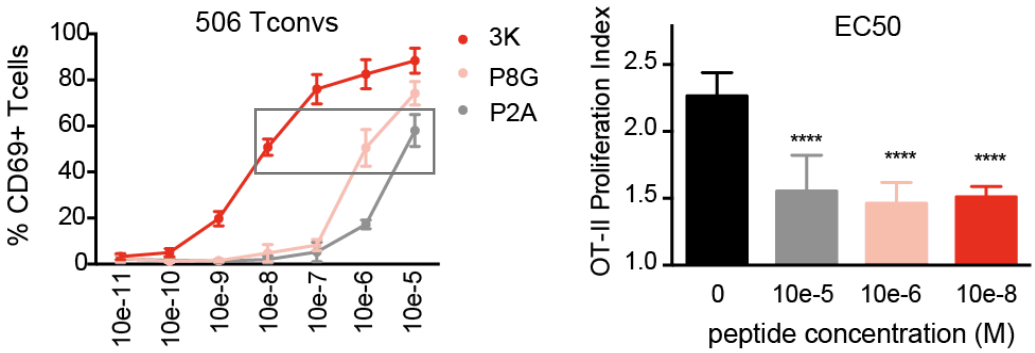

Figure 5.1.15 EC50 peptide concentrations

Left: Graph shows mean % of CD69^{+} B3K506 Tconvs +/-SEM in response to various peptide antigens used at various concentrations. Cells were cultured for 24 hours, n=3. Right: Bar graph shows mean OT-II proliferation index +/-SD from suppressive co-cultures at 72h where B3K506 Tregs were stimulated with various altered peptide ligands at their EC50 concentration, n=8.

In cultures stimulated with various altered peptide ligands at various concentrations, live, CD4^{high}, Foxp3^{high} B3K506 Tregs were assessed for frequency, absolute cell numbers (Figure 5.1.16 A), CD25 expression (Figure 5.1.16 B) and suppressive capacity (Figure 5.1.16 C). Independent of concentration, stimulation with the high affinity ligand 3K resulted in high numbers of surviving/expanding B3K506 Tregs and induction of significant OT-II Tconv suppression. However, the intermediate affinity ligand, P8G only led to Treg survival and significant suppression when added at a high concentration (Figure 5.1.16 A, C). B3K506 Treg survival decreased even more when stimulated with the threshold affinity ligand, P2A (Figure 5.1.16 A). However, significant suppression could still be achieved in co-cultures with high P2A peptide concentrations (Figure 5.1.16 C).

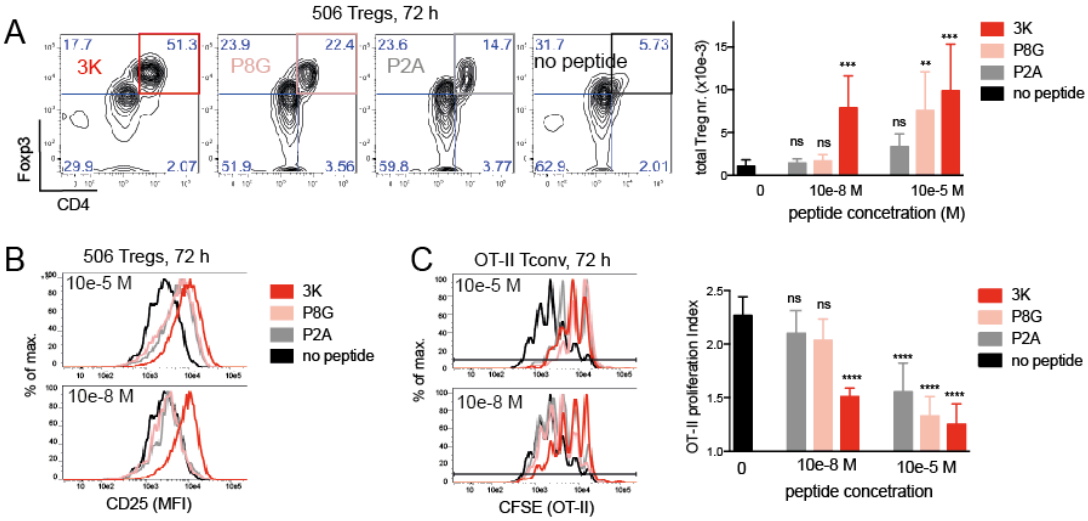

Figure 5.1.16 Suppression assays using altered peptide ligands for B3K506 Tregs

A) Representative flow cytometry plots show live B3K506 Tregs from suppressive co-cultures at 72h stimulated with various B3K506 altered peptide ligands used at 10e-5 peptide concentration. Numbers in the plots depict % of cells in each quadrant. Bar graph shows mean number of live B3K506 Tregs +/-SD from these cultures at 72h, n=5. B) Representative histograms show CD25 expression (MFI) on $CD4^{high}$ $Foxp3^{high}$ B3K506 Tregs from suppressive co-cultures stimulated with various altered peptide ligands or no peptide at 72h. C) Representative histograms depict proliferation of CFSE labelled live OT-II Tconvs form suppressive co-cultures described in A). Bar graph shows OT-II mean proliferation index +/-SD at 72h, n=4-8. A,C) Statistical significance was calculated using an one-way ANOVA and subsequently Bonferroni's multiple comparisons test. Ns=p>0.05, *=p≤0.05, **=p≤0.01, ***=p≤0.001, ****=p≤0.0001

To further deconstruct the role of TCR signalling in Treg suppression, we plotted the suppressive capacity of B3K506 Tregs against surviving B3K506 Treg numbers (Figure 5.1.17 C) or B3K506 Treg CD25 expression (Figure 5.1.17 D). Suppression clearly correlated with pMHC affinity and concentration (Figure 5.1.17 A, B), surviving Treg numbers and the amount of CD25 expression on surviving Tregs. High Treg cell numbers can compensate for low CD25 expression (3K 10e-7M, compare red triangle in C and D) and vice versa (3K 10e-5 compare red circle in C and 3D). There is a clear threshold below which low Treg cell numbers and CD25 expression fail to induce suppression.

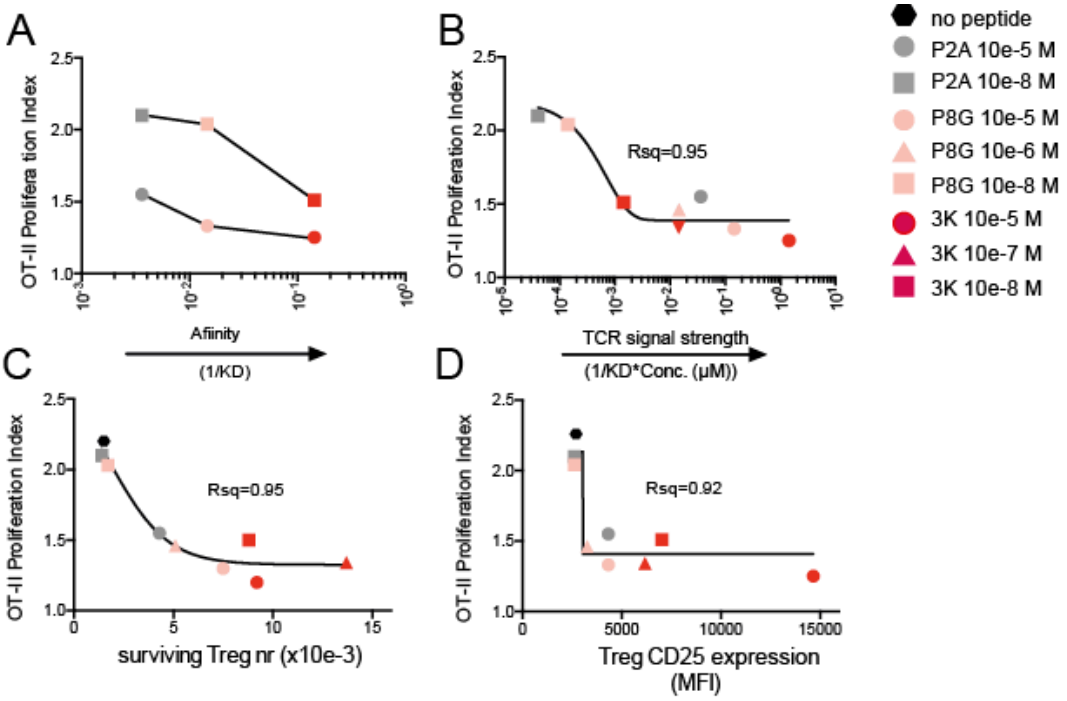

Figure 5.1.17 Suppression correlates with Treg cell number, CD25 expression and peptide affinity

A) Curve shows correlation between peptide-MHC affinity (1/KD) for the B3K506 TCR and OT-II proliferation index from suppressive co-cultures described in Figure 5.1.16. APCs were pulsed with 10e-8M peptides (squares) or 10e-5M peptides (circles). B) Curve shows correlation between B3K506 TCR stimulus strength (defined as pMHC affinity [1/KD x peptide conc. (µM)] and OT-II proliferation index from suppressive co-cultures described in Figure 5.1.16. Curve is a nonlinear fit with variable slope (4 parameters). C) Correlation between OT-II proliferation index and number of surviving Tregs from suppressive co-cultures described in Figure 5.1.16. Curve is a nonlinear fit with variable slope (4 parameters). D) Correlation between OT-II proliferation index and CD25 levels on surviving Tregs from suppressive co-cultures described in Figure 5.1.16. Curve is a nonlinear fit with variable slope (4 parameters).

From these results we conclude that Treg TCR stimulation strength drives suppression through maintenance and induction of Treg cell survival/expansion and CD25 expression.
With extent to the fact that suppression correlates with the numbers of Tregs, we further aimed to understand suppression on a cellular, mechanistic level. By stimulating OT-II Tconvs with peptide loaded APCs in the presence of culture supernatants form antigen stimulated B3K506 Treg cultures, no evidence for a soluble suppressive molecule was observed (Figure 5.1.18)

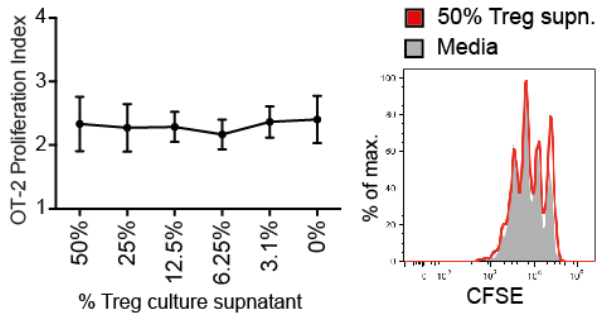

Figure 5.1.18 B3K 506 Treg culture supernatant

Supernatants from stimulated Treg cultures are not suppressive. Graph depicts mean proliferation index +/- SEM of OT-II T convs cultured in various concentrations of supernatant from stimulated B3K506 Treg cultures, n=3. Representative histograms depict proliferation of OT-II Tconvs cultured in media containing 50% Treg supernatant (red) or in media alone (grey).

In suppressive (with 3K peptide) and non-suppressive (without 3K peptide) co-cultures, expression of CD86 on splenic B cell APCs and surviving splenic B cell numbers was similar (Figure 5.1.19). This argues that a Treg-induced decrease of CD86 on APCs (i.e. trans endocytosis) or a Treg-mediated killing of APCs was not obviously required for suppression in our cultures.

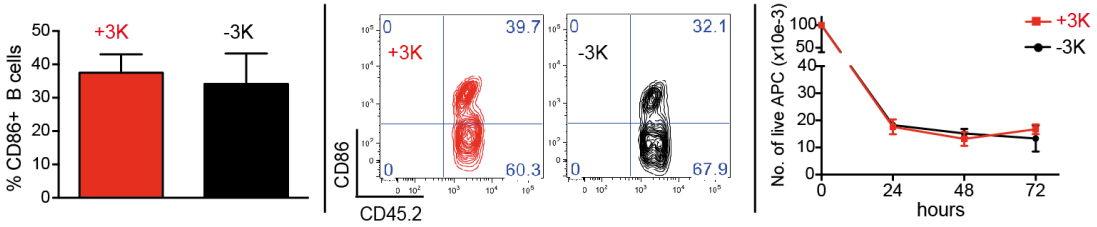

Figure 5.1.19 Tregs do not affect CD86 expression on APCs or APC cell numbers

Left: Bar graph depicts % of $CD86^+$ splenic B cell APCs from suppressive (with 3K peptide, red) and non-suppressive (without 3K peptide, black) co-cultures. Middle: Representative flow cytometry plots show CD86 expression on live, $CD19^+CD4^-$ splenic B cell APCs at 72h from these cultures. Numbers in the plots depict % of cells in each quadrant. Right: Graph shows mean number of live splenic B cell APCs +/- SD vs. time in suppressive vs. non-suppressive co-cultures, n=3.

Even though B3K506 Tregs from suppressive co-cultures expressed surface latency associated peptide of TGFβ (LAP) (Figure 5.1.20 A) we didn't observe conversion of OT-II Tconvs into iTregs (Figure 5.1.20 B). This mechanism of suppression is not evident in our experimental system.

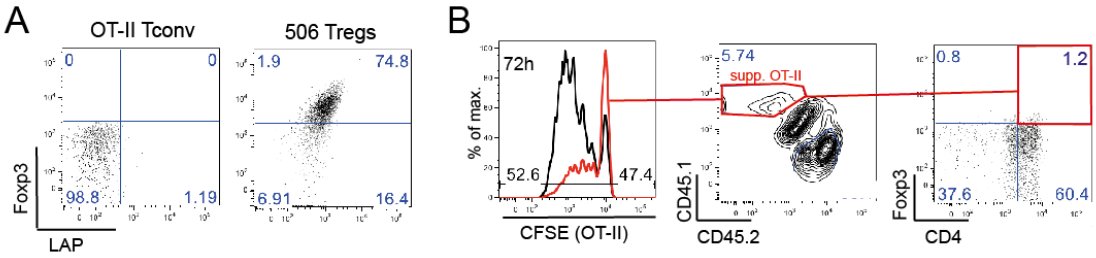

Figure 5.1.20 B3K506 Tregs do not convert OT-II Tconvs into iTregs

A) Representative flow cytometry plots show Foxp3 and LAP expression on OT-II Tconvs and B3K506 Tregs from suppressive cultures at 72 hours. Numbers in the plots represent % of cells in each gate. B) B3K506 Tregs do not convert OT-II Tconvs into induced Tregs (iTregs). Representative flow cytometry plots show Foxp3 and CD4 expression on OT-IIs from suppressive co-cultures at 72h. Numbers in the plots depict % of cells in each quadrant or gate.

Finally we wondered if Tregs and Tconvs needed to encounter their cognate peptide on the same APC for effective suppression to occur. To avoid cross-presentation, we used $I\text{-}E^d$ restricted HA transgenic Tconvs. In this system, peptide cross presentation and alloreactions

did not occur (Figure 5.1.21 B). We co-cultured I-A^b restricted B3K506 Tregs and I-E^d restricted HA Tconvs on the same APCs (i.e. F1, B6xBalb/c splenic B cells with 3K and HA peptides) or on separate APCs (i.e. B6 splenic B cells loaded with 3K peptide only and BALB/c splenic B cells loaded with HA peptide only). The results show that suppression is more complete when both antigens are presented on the same APC (Figure 5.1.21 A)

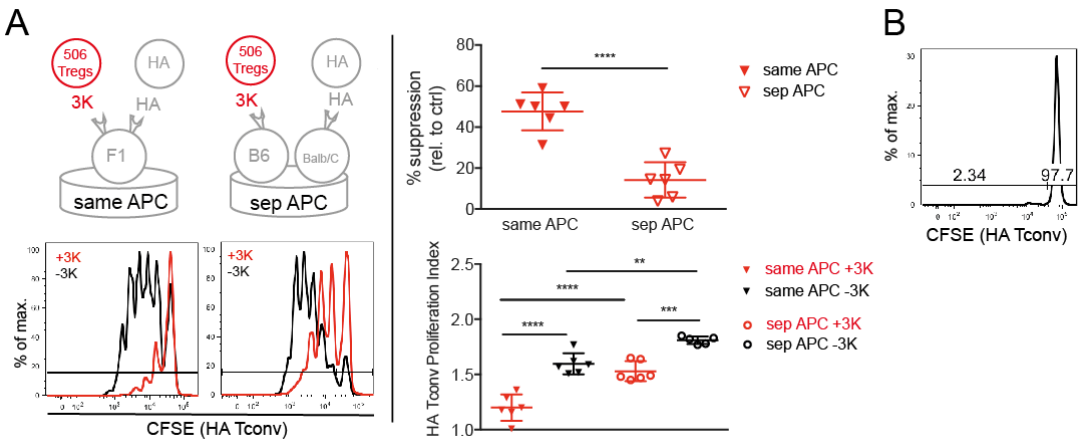

Figure 5.1.21 Peptide encounter on same vs. separate APCs

A) Suppression is enhanced when Treg and Tconv antigens are presented on the same APC. Left: Representative histograms show proliferation of CFSE labelled HA Tconv co-cultured with B3K506 Tregs. HA Tconvs and 506 Tregs encounter their cognate ligand either on the same (left) or on separate (right) splenic B cell APCs (see diagram). Both conditions were compared to non-suppressive cultures where 3K peptide was omitted (black). Right: Graph shows mean % suppression and proliferation index +/-SD of HA-Tconvs co-cultured in the different conditions described above, n=4-5. B) Representative histogram shows CFSE-labelled HA Tconv on an I-E^d background in culture with B6 splenic B cells on an I-A^b background after 72 hours. Gated on live, CD45.1$^+$CD4$^+$ cells (HA-Tconvs).

However, antigens presented on separate APCs were able to support some degree of suppression, as up regulation of CD25 on HA Tconvs was suppressed in these separate APC co-cultures (Figure 5.1.22).

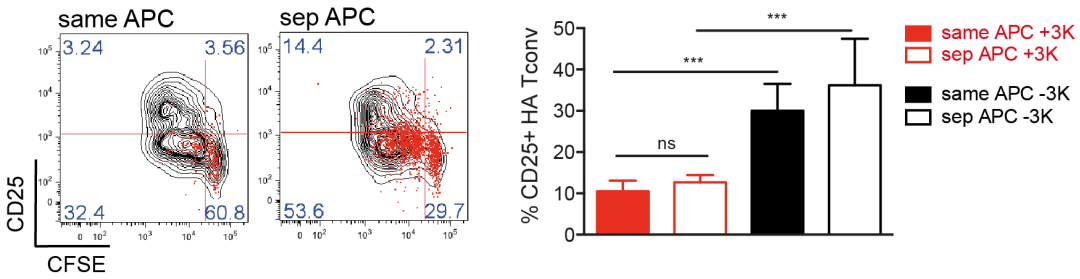

Figure 5.1.22 Suppression of CD25 on HA-Tconvs

Representative flow cytometry plots show CD25 expression on live HA Tconvs in cultures described in 4.1.21. Numbers in the plots represent % of cells in each quadrant. Bar graph depicts mean % $CD25^+$ HA-Tconvs +/-SD in these cultures at 72h, n=4.

Manuscript submitted at *Scientific Reports*

Monoclonal regulatory T cells provide insights into T cell suppression

Gubser, C. Schmaler, M. Rossi, S. W. Palmer, E.

5.2 Part B

To quantify the amount of Lck coupled to CD8 or CD4 coreceptors we made use of a method where multiprotein complexes are analyzed via immunoprecipitation and quantitative flow cytometry (IP-FCM[162] Figure 5.2.1).

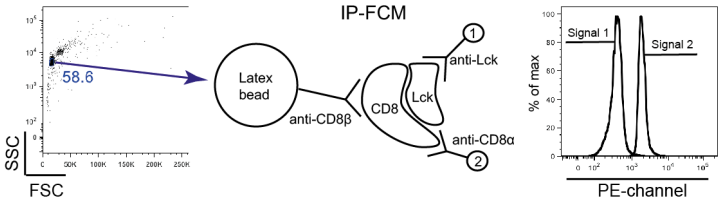

Figure 5.2.1 IP-FCM principle

Scheme of immunoprecipitation and quantitative flow cytometry

Sorting TCRβ low B6 thymocytes resulted in a 96.3 % pure population of DP thymocytes (Figure 5.2.3 A). In this sorted population, 0.6% of CD8 co-receptor were coupled to Lck where as 6.7% of CD4 co-receptors carried Lck (Figure 5.2.3 C: black bars and A: black/grey histograms) To further investigate this difference between CD8 and CD4 co-receptor-Lck coupling ratios, OT-1 TCR transgenic mice were bred to a CD8.4 co-receptor chimera knock-in strain. In this mouse, thymocytes express a co-receptor consisting of the extracellular CD8α chain and the intracellular CD4 tail carrying Lck (Figure 5.2.2).

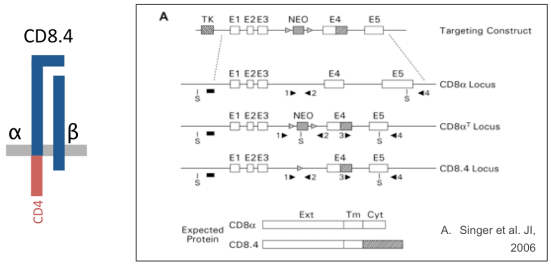

Figure 5.2.2 Chimeric CD8.4 receptor

A. Singer et al. JI, 2006

In DP thymocytes from OT-1 CD8.4 mice, 6% of CD8.4 molecules were loaded with Lck compared to 1.1% in OT-1 WT mice (Figure 5.2.3 C compare light blue and dark blue bars and Figure 5.2.3 B compare light blue and dark blue histograms).

Interestingly, CD4 co-receptors in CD8.4 mice carried less Lck than CD4 co-receptors from OT-1 WT mice (Figure 5.2.3 C compare light blue bars and dark blue bars). These

differences were also apparent in co-immunoprecipitations of CD8 and CD4 co-receptors in DP thymocytes from these mice (Figure 5.2.3 D).

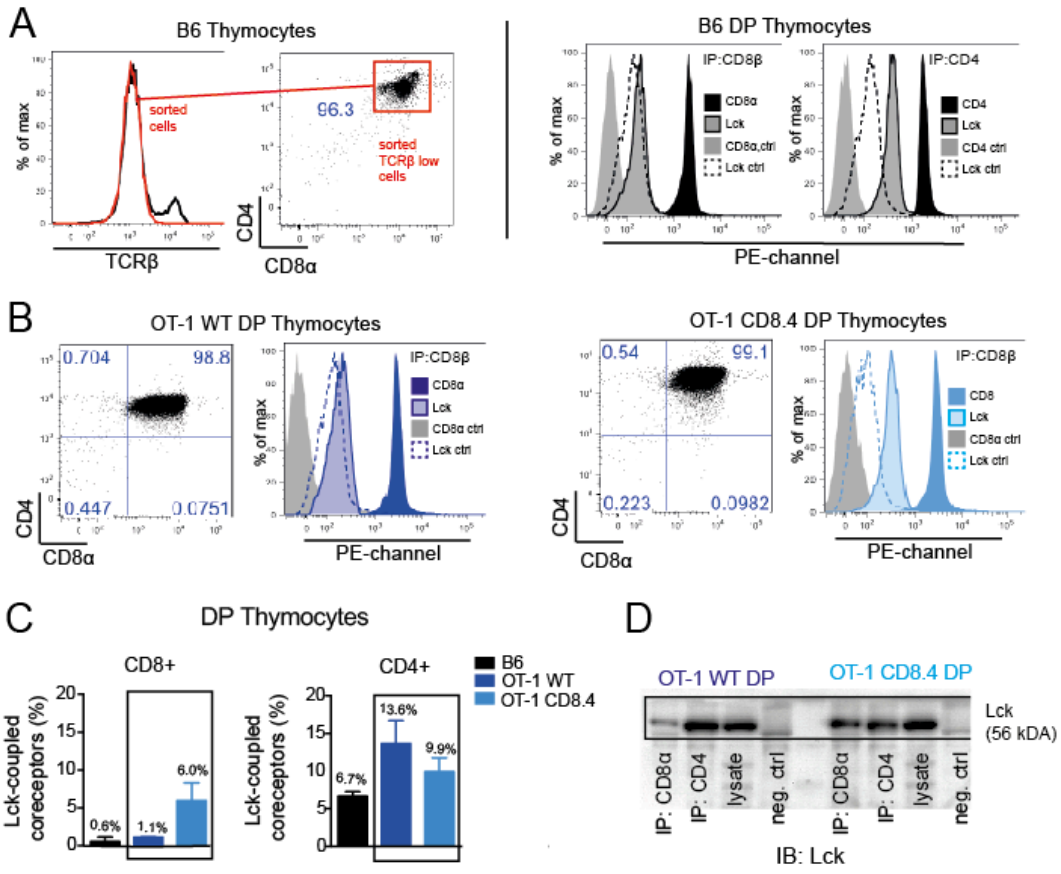

Figure 5.2.3 Co-receptor Lck coupling ratios in WT and CD8.4 OT-I DP thymocytes compared to B6 DP thymocytes

A) Left: representative histogram and flow cytometry blot show TCRβ high (SP) and low (DP) thymocytes from B6 mice. TCRβ low cells were sorted to exclude contamination with single positive thymocytes. Number in the plot depicts % of cells in the gate. Right: Cell lysates were incubated with beads coated with antibodies to CD4, CD8β or isotype controls. Beads were probed with PE-conjugated antibodies to Lck, CD8α or CD4 and analyzed by flow cytometry. Histograms show PE-signal intensity of immunoprecipitated proteins from sorted TCRβ low B6 thymocytes. B) Thymocytes from OT-I WT (dark blue) and OT-I CD8.4 (light blue) were analyzed. Histograms show PE-signal intensity of immunoprecipitated proteins. Number in the plots depict % of cells in each gate. C) Bar graph show mean % Lck co-receptor coupling rations, +/- SD of DP thymocytes from B6 (black), OT-1 WT (dark blue) and OT-I CD8.4 (light blue) mice, n=3-5. D) Thymocyte lysates were immunoprecipitated with protein G beads coated with antibodies to CD4, CD8α or isotype controls and analyzed by western blotting. Membrane was probed with anti-Lck antibody, n=2.

We examined if there was a competition for Lck between the intracellular CD4 tail of the CD8.4 chimeric co-receptor and the wild type CD4 co-receptor. Therefore MHC class II restricted B3K508 TCR transgenic mice were bred to the CD8.4 co-receptor chimera knock-in strain. While CD8.4 co-receptors from these mice had increased Lck coupling ratios, they also showed increased CD4 co-receptor Lck coupling ratios (16.4% vs. 9.9%, Figure 5.2.4). This argued against a competition for Lck between the intracellular CD4 WT tail and the CD8.4 chimeric co-receptor tail.

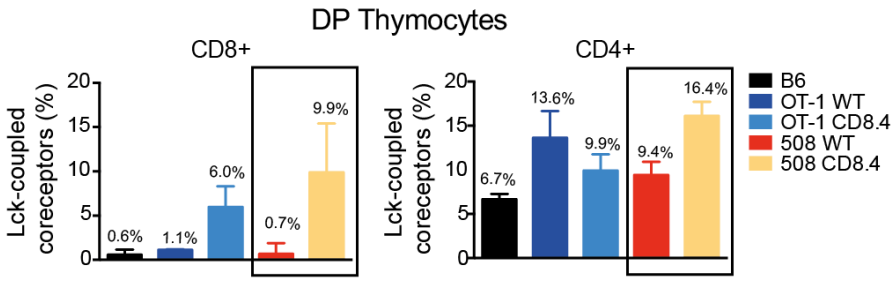

Figure 5.2.4 Co-receptor coupling rations in MHC class II restricted B3K508 WT and B3K508 CD8.4 mice

Cell lysates were incubated with beads coated with antibodies to CD4, CD8β or isotype controls. Beads were probed with PE-conjugated antibodies to Lck, CD8α or CD4 and analyzed by flow cytometry. Bar graph show mean % Lck co-receptor coupling rations, +/- SD of DP thymocytes from B3K508 WT (red) and B3K508 CD8.4 (yellow) mice compared to B6 (black), OT-1 WT (dark blue) and OT-I CD8.4 (light blue) mice, n=3-5

Next we wondered if mature, single positive T cells showed increased CD8 and CD4 co-receptor Lck coupling ratios compared to immature DP thymocytes (Figure 5.2.5). No significant difference was seen comparing CD4-coupled Lck ratios from peripheral T cells and CD4 Lck coupling ratios from DP thymocytes (Figure 5.2.5 and Figure 5.2.4, compare black and red bars). However there was a difference in CD8 coupled Lck ratios; while co-receptors from peripheral B6 $CD8^+$ T cells carried 9.5% of Lck, only 0.6% of CD8 coreceptors in DP thymocytes form these mice carried Lck (Figure 5.2.5 and Figure 5.2.4, compare black bars). The same was true in the OT-1 WT strain: 8.9% of CD8 co-receptors from peripheral $CD8^+$ T cells were coupled to Lck, but only 1.1% of CD8 co-receptors in DP thymocytes were coupled to Lck (Figure 5.2.4 and Figure 5.2.4, compare blue bars). A possible explanation for this finding might be the sialyation of the CD8β co-receptor chain following positive selection in the thymus[7]. To compensate for decreased binding capacity of

the sialylated CD8β chain to peptide–MHC complexes, peripheral CD8 co-receptor Lck coupling ratios might therefore be increased,.

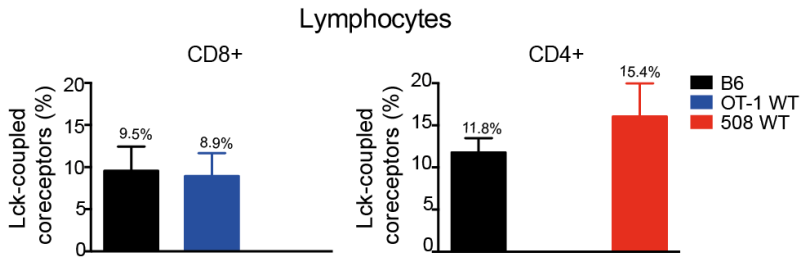

Figure 5.2.5 Co-receptor Lck coupling ratios in mature peripheral T cells

Bar graph show mean % Lck co-receptor coupling rations, +/- SD of mature T lymphocytes from B6 (black bars) OT-I WT (blue) and B3K508 WT (red) mice, n=4-5

Finally, to calculate the exact Lck molecule numbers, we determined the absolute amount of TCR, CD4 and CD8 surface molecules on DP thymocytes of B6, OT-1 WT and OT-1 CD8.4 mice. By generating a standard curve based on the fluorescence signal of calibration beads, the mean fluorescence intensity of surface staining, i.e. CD3ε, CD4 and CD8, could be transformed into absolute numbers of surface molecules (Figure 5.2.6).

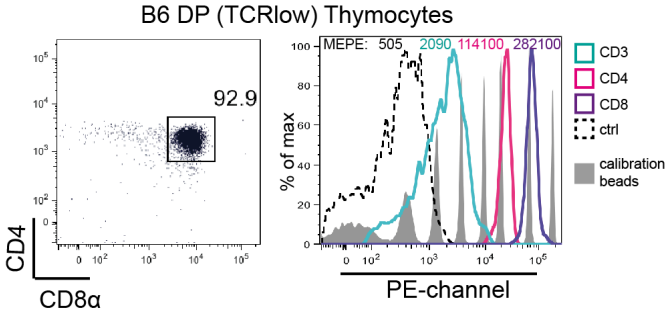

Figure 5.2.6 Mean equivalent soluble PE molecules (MEPE) for B6 DP thymocytes

DP TCRβ low B6 thymocytes were stained with saturating concentrations of PE-conjugated antibodies to CD4, CD8α or CD3 and analyzed by flow cytometry together with PE calibration beads. Florescence signals from stained thymocytes and calibration beads (grey histograms) are shown (i.e. CD4 (pink), CD8α (purple), CD3 (turquoise) and negative B cell control (dotted black)). Left: number in the plot depict % of cells in the gate. Right: number of mean equivalent soluble PE molecules (MEPE) is shown for each peak.

We counted approximately 2500 TCR molecules on the surface of a DP B6 thymocyte (Figure 5.2.7 A). The same cell expressed approximately 1.15x10e5 CD4 and 2.8x10e5 CD8 co-receptors (Figure 5.2.7 B, C). A 50 to 100-fold increase of TCR expression was observed on peripheral T lymphocytes compared to DP thymocytes, indicating that TCR expression increased after successful thymic selection (Figure 5.2.7 A).

Compared to DP thymocytes, there is a twofold increase of CD4 co-receptors expressed by peripheral $CD4^+$ T cells (Figure 5.2.7 B). However no such increase was seen in the expression levels of CD8 co-receptors. DP and SP thymocytes from B6, OT-1 WT and OT-1 CD8.4 mice expressed similar levels of CD8 co-receptors and no significant increase was seen in $CD8^+$ peripheral T cells (Figure 5.2.7 C).

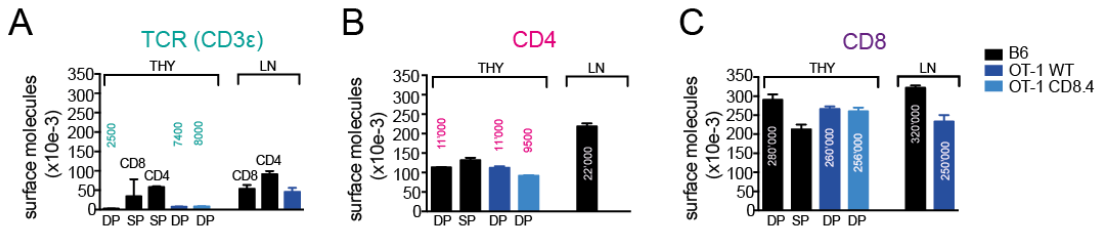

Figure 5.2.7 Surface molecules

A) Bar graph show mean number of CD3 surface molecules on DP, SP thymocytes (left) and T lymphocytes (right). Cells from B6 (black), OT-1 WT (dark blue) and OT-1 CD8.4 (light blue) were analyzed. B) Bar graph show mean number of CD4 surface molecules on DP, SP thymocytes (left) and T lymphocytes (right). Cells from B6 (black), OT-1 WT (dark blue) and OT-1 CD8.4 (light blue) were analyzed. C) Bar graph show mean number of CD8α surface molecules on DP, SP thymocytes (left) and T lymphocytes (right). Cells from B6 (black), OT-1 WT (dark blue) and OT-1 CD8.4 (light blue) were analyzed. Data show mean numbers +/- SEM, n=3-6.

Taken together, we show that in DP thymocytes, CD4 co-receptors carry more Lck than CD8 co-receptors. In a system where MHC class I restricted thymocytes express a chimeric CD8.4 co-receptor, Lck coupling ratios are increased. In addition, DP thymocytes express more CD8 than CD4 surface co-receptors. These data add to the idea that the affinity threshold for MHC class I and II restricted thymocytes depend on the probability of a peptide-MHC-TCR complex colliding with a co-receptor coupled to Lck to during the time pMHC occupies the TCR. We therefor believe co-receptor Lck coupling ratios have an important role in setting the affinity threshold for negative selection.

6 Discussion

6.1 Studies of suppression using monoclonal regulatory T cells

In the first part of the thesis we examined the role of various Treg suppressive mechanisms using a source of monoclonal TCR and Foxp3 transgenic Tregs (i.e. B3K506 Tregs). Here we show that monoclonal B3K506 Tregs are functional in vitro and in vivo and clearly require cognate peptide stimulation through their TCR to be suppressive. Our data show that the strength of Treg TCR stimulation correlates with the extent of Treg mediated suppression. Increasing the affinity and/or concentration of Treg antigen drives Treg proliferation and CD25 expression, which is likely related to the extent of suppression in the system.

B3K506 (monoclonal) Tregs differed from polyclonal, thymus derived Tregs observed in B6 mice in that B3K506 monoclonal Tregs express neither Helios nor NRP-1. Thymic Tregs in polyclonal mice are normally generated through antigen selection[28,29]; they likely acquire Helios and NRP1 expression following a high affinity encounter with self-antigen[31]. In contrast, thymocytes bearing the B3K506 TCR are normally positively selected but are directed into the Treg lineage due to the presence of the Foxp3 transgene. Since B3K506 monoclonal Tregs did not encounter a high affinity self-antigen during their development, they are Helios- and NRP1- negative[32].

B3K506TCR Tg Foxp3 Tg mice are lymphopenic and only 40-50 % of CD4 T cells are $Foxp3^+$. To increase Treg numbers, we injected mice with Il-2 complexed to the monoclonal antibody JES6-1[164]. Although $CD4^+$ T cells expanded in treated mice the proportion of $CD4^+Foxp3^+$ cells did not alter. Treatment with IL-2/mAb complexes did not increase the number of NK Tcells in these mice. Sorting a $CD4^+GITR^{high}$ population from the B3K506 Foxp3 Tg mouse, resulted in >96% pure monoclonal Treg population. Previous work describing the ablation of Treg suppression after application of anti-GITR antibodies was not observed in our system, as GITR sorted Tregs were suppressive in vitro and in vivo[165].

B3K506 Tregs are suppressive in vitro upon cognate antigen encounter. This led us to examine how TCR signalling between B3K506 Tregs and B3K506 Tconvs might differ. Proximal TCR signalling (measured by pCD3ζ and pZap-70) seems to be reduced in Tregs. Previous work, stating that Tregs maintain a hypo-responsive state by suppressing the induction of TCR initiated signals support these findings[99,100]. However, we measured a similar increase of pc-JUN levels in pMHC stimulated B3K506 Tregs and B3KTconvs over time (0-150 minutes). C-JUN is critically involved in the cycle progression process of a T cell, indicating that the Treg's capacity to proliferate upon TCR signalling is not diminished.

Recent data using a model where the TCR can be depleted in peripheral Tregs, show that continuous expression and signalling of the TRC is required for effective suppression to occur[106]. This supports our observation that monoclonal B3K506 Tregs clearly require cognate peptide stimulation through their TCR in order to be suppressive.

Using a skin-graft-transplantation model we observed that B3K506 monoclonal Tregs receiving cognate peptide 3K, are less suppressive than polyclonal Tregs (50% vs. 100% graft survival). This might be explained by a short half-life of 3K peptide in vivo, leading to suboptimal priming in the host. However, recipient mice that had accepted their skin graft achieved stable (75d) tolerance and did not require peptide administration past day 15.

In the presence of cognate antigen B3K506 Tregs expanded between 48 and 72h. This contradicts previous work describing a requirement for Treg anergy to achieve effective suppression[108]. There is data showing that Tconv proliferation is limited in suppressed cultures and cytokine production (IFNγ and IL-2) is inhibited at a level of RNA transcription[109]. Similar to what is reported, we observed decreased IFNγ and IL-2 cytokine levels in culture supernatants from suppressive co-cultures. Although suppressed OT-II Tconv produced very little IFNγ (as measured by intracellular staining) using an IL-2^{EGFP} reporter, suppression of measured IL-2 production was incomplete.

To investigate the role of TCR signal strength in B3K506 Treg suppression we used three altered peptide ligands (i.e. 3K, P8G, P2A). Although they display an affinity hierarchy for the B3K506 TCR (3K>P8G>P2A) all three peptides are above the affinity threshold for negative selection[9]. All three peptides induced suppression when used at their EC50 concentration for CD69. However, low affinity peptides were more suppressive when used at increased concentrations. Peptide concentration could compensate decreased affinity to some extent. Overall suppressive capacity correlates with pMHC affinity, peptide concentration, TCR signal strength, B3K506 Treg proliferation and CD25 expression.

In accordance with published data[166], we did not detect a soluble suppressive molecule in culture supernatants from antigen stimulated B3K506 Tregs. However suppressive cytokines like IL-10, IL-35 and TGFβ or tryptophan metabolites, granzymes A or B and adenosine may be too diluted or unstable to be suppressive in a relatively large culture volume (200µl). In this experimental system, CTLA-4 mediated trans-endocytosis of CD86 was not observed[116-118]. CD86 expression on APCs (splenic B cells) from suppressive vs. non-suppressive co-cultures was similar. Suppressive mechanisms involving the induction of APC apoptosis can also be excluded due to the fact that the numbers of surviving APCs in suppressive and non-suppressive co-cultures are similar and previous work showing that

paraformaldehyde fixation of APCs had no significant effect on the degree of Treg mediated suppression[108].

Furthermore as polyclonal Tregs express higher amounts of LFA-1 than Tconvs[121], suppression was suggested to work through the physical interference of Tregs with the interaction between APCs and Tconvs. However B3K506 monoclonal Tregs express lower levels of LFA-1 compared to B3K506 Tconvs. Therefor it does not seem likely that LFA-1 by itself accounts for suppression in our system. Finally we didn't observe conversion of OT-II Tconv into iTregs, although B3K506 Tregs from suppressive co-cultures expressed surface latency associated peptide of TGFβ (LAP).

Experiments using transwell culture settings failed to observe suppression[108,109]. The authors concluded that Treg-to-Tconv-cell-contact has a predominant role in mediating suppression. Along this line we designed an experiment where I-Ab restricted B3K506 Tregs and I-Ed restricted HA Tconvs were either co-cultured on B6xBALB/c F1 APCs presenting Treg and Tconv peptides or on separate B6 and BALB/c APCs each presenting the Treg and Tconv peptides respectively. In this system, peptide cross presentation and alloreactions of the two MHC class 2 types did not occur. Suppression is more complete when Tregs and Tconvs received antigen stimulation from F1 APCs presenting both peptides. However, a partial suppression was detected when cells were cultured on separate APCs: using separate APCs for each antigen, HA Tconv were able to proliferate but did not up regulate CD25.

Taken together we conclude that suppression requires high Treg numbers with high CD25 surface expression and close proximity between Tregs and Tconvs. These results, along with the observation that addition of exogenous IL-2 abrogates suppression (in vitro)[108,109], are consistent with the idea for a model of suppression, where Tregs scavenge IL-2 produced by Tconvs. Tregs continuously, and upon TCR signalling even more so, express high affinity CD25. Due to the direct repression of the IL-2 promoter via the transcription factor Foxp3 they are unable to produce autocrine IL-2[59]. A potential, reliable source of paracrine IL-2 could be a naïve neighbouring CD4+ T cell encountering ubiquitously present self-peptide in the periphery. The uptake of excess paracrine IL-2 by Tregs has beneficial effects on the maintenance of immune homeostasis[155]: (i) consuming IL-2 gives the Treg a survival signal and maintains elevated CD25 expression and (ii) by decreasing the amounts of IL-2 available to Tconvs, Tregs limit the ability of Tconvs to respond to self-antigens.

There are few reports in the literature arguing against IL-2 scavenging as a major mechanism of suppression. CD25 KO mice are suppressive in vitro and mice with specific deletion of peripheral CD122 in Tregs do not suffer from autoimmune disorders[85]. However these arguments have been mitigated by work showing that CD122 deficient Tregs still respond,

albeit to a diminished extent, to IL-2 signalling[138] and Tregs from CD25 KO mice failed to prevent spontaneous encephalomyelitis in vivo[167].

We show here that proximity imposed by Treg and Tconv peptide recognition on the same (F1) APC renders suppression more complete. This mechanism may be partially active in cultures using two separate APC's due to the high density of Tregs. However, in vivo it seems unlikely that Tregs and Tconvs responding to separate APCs will achieve sufficient proximity to induce suppression. In the lymph node there is a large excess of bystander CD4 and CD8 T cells, which decrease the proximity of Tregs and self-reactive Tconvs. In this light, the most efficient mechanism to achieve Treg-Tconv proximity is for the Treg and Tconv to be stimulated by the same APC. Recent data using a two-photon microscopy for LN-live imaging showed that Tregs migrate at high velocities and engage both Tconvs and DCs in brief but frequent contacts. The authors conclude that, under non-inflammatory conditions, a LN-resident DC is in contact with at least one Treg for 36-47% of the time[168]. The Treg TCR receptor repertoire is skewed towards self-antigen recognition and TCR expressed by Tregs are thought to be of higher affinity for self-antigens than conventional T cells[169,170]. Resident LN DCs constitutively present self-peptides. Accordingly if a Treg in the LN often occupies a DC, this provides an ideal platform for a Treg and a potentially self-reactive Tconv to encounter (self)-peptide in close proximity (i.e. on the same APC). This might create a localized "IL-2-sink" which abrogates further activation and proliferation of self-reactive Tconvs.

Even though we favour IL-2 steeling as the starring mechanism among all others proposed, this thesis couldn't exclude a role for cell-to-cell contact suppressive mechanisms. It is well possible that Tregs, in addition to scavenging IL-2, physically interact with Tconv and mediate suppression, for example, through gap-junction formation, shunting high levels of inhibitory cyclic adenosine monophosphate (cAMP) from Tregs to Tconv[135]. In addition a requirement for Treg-Tconv proximity is also compatible with the Treg secreting suppressive mediators which are only effective (i.e. at sufficiently high concentrations) at short distance from the Treg. Additional work is needed to fully characterize the multiple mechanism of Treg-mediated suppression and monoclonal Tregs may be a useful tool for the future.

6.2 The importance of co-receptor Lck coupling ratios for negative selection

In the second part of the thesis we examined the importance of co-receptor Lck coupling ratios for negative selection. Here we show, that unequal proportions of CD8 and CD4 co-

receptors from DP thymocytes carry the tyrosine kinase Lck (i.e. 0.6% vs. 6.7%, respectively). Further analysis showed that only 25-28% of coupled Lck is active. This implies that ~0.16% of CD8 and ~1.8% of CD4 molecules in B6 DP thymocytes are actually capable of initiating a TCR signal.

Using a chimeric CD8.4 co-receptor, consisting of an extracellular CD8α chain and an intracellular CD4 tail, we measured an increase in the co-receptor Lck coupling ratio (i.e. 1.1% for the CD8 WT and 6% for the CD8.4 co-receptor). Additional experiments making use of TCR Tg OT-I WT and OT-I CD8.4 DP thymocytes, revealed that a difference in co-receptor Lck coupling ratios results in a shift of the affinity threshold for negative selection. In OT-I CD8.4 mice, below threshold ligands, with decreased affinity for the OT-I TCR, were able to induce negative selection (Fig. 3A, Stepanek, O. et al. Cell, 2014).

Upon recruitment, active Lck phosphorylates the ITAMs in the CD3 complex and activates the tyrosines on Zap-70. Since TCR-pMHC complexes scan up to hundreds of co-receptors before colliding with one that carries active Lck, we measured the time an antigen needed to occupy the TCR (i.e. antigen dwell time) to induce a negative selection signal. A MHC class I-restricted TCR required antigens with a median dwell time (i.e. half life) > 0.9s to induce negative selection, while the negative selection threshold for MHCII-restricted TCRs is > 0.2s[9].

Modeling studies revealed that the co-receptor Lck coupling ratio is a critical parameter for the establishment of the affinity threshold for negative selection. The decrease in antigen dwell time threshold of negative selection seen in MHC-II restricted TCRs compared to MHC-I restricted TCRs is a direct consequence of the CD4's increased Lck coupling ratio.

With our experimental results and additional mathematical calculations the 'Lck come and stay/signal duration' model based on the principle of kinetic proofreading[171] was generated. The model assumes that transient CD4-MHCII or CD8-MHCI interactions allow the TCR-pMHC complex to scan multiple coreceptors via co-receptor exchange before finding a co-receptor carrying catalytically active Lck. This model can explain how the TCR actually measures antigen affinity to initiate a negative selection signal; long lasting antigen binding events are more likely to be converted into a signaling event and trigger negative selection.

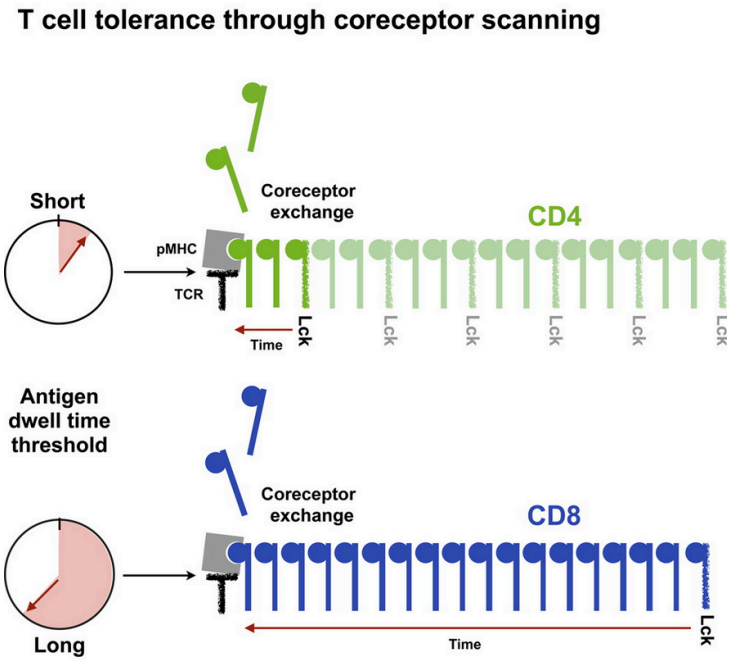

Figure 6.2.1 Graphical abstract of co-receptor scanning

Stepanek, O. et al. Cell, 2014

7 References

1 Burnet, F. M. The immunological significance of the thymus: an extension of the clonal selection theory of immunity. *Australasian annals of medicine* **11**, 79-91 (1962).

2 Mathis, D. & Benoist, C. A decade of AIRE. *Nat Rev Immunol* **7**, 645-650, doi:10.1038/nri2136 (2007).

3 Kappler, J. W., Roehm, N. & Marrack, P. T cell tolerance by clonal elimination in the thymus. *Cell* **49**, 273-280 (1987).

4 Hogquist, K. A. *et al.* T cell receptor antagonist peptides induce positive selection. *Cell* **76**, 17-27 (1994).

5 Williams, C. B., Engle, D. L., Kersh, G. J., Michael White, J. & Allen, P. M. A kinetic threshold between negative and positive selection based on the longevity of the T cell receptor-ligand complex. *J Exp Med* **189**, 1531-1544 (1999).

6 Naeher, D. *et al.* A constant affinity threshold for T cell tolerance. *J Exp Med* **204**, 2553-2559, doi:10.1084/jem.20070254 (2007).

7 Palmer, E. & Naeher, D. Affinity threshold for thymic selection through a T-cell receptor-co-receptor zipper. *Nat Rev Immunol* **9**, 207-213, doi:10.1038/nri2469 (2009).

8 Daniels, M. A. *et al.* Thymic selection threshold defined by compartmentalization of Ras/MAPK signalling. *Nature* **444**, 724-729, doi:10.1038/nature05269 (2006).

9 Stepanek, O. *et al.* Coreceptor scanning by the T cell receptor provides a mechanism for T cell tolerance. *Cell* **159**, 333-345, doi:10.1016/j.cell.2014.08.042 (2014).

10 Jenkins, M. K., Pardoll, D. M., Mizuguchi, J., Quill, H. & Schwartz, R. H. T-cell unresponsiveness in vivo and in vitro: fine specificity of induction and molecular characterization of the unresponsive state. *Immunol Rev* **95**, 113-135 (1987).

11 Jenkins, M. K. & Schwartz, R. H. Antigen presentation by chemically modified splenocytes induces antigen-specific T cell unresponsiveness in vitro and in vivo. *J Exp Med* **165**, 302-319 (1987).

12 Gershon, R. K. & Kondo, K. Infectious immunological tolerance. *Immunology* **21**, 903-914 (1971).

13 Gershon, R. K., Cohen, P., Hencin, R. & Liebhaber, S. A. Suppressor T cells. *J Immunol* **108**, 586-590 (1972).

14 Nishizuka, Y. & Sakakura, T. Thymus and reproduction: sex-linked dysgenesia of the gonad after neonatal thymectomy in mice. *Science* **166**, 753-755 (1969).

15 Sakaguchi, S., Sakaguchi, N., Asano, M., Itoh, M. & Toda, M. Immunologic self-tolerance maintained by activated T cells expressing IL-2 receptor alpha-chains (CD25). Breakdown of a single mechanism of self-tolerance causes various autoimmune diseases. *J Immunol* **155**, 1151-1164 (1995).

16 Asano, M., Toda, M., Sakaguchi, N. & Sakaguchi, S. Autoimmune disease as a consequence of developmental abnormality of a T cell subpopulation. *J Exp Med* **184**, 387-396 (1996).

17 Powell, B. R., Buist, N. R. & Stenzel, P. An X-linked syndrome of diarrhea, polyendocrinopathy, and fatal infection in infancy. *The Journal of pediatrics* **100**, 731-737 (1982).

18 Godfrey, V. L., Wilkinson, J. E., Rinchik, E. M. & Russell, L. B. Fatal lymphoreticular disease in the scurfy (sf) mouse requires T cells that mature in a sf thymic environment: potential model for thymic education. *Proc Natl Acad Sci U S A* **88**, 5528-5532 (1991).

19 Godfrey, V. L., Wilkinson, J. E. & Russell, L. B. X-linked lymphoreticular disease in the scurfy (sf) mutant mouse. *Am J Pathol* **138**, 1379-1387 (1991).

20 Brunkow, M. E. *et al.* Disruption of a new forkhead/winged-helix protein, scurfin, results in the fatal lymphoproliferative disorder of the scurfy mouse. *Nat Genet* **27**, 68-73, doi:10.1038/83784 (2001).

21 Wildin, R. S. *et al.* X-linked neonatal diabetes mellitus, enteropathy and endocrinopathy syndrome is the human equivalent of mouse scurfy. *Nat Genet* **27**, 18-20, doi:10.1038/83707 (2001).

22 Schubert, L. A., Jeffery, E., Zhang, Y., Ramsdell, F. & Ziegler, S. F. Scurfin (FOXP3) acts as a repressor of transcription and regulates T cell activation. *J Biol Chem* **276**, 37672-37679, doi:10.1074/jbc.M104521200 (2001).

23 Khattri, R., Cox, T., Yasayko, S. A. & Ramsdell, F. An essential role for Scurfin in CD4+CD25+ T regulatory cells. *Nat Immunol* **4**, 337-342, doi:10.1038/ni909 (2003).

24 Fontenot, J. D., Gavin, M. A. & Rudensky, A. Y. Foxp3 programs the development and function of CD4+CD25+ regulatory T cells. *Nat Immunol* **4**, 330-336, doi:10.1038/ni904 (2003).

25 Hori, S., Nomura, T. & Sakaguchi, S. Control of regulatory T cell development by the transcription factor Foxp3. *Science* **299**, 1057-1061, doi:10.1126/science.1079490 (2003).

26 Liston, A. & Gray, D. H. Homeostatic control of regulatory T cell diversity. *Nat Rev Immunol* **14**, 154-165, doi:10.1038/nri3605 (2014).

27 Jordan, M. S. *et al.* Thymic selection of CD4+CD25+ regulatory T cells induced by an agonist self-peptide. *Nat Immunol* **2**, 301-306, doi:10.1038/86302 (2001).

28 Lee, H. M., Bautista, J. L., Scott-Browne, J., Mohan, J. F. & Hsieh, C. S. A broad range of self-reactivity drives thymic regulatory T cell selection to limit responses to self. *Immunity* **37**, 475-486, doi:10.1016/j.immuni.2012.07.009 (2012).

29 Apostolou, I., Sarukhan, A., Klein, L. & von Boehmer, H. Origin of regulatory T cells with known specificity for antigen. *Nat Immunol* **3**, 756-763, doi:10.1038/ni816 (2002).

30 Thornton, A. M. *et al.* Expression of Helios, an Ikaros transcription factor family member, differentiates thymic-derived from peripherally induced Foxp3+ T regulatory cells. *J Immunol* **184**, 3433-3441, doi:10.4049/jimmunol.0904028 (2010).

31 Daley, S. R., Hu, D. Y. & Goodnow, C. C. Helios marks strongly autoreactive CD4+ T cells in two major waves of thymic deletion distinguished by induction of PD-1 or NF-kappaB. *J Exp Med* **210**, 269-285, doi:10.1084/jem.20121458 (2013).

32 Yadav, M. *et al.* Neuropilin-1 distinguishes natural and inducible regulatory T cells among regulatory T cell subsets in vivo. *J Exp Med* **209**, 1713-1722, S1711-1719, doi:10.1084/jem.20120822 (2012).

33 Haribhai, D. *et al.* A requisite role for induced regulatory T cells in tolerance based on expanding antigen receptor diversity. *Immunity* **35**, 109-122, doi:10.1016/j.immuni.2011.03.029 (2011).

34 Andersson, J. *et al.* CD4+ FoxP3+ regulatory T cells confer infectious tolerance in a TGF-beta-dependent manner. *J Exp Med* **205**, 1975-1981, doi:10.1084/jem.20080308 (2008).

35 Chen, W. *et al.* Conversion of peripheral CD4+CD25- naive T cells to CD4+CD25+ regulatory T cells by TGF-beta induction of transcription factor Foxp3. *J Exp Med* **198**, 1875-1886, doi:10.1084/jem.20030152 (2003).

36 Knoechel, B., Lohr, J., Kahn, E., Bluestone, J. A. & Abbas, A. K. Sequential development of interleukin 2-dependent effector and regulatory T cells in response to endogenous systemic antigen. *J Exp Med* **202**, 1375-1386, doi:10.1084/jem.20050855 (2005).

37 Amado, I. F. *et al.* IL-2 coordinates IL-2-producing and regulatory T cell interplay. *J Exp Med* **210**, 2707-2720, doi:10.1084/jem.20122759 (2013).

38 Tai, X. *et al.* Foxp3 transcription factor is proapoptotic and lethal to developing regulatory T cells unless counterbalanced by cytokine survival signals. *Immunity* **38**, 1116-1128, doi:10.1016/j.immuni.2013.02.022 (2013).

39 Pierson, W. *et al.* Antiapoptotic Mcl-1 is critical for the survival and niche-filling capacity of Foxp3(+) regulatory T cells. *Nat Immunol* **14**, 959-965, doi:10.1038/ni.2649 (2013).

40 Huehn, J. *et al.* Developmental stage, phenotype, and migration distinguish naive- and effector/memory-like CD4+ regulatory T cells. *J Exp Med* **199**, 303-313, doi:10.1084/jem.20031562 (2004).

41 Cretney, E. *et al.* The transcription factors Blimp-1 and IRF4 jointly control the differentiation and function of effector regulatory T cells. *Nat Immunol* **12**, 304-311, doi:10.1038/ni.2006 (2011).

42 Feuerer, M. *et al.* Genomic definition of multiple ex vivo regulatory T cell subphenotypes. *Proc Natl Acad Sci U S A* **107**, 5919-5924, doi:10.1073/pnas.1002006107 (2010).

43 Duhen, T., Duhen, R., Lanzavecchia, A., Sallusto, F. & Campbell, D. J. Functionally distinct subsets of human FOXP3+ Treg cells that phenotypically mirror effector Th cells. *Blood* **119**, 4430-4440, doi:10.1182/blood-2011-11-392324 (2012).

44 Burzyn, D., Benoist, C. & Mathis, D. Regulatory T cells in nonlymphoid tissues. *Nat Immunol* **14**, 1007-1013, doi:10.1038/ni.2683 (2013).

45 Atarashi, K. *et al.* Treg induction by a rationally selected mixture of Clostridia strains from the human microbiota. *Nature* **500**, 232-236, doi:10.1038/nature12331 (2013).

46 Smith, P. M. *et al.* The microbial metabolites, short-chain fatty acids, regulate colonic Treg cell homeostasis. *Science* **341**, 569-573, doi:10.1126/science.1241165 (2013).

47 Vasanthakumar, A. *et al.* The transcriptional regulators IRF4, BATF and IL-33 orchestrate development and maintenance of adipose tissue-resident regulatory T cells. *Nat Immunol* **16**, 276-285, doi:10.1038/ni.3085 (2015).

48 Cipolletta, D. *et al.* PPAR-gamma is a major driver of the accumulation and phenotype of adipose tissue Treg cells. *Nature* **486**, 549-553, doi:10.1038/nature11132 (2012).

49 Feuerer, M. *et al.* Lean, but not obese, fat is enriched for a unique population of regulatory T cells that affect metabolic parameters. *Nat Med* **15**, 930-939, doi:10.1038/nm.2002 (2009).

50 Sather, B. D. *et al.* Altering the distribution of Foxp3(+) regulatory T cells results in tissue-specific inflammatory disease. *J Exp Med* **204**, 1335-1347, doi:10.1084/jem.20070081 (2007).

51 Rosenblum, M. D. *et al.* Response to self antigen imprints regulatory memory in tissues. *Nature* **480**, 538-542, doi:10.1038/nature10664 (2011).

52 Chung, Y. *et al.* Follicular regulatory T cells expressing Foxp3 and Bcl-6 suppress germinal center reactions. *Nat Med* **17**, 983-988, doi:10.1038/nm.2426 (2011).

53 Linterman, M. A. *et al.* Foxp3+ follicular regulatory T cells control the germinal center response. *Nat Med* **17**, 975-982, doi:10.1038/nm.2425 (2011).

54 Burzyn, D. *et al.* A special population of regulatory T cells potentiates muscle repair. *Cell* **155**, 1282-1295, doi:10.1016/j.cell.2013.10.054 (2013).

55 Rowe, J. H., Ertelt, J. M., Xin, L. & Way, S. S. Pregnancy imprints regulatory memory that sustains anergy to fetal antigen. *Nature* **490**, 102-106, doi:10.1038/nature11462 (2012).

56 Rudensky, A. Y. Regulatory T cells and Foxp3. *Immunol Rev* **241**, 260-268, doi:10.1111/j.1600-065X.2011.01018.x (2011).

57 Khattri, R. *et al.* The amount of scurfin protein determines peripheral T cell number and responsiveness. *J Immunol* **167**, 6312-6320 (2001).

58 Lopes, J. E. *et al.* Analysis of FOXP3 reveals multiple domains required for its function as a transcriptional repressor. *J Immunol* **177**, 3133-3142 (2006).

59 Wu, Y. *et al.* FOXP3 controls regulatory T cell function through cooperation with NFAT. *Cell* **126**, 375-387, doi:10.1016/j.cell.2006.05.042 (2006).

60 Polansky, J. K. *et al.* DNA methylation controls Foxp3 gene expression. *Eur J Immunol* **38**, 1654-1663, doi:10.1002/eji.200838105 (2008).

61 Zheng, Y. *et al.* Role of conserved non-coding DNA elements in the Foxp3 gene in regulatory T-cell fate. *Nature* **463**, 808-812, doi:10.1038/nature08750 (2010).

62 Samstein, R. M., Josefowicz, S. Z., Arvey, A., Treuting, P. M. & Rudensky, A. Y. Extrathymic generation of regulatory T cells in placental mammals mitigates maternal-fetal conflict. *Cell* **150**, 29-38, doi:10.1016/j.cell.2012.05.031 (2012).

63 Deenick, E. K. *et al.* c-Rel but not NF-kappaB1 is important for T regulatory cell development. *Eur J Immunol* **40**, 677-681, doi:10.1002/eji.201040298 (2010).

64 Long, M., Park, S. G., Strickland, I., Hayden, M. S. & Ghosh, S. Nuclear factor-kappaB modulates regulatory T cell development by directly regulating expression of Foxp3 transcription factor. *Immunity* **31**, 921-931, doi:10.1016/j.immuni.2009.09.022 (2009).

65 Samstein, R. M. *et al.* Foxp3 exploits a pre-existent enhancer landscape for regulatory T cell lineage specification. *Cell* **151**, 153-166, doi:10.1016/j.cell.2012.06.053 (2012).

66 Fu, W. *et al.* A multiply redundant genetic switch 'locks in' the transcriptional signature of regulatory T cells. *Nat Immunol* **13**, 972-980, doi:10.1038/ni.2420 (2012).

67 Walker, M. R. *et al.* Induction of FoxP3 and acquisition of T regulatory activity by stimulated human CD4+CD25- T cells. *J Clin Invest* **112**, 1437-1443, doi:10.1172/JCI19441 (2003).

68 Smith, E. L., Finney, H. M., Nesbitt, A. M., Ramsdell, F. & Robinson, M. K. Splice variants of human FOXP3 are functional inhibitors of human CD4+ T-cell activation. *Immunology* **119**, 203-211, doi:10.1111/j.1365-2567.2006.02425.x (2006).

69 Huang, C. *et al.* Cutting Edge: A Novel, Human-Specific Interacting Protein Couples FOXP3 to a Chromatin-Remodeling Complex That Contains KAP1/TRIM28. *J Immunol* **190**, 4470-4473, doi:10.4049/jimmunol.1203561 (2013).

70 Fontenot, J. D., Rasmussen, J. P., Gavin, M. A. & Rudensky, A. Y. A function for interleukin 2 in Foxp3-expressing regulatory T cells. *Nat Immunol* **6**, 1142-1151, doi:10.1038/ni1263 (2005).

71 Donohue, J. H. & Rosenberg, S. A. The fate of interleukin-2 after in vivo administration. *J Immunol* **130**, 2203-2208 (1983).

72 Malek, T. R. & Castro, I. Interleukin-2 receptor signaling: at the interface between tolerance and immunity. *Immunity* **33**, 153-165, doi:10.1016/j.immuni.2010.08.004 (2010).

73 Malek, T. R. The biology of interleukin-2. *Annu Rev Immunol* **26**, 453-479, doi:10.1146/annurev.immunol.26.021607.090357 (2008).

74 Gong, D. & Malek, T. R. Cytokine-dependent Blimp-1 expression in activated T cells inhibits IL-2 production. *J Immunol* **178**, 242-252 (2007).

75 Villarino, A. V. *et al.* Helper T cell IL-2 production is limited by negative feedback and STAT-dependent cytokine signals. *J Exp Med* **204**, 65-71, doi:10.1084/jem.20061198 (2007).

76 Hemar, A. *et al.* Endocytosis of interleukin 2 receptors in human T lymphocytes: distinct intracellular localization and fate of the receptor alpha, beta, and gamma chains. *J Cell Biol* **129**, 55-64 (1995).

77 Nelson, B. H. & Willerford, D. M. Biology of the interleukin-2 receptor. *Advances in immunology* **70**, 1-81 (1998).
78 Gaffen, S. L. Signaling domains of the interleukin 2 receptor. *Cytokine* **14**, 63-77, doi:10.1006/cyto.2001.0862 (2001).
79 Burchill, M. A., Yang, J., Vogtenhuber, C., Blazar, B. R. & Farrar, M. A. IL-2 receptor beta-dependent STAT5 activation is required for the development of Foxp3+ regulatory T cells. *J Immunol* **178**, 280-290 (2007).
80 Bensinger, S. J. *et al.* Distinct IL-2 receptor signaling pattern in CD4+CD25+ regulatory T cells. *J Immunol* **172**, 5287-5296 (2004).
81 Suzuki, H. *et al.* Deregulated T cell activation and autoimmunity in mice lacking interleukin-2 receptor beta. *Science* **268**, 1472-1476 (1995).
82 Sadlack, B. *et al.* Ulcerative colitis-like disease in mice with a disrupted interleukin-2 gene. *Cell* **75**, 253-261 (1993).
83 Willerford, D. M. *et al.* Interleukin-2 receptor alpha chain regulates the size and content of the peripheral lymphoid compartment. *Immunity* **3**, 521-530 (1995).
84 Boyman, O. & Sprent, J. The role of interleukin-2 during homeostasis and activation of the immune system. *Nat Rev Immunol* **12**, 180-190, doi:10.1038/nri3156 (2012).
85 Malek, T. R., Yu, A., Vincek, V., Scibelli, P. & Kong, L. CD4 regulatory T cells prevent lethal autoimmunity in IL-2Rbeta-deficient mice. Implications for the nonredundant function of IL-2. *Immunity* **17**, 167-178 (2002).
86 Klapper, J. A. *et al.* High-dose interleukin-2 for the treatment of metastatic renal cell carcinoma : a retrospective analysis of response and survival in patients treated in the surgery branch at the National Cancer Institute between 1986 and 2006. *Cancer* **113**, 293-301, doi:10.1002/cncr.23552 (2008).
87 Smith, F. O. *et al.* Treatment of metastatic melanoma using interleukin-2 alone or in conjunction with vaccines. *Clin Cancer Res* **14**, 5610-5618, doi:10.1158/1078-0432.CCR-08-0116 (2008).
88 Kosmaczewska, A. Low-dose interleukin-2 therapy: a driver of an imbalance between immune tolerance and autoimmunity. *International journal of molecular sciences* **15**, 18574-18592, doi:10.3390/ijms151018574 (2014).
89 Boyman, O., Surh, C. D. & Sprent, J. Potential use of IL-2/anti-IL-2 antibody immune complexes for the treatment of cancer and autoimmune disease. *Expert Opin Biol Ther* **6**, 1323-1331, doi:10.1517/14712598.6.12.1323 (2006).
90 Letourneau, S., Krieg, C., Pantaleo, G. & Boyman, O. IL-2- and CD25-dependent immunoregulatory mechanisms in the homeostasis of T-cell subsets. *J Allergy Clin Immunol* **123**, 758-762, doi:10.1016/j.jaci.2009.02.011 (2009).
91 Letourneau, S. *et al.* IL-2/anti-IL-2 antibody complexes show strong biological activity by avoiding interaction with IL-2 receptor alpha subunit CD25. *Proc Natl Acad Sci U S A* **107**, 2171-2176, doi:10.1073/pnas.0909384107 (2010).
92 Krieg, C., Letourneau, S., Pantaleo, G. & Boyman, O. Improved IL-2 immunotherapy by selective stimulation of IL-2 receptors on lymphocytes and endothelial cells. *Proc Natl Acad Sci U S A* **107**, 11906-11911, doi:10.1073/pnas.1002569107 (2010).
93 Webster, K. E. *et al.* In vivo expansion of T reg cells with IL-2-mAb complexes: induction of resistance to EAE and long-term acceptance of islet allografts without immunosuppression. *J Exp Med* **206**, 751-760, doi:10.1084/jem.20082824 (2009).
94 Cozzo, C., Larkin, J., 3rd & Caton, A. J. Cutting edge: self-peptides drive the peripheral expansion of CD4+CD25+ regulatory T cells. *J Immunol* **171**, 5678-5682 (2003).
95 Palacios, E. H. & Weiss, A. Function of the Src-family kinases, Lck and Fyn, in T-cell development and activation. *Oncogene* **23**, 7990-8000, doi:10.1038/sj.onc.1208074 (2004).

96 Dustin, M. L. PKC-theta: hitting the bull's eye. *Nat Immunol* **12**, 1031-1032, doi:10.1038/ni.2141 (2011).

97 Weil, R. & Israel, A. Deciphering the pathway from the TCR to NF-kappaB. *Cell Death Differ* **13**, 826-833, doi:10.1038/sj.cdd.4401856 (2006).

98 Crellin, N. K., Garcia, R. V. & Levings, M. K. Altered activation of AKT is required for the suppressive function of human CD4+CD25+ T regulatory cells. *Blood* **109**, 2014-2022, doi:10.1182/blood-2006-07-035279 (2007).

99 Hickman, S. P., Yang, J., Thomas, R. M., Wells, A. D. & Turka, L. A. Defective activation of protein kinase C and Ras-ERK pathways limits IL-2 production and proliferation by CD4+CD25+ regulatory T cells. *J Immunol* **177**, 2186-2194 (2006).

100 Au-Yeung, B. B. *et al.* A genetically selective inhibitor demonstrates a function for the kinase Zap70 in regulatory T cells independent of its catalytic activity. *Nat Immunol* **11**, 1085-1092, doi:10.1038/ni.1955 (2010).

101 Gavin, M. A., Clarke, S. R., Negrou, E., Gallegos, A. & Rudensky, A. Homeostasis and anergy of CD4(+)CD25(+) suppressor T cells in vivo. *Nat Immunol* **3**, 33-41, doi:10.1038/ni743 (2002).

102 Dong, S. *et al.* T cell receptor for antigen induces linker for activation of T cell-dependent activation of a negative signaling complex involving Dok-2, SHIP-1, and Grb-2. *J Exp Med* **203**, 2509-2518, doi:10.1084/jem.20060650 (2006).

103 Zhao, M., Janas, J. A., Niki, M., Pandolfi, P. P. & Van Aelst, L. Dok-1 independently attenuates Ras/mitogen-activated protein kinase and Src/c-myc pathways to inhibit platelet-derived growth factor-induced mitogenesis. *Mol Cell Biol* **26**, 2479-2489, doi:10.1128/MCB.26.7.2479-2489.2006 (2006).

104 Okada, M., Nada, S., Yamanashi, Y., Yamamoto, T. & Nakagawa, H. CSK: a protein-tyrosine kinase involved in regulation of src family kinases. *J Biol Chem* **266**, 24249-24252 (1991).

105 Bettelli, E., Dastrange, M. & Oukka, M. Foxp3 interacts with nuclear factor of activated T cells and NF-kappa B to repress cytokine gene expression and effector functions of T helper cells. *Proc Natl Acad Sci U S A* **102**, 5138-5143, doi:10.1073/pnas.0501675102 (2005).

106 Levine, A. G., Arvey, A., Jin, W. & Rudensky, A. Y. Continuous requirement for the TCR in regulatory T cell function. *Nat Immunol* **15**, 1070-1078, doi:10.1038/ni.3004 (2014).

107 Schmidt, A. M. *et al.* Regulatory T cells require TCR signaling for their suppressive function. *J Immunol* **194**, 4362-4370, doi:10.4049/jimmunol.1402384 (2015).

108 Takahashi, T. *et al.* Immunologic self-tolerance maintained by CD25+CD4+ naturally anergic and suppressive T cells: induction of autoimmune disease by breaking their anergic/suppressive state. *Int Immunol* **10**, 1969-1980 (1998).

109 Thornton, A. M. & Shevach, E. M. CD4+CD25+ immunoregulatory T cells suppress polyclonal T cell activation in vitro by inhibiting interleukin 2 production. *J Exp Med* **188**, 287-296 (1998).

110 Hofer, T., Krichevsky, O. & Altan-Bonnet, G. Competition for IL-2 between Regulatory and Effector T Cells to Chisel Immune Responses. *Frontiers in immunology* **3**, 268, doi:10.3389/fimmu.2012.00268 (2012).

111 Read, S., Malmstrom, V. & Powrie, F. Cytotoxic T lymphocyte-associated antigen 4 plays an essential role in the function of CD25(+)CD4(+) regulatory cells that control intestinal inflammation. *J Exp Med* **192**, 295-302 (2000).

112 Wing, K. *et al.* CTLA-4 control over Foxp3+ regulatory T cell function. *Science* **322**, 271-275, doi:10.1126/science.1160062 (2008).

113 Fallarino, F. *et al.* Modulation of tryptophan catabolism by regulatory T cells. *Nat Immunol* **4**, 1206-1212, doi:10.1038/ni1003 (2003).

114 Fallarino, F. *et al.* Tryptophan catabolism generates autoimmune-preventive regulatory T cells. *Transplant immunology* **17**, 58-60, doi:10.1016/j.trim.2006.09.017 (2006).

115 Fallarino, F. *et al.* The combined effects of tryptophan starvation and tryptophan catabolites down-regulate T cell receptor zeta-chain and induce a regulatory phenotype in naive T cells. *J Immunol* **176**, 6752-6761 (2006).

116 Cederbom, L., Hall, H. & Ivars, F. CD4+CD25+ regulatory T cells down-regulate co-stimulatory molecules on antigen-presenting cells. *Eur J Immunol* **30**, 1538-1543, doi:10.1002/1521-4141(200006)30:6<1538::AID-IMMU1538>3.0.CO;2-X (2000).

117 Qureshi, O. S. *et al.* Trans-endocytosis of CD80 and CD86: a molecular basis for the cell-extrinsic function of CTLA-4. *Science* **332**, 600-603, doi:10.1126/science.1202947 (2011).

118 Kong, K. F. *et al.* Protein kinase C-eta controls CTLA-4-mediated regulatory T cell function. *Nat Immunol* **15**, 465-472, doi:10.1038/ni.2866 (2014).

119 Oderup, C., Cederbom, L., Makowska, A., Cilio, C. M. & Ivars, F. Cytotoxic T lymphocyte antigen-4-dependent down-modulation of costimulatory molecules on dendritic cells in CD4+ CD25+ regulatory T-cell-mediated suppression. *Immunology* **118**, 240-249, doi:10.1111/j.1365-2567.2006.02362.x (2006).

120 Fehervari, Z. & Sakaguchi, S. Control of Foxp3+ CD25+CD4+ regulatory cell activation and function by dendritic cells. *Int Immunol* **16**, 1769-1780, doi:10.1093/intimm/dxh178 (2004).

121 Onishi, Y., Fehervari, Z., Yamaguchi, T. & Sakaguchi, S. Foxp3+ natural regulatory T cells preferentially form aggregates on dendritic cells in vitro and actively inhibit their maturation. *Proc Natl Acad Sci U S A* **105**, 10113-10118, doi:10.1073/pnas.0711106105 (2008).

122 Huang, C. T. *et al.* Role of LAG-3 in regulatory T cells. *Immunity* **21**, 503-513, doi:10.1016/j.immuni.2004.08.010 (2004).

123 Miyazaki, T., Dierich, A., Benoist, C. & Mathis, D. Independent modes of natural killing distinguished in mice lacking Lag3. *Science* **272**, 405-408 (1996).

124 von Boehmer, H. Mechanisms of suppression by suppressor T cells. *Nat Immunol* **6**, 338-344, doi:10.1038/ni1180 (2005).

125 Nakamura, K., Kitani, A. & Strober, W. Cell contact-dependent immunosuppression by CD4(+)CD25(+) regulatory T cells is mediated by cell surface-bound transforming growth factor beta. *J Exp Med* **194**, 629-644 (2001).

126 Piccirillo, C. A. *et al.* CD4(+)CD25(+) regulatory T cells can mediate suppressor function in the absence of transforming growth factor beta1 production and responsiveness. *J Exp Med* **196**, 237-246 (2002).

127 Annacker, O. *et al.* CD25+ CD4+ T cells regulate the expansion of peripheral CD4 T cells through the production of IL-10. *J Immunol* **166**, 3008-3018 (2001).

128 Uhlig, H. H. *et al.* Characterization of Foxp3+CD4+CD25+ and IL-10-secreting CD4+CD25+ T cells during cure of colitis. *J Immunol* **177**, 5852-5860 (2006).

129 Asseman, C., Mauze, S., Leach, M. W., Coffman, R. L. & Powrie, F. An essential role for interleukin 10 in the function of regulatory T cells that inhibit intestinal inflammation. *J Exp Med* **190**, 995-1004 (1999).

130 Rubtsov, Y. P. *et al.* Regulatory T cell-derived interleukin-10 limits inflammation at environmental interfaces. *Immunity* **28**, 546-558, doi:10.1016/j.immuni.2008.02.017 (2008).

131 Sakaguchi, S. Naturally arising CD4+ regulatory t cells for immunologic self-tolerance and negative control of immune responses. *Annu Rev Immunol* **22**, 531-562, doi:10.1146/annurev.immunol.21.120601.141122 (2004).

132 Gondek, D. C., Lu, L. F., Quezada, S. A., Sakaguchi, S. & Noelle, R. J. Cutting edge: contact-mediated suppression by CD4+CD25+ regulatory cells involves a

granzyme B-dependent, perforin-independent mechanism. *J Immunol* **174**, 1783-1786 (2005).

133 Zhao, D. M., Thornton, A. M., DiPaolo, R. J. & Shevach, E. M. Activated CD4+CD25+ T cells selectively kill B lymphocytes. *Blood* **107**, 3925-3932, doi:10.1182/blood-2005-11-4502 (2006).

134 Grossman, W. J. *et al.* Differential expression of granzymes A and B in human cytotoxic lymphocyte subsets and T regulatory cells. *Blood* **104**, 2840-2848, doi:10.1182/blood-2004-03-0859 (2004).

135 Bopp, T. *et al.* Cyclic adenosine monophosphate is a key component of regulatory T cell-mediated suppression. *J Exp Med* **204**, 1303-1310, doi:10.1084/jem.20062129 (2007).

136 Deaglio, S. *et al.* Adenosine generation catalyzed by CD39 and CD73 expressed on regulatory T cells mediates immune suppression. *J Exp Med* **204**, 1257-1265, doi:10.1084/jem.20062512 (2007).

137 Scheffold, A., Murphy, K. M. & Hofer, T. Competition for cytokines: T(reg) cells take all. *Nat Immunol* **8**, 1285-1287, doi:10.1038/ni1207-1285 (2007).

138 Bayer, A. L., Yu, A. & Malek, T. R. Function of the IL-2R for thymic and peripheral CD4+CD25+ Foxp3+ T regulatory cells. *J Immunol* **178**, 4062-4071 (2007).

139 Li, X. C. *et al.* IL-15 and IL-2: a matter of life and death for T cells in vivo. *Nat Med* **7**, 114-118, doi:10.1038/83253 (2001).

140 Joshi, N. S. *et al.* Regulatory T Cells in Tumor-Associated Tertiary Lymphoid Structures Suppress Anti-tumor T Cell Responses. *Immunity* **43**, 579-590, doi:10.1016/j.immuni.2015.08.006 (2015).

141 Jeker, L. T., Bour-Jordan, H. & Bluestone, J. A. Breakdown in peripheral tolerance in type 1 diabetes in mice and humans. *Cold Spring Harbor perspectives in medicine* **2**, a007807, doi:10.1101/cshperspect.a007807 (2012).

142 Monti, P. *et al.* Rapamycin monotherapy in patients with type 1 diabetes modifies CD4+CD25+FOXP3+ regulatory T-cells. *Diabetes* **57**, 2341-2347, doi:10.2337/db08-0138 (2008).

143 McMurchy, A. N., Bushell, A., Levings, M. K. & Wood, K. J. Moving to tolerance: clinical application of T regulatory cells. *Semin Immunol* **23**, 304-313, doi:10.1016/j.smim.2011.04.001 (2011).

144 Schuppan, D., Junker, Y. & Barisani, D. Celiac disease: from pathogenesis to novel therapies. *Gastroenterology* **137**, 1912-1933, doi:10.1053/j.gastro.2009.09.008 (2009).

145 Tye-Din, J. A. *et al.* Comprehensive, quantitative mapping of T cell epitopes in gluten in celiac disease. *Sci Transl Med* **2**, 41ra51, doi:10.1126/scitranslmed.3001012 (2010).

146 Tye-Din, J. A. *et al.* The effects of ALV003 pre-digestion of gluten on immune response and symptoms in celiac disease in vivo. *Clin Immunol* **134**, 289-295, doi:10.1016/j.clim.2009.11.001 (2010).

147 Allan, S. E. *et al.* Generation of potent and stable human CD4+ T regulatory cells by activation-independent expression of FOXP3. *Mol Ther* **16**, 194-202, doi:10.1038/sj.mt.6300341 (2008).

148 Hippen, K. L. *et al.* Generation and large-scale expansion of human inducible regulatory T cells that suppress graft-versus-host disease. *Am J Transplant* **11**, 1148-1157, doi:10.1111/j.1600-6143.2011.03558.x (2011).

149 Hippen, K. L. *et al.* Massive ex vivo expansion of human natural regulatory T cells (T(regs)) with minimal loss of in vivo functional activity. *Sci Transl Med* **3**, 83ra41, doi:10.1126/scitranslmed.3001809 (2011).

150 Ermann, J. *et al.* Only the CD62L+ subpopulation of CD4+CD25+ regulatory T cells protects from lethal acute GVHD. *Blood* **105**, 2220-2226, doi:10.1182/blood-2004-05-2044 (2005).

151 Magenau, J. M. *et al.* Frequency of CD4(+)CD25(hi)FOXP3(+) regulatory T cells has diagnostic and prognostic value as a biomarker for acute graft-versus-host-disease. *Biol Blood Marrow Transplant* **16**, 907-914, doi:10.1016/j.bbmt.2010.02.026 (2010).
152 Canavan, J. B. *et al.* Developing in vitro expanded CD45RA+ regulatory T cells as an adoptive cell therapy for Crohn's disease. *Gut*, doi:10.1136/gutjnl-2014-306919 (2015).
153 Intlekofer, A. M. & Thompson, C. B. At the bench: preclinical rationale for CTLA-4 and PD-1 blockade as cancer immunotherapy. *J Leukoc Biol* **94**, 25-39, doi:10.1189/jlb.1212621 (2013).
154 Callahan, M. K. & Wolchok, J. D. At the bedside: CTLA-4- and PD-1-blocking antibodies in cancer immunotherapy. *J Leukoc Biol* **94**, 41-53, doi:10.1189/jlb.1212631 (2013).
155 Huseby, E. S. *et al.* How the T cell repertoire becomes peptide and MHC specific. *Cell* **122**, 247-260, doi:10.1016/j.cell.2005.05.013 (2005).
156 Wang, Y. *et al.* Th2 lymphoproliferative disorder of LatY136F mutant mice unfolds independently of TCR-MHC engagement and is insensitive to the action of Foxp3+ regulatory T cells. *J Immunol* **180**, 1565-1575 (2008).
157 Backstrom, B. T., Muller, U., Hausmann, B. & Palmer, E. Positive selection through a motif in the alphabeta T cell receptor. *Science* **281**, 835-838 (1998).
158 Naramura, M., Hu, R. J. & Gu, H. Mice with a fluorescent marker for interleukin 2 gene activation. *Immunity* **9**, 209-216 (1998).
159 Liu, C. P., Lin, W. J., Huang, M., Kappler, J. W. & Marrack, P. Development and function of T cells in T cell antigen receptor/CD3 zeta knockout mice reconstituted with Fc epsilon RI gamma. *Proc Natl Acad Sci U S A* **94**, 616-621 (1997).
160 Kirberg, J. *et al.* Thymic selection of CD8+ single positive cells with a class II major histocompatibility complex-restricted receptor. *J Exp Med* **180**, 25-34 (1994).
161 Erman, B. *et al.* Coreceptor signal strength regulates positive selection but does not determine CD4/CD8 lineage choice in a physiologic in vivo model. *J Immunol* **177**, 6613-6625 (2006).
162 Schrum, A. G. *et al.* High-sensitivity detection and quantitative analysis of native protein-protein interactions and multiprotein complexes by flow cytometry. *Sci STKE* **2007**, pl2, doi:10.1126/stke.3892007pl2 (2007).
163 Davis, K. A., Abrams, B., Iyer, S. B., Hoffman, R. A. & Bishop, J. E. Determination of CD4 antigen density on cells: role of antibody valency, avidity, clones, and conjugation. *Cytometry* **33**, 197-205 (1998).
164 Boyman, O., Kovar, M., Rubinstein, M. P., Surh, C. D. & Sprent, J. Selective stimulation of T cell subsets with antibody-cytokine immune complexes. *Science* **311**, 1924-1927, doi:10.1126/science.1122927 (2006).
165 Shimizu, J., Yamazaki, S., Takahashi, T., Ishida, Y. & Sakaguchi, S. Stimulation of CD25(+)CD4(+) regulatory T cells through GITR breaks immunological self-tolerance. *Nat Immunol* **3**, 135-142, doi:10.1038/ni759 (2002).
166 Sakaguchi, S., Wing, K., Onishi, Y., Prieto-Martin, P. & Yamaguchi, T. Regulatory T cells: how do they suppress immune responses? *Int Immunol* **21**, 1105-1111, doi:10.1093/intimm/dxp095 (2009).
167 Furtado, G. C., Curotto de Lafaille, M. A., Kutchukhidze, N. & Lafaille, J. J. Interleukin 2 signaling is required for CD4(+) regulatory T cell function. *J Exp Med* **196**, 851-857 (2002).
168 Matheu, M. P. *et al.* Imaging regulatory T cell dynamics and CTLA4-mediated suppression of T cell priming. *Nature communications* **6**, 6219, doi:10.1038/ncomms7219 (2015).

169 Hsieh, C. S., Zheng, Y., Liang, Y., Fontenot, J. D. & Rudensky, A. Y. An intersection between the self-reactive regulatory and nonregulatory T cell receptor repertoires. *Nat Immunol* **7**, 401-410, doi:10.1038/ni1318 (2006).

170 Pacholczyk, R., Ignatowicz, H., Kraj, P. & Ignatowicz, L. Origin and T cell receptor diversity of Foxp3+CD4+CD25+ T cells. *Immunity* **25**, 249-259, doi:10.1016/j.immuni.2006.05.016 (2006).

171 McKeithan, T. W. Kinetic proofreading in T-cell receptor signal transduction. *Proc Natl Acad Sci U S A* **92**, 5042-5046 (1995).

8 Abbreviations

Ab	Antibody
Ag	Antigen
AIRE	Human autoimmune regulator protein
Akt	Also known as PKB, Protein kinase B
APC	Allophycocyanin
APC	Antigen-presenting cell
AP-1	Activator protein 1
B6	C57BL/6
β2m	Beta two microglobulin
BCL	B cell lymphoma
Bim	BCL2L11 protein
Blimp-1	Domain zinc finger protein 1, also know as PRDM1
BSA	Bovine serum albumin
Ca^{2+}	Calcium
cAMP	Cyclic adenosine monophosphate
CBA	Cytometric bead array
CBFβ	Core-binding factor subunit beta
CCR	Chemokine receptor
CD	Cluster of differentiation
CD25	IL-2 receptor alpha chain
CD122	IL-2 receptor beta chain
CD132	Common gamma chain
CFSE	Carboxyfluorescein diacetatsuccinimidyl ester
CML	Carboxylate modified latex
CNS	Conserved non-coding regions
Cre	Cyclization recombination
C-rel	Protoncogene
Csk	C-terminal Scr kinase
cTEC	Cortical thymic epithelial cell
CTLA-4	Cytotoxic T-lymphocyte antigen 4

CXCR5	C-X-C chemokine receptor type 5
DC	Dendritic cell
DMEM	Dulbecco's modified eagle medium
DNA	Desoxyribonucleinacid
DP	Double positive
EC50	Half maximal effect concentration
EDTA	Ethylenediaminetetraacetic acid
ERK	Extracellular signal-regulated kinase
FACS	Fluorescent activated cell scanning/sorting
FCS	Fetal calf serum
FITC	Fluorescein isothiocyanat
FIK	Foxp3-interacting KRAB domain containing protein
Foxp3	Forkhead box protein 3
Foxo-1	Forkhead box protein O1
GITR	Glucocorticoid-induced TNFR-related protein
GFP	Green fluorescent protein
GVHD	Graft versus host disease
HATs	Histone acetyltransferases
HCS	Hematopoietic stem cell
HDACcs	Histone deacetyltransferases
HRPO	Horseradish peroxidase
IFNγ	Interferon gamma
Ig	Immuneglobulin
IL	Interleukine
i.p.	Intraperitoneal
IPEX	Immunodysregulation polyendocrinopathy enteropathy X-linked syndrome
IP-FCM	Immunoprecipitation and quantitative flow cytometry
IRF-4	Interferon regulatory factor 4
ITAM	Immunoreceptor tyrosine activator motif
i.v.	Intravenous
JAK	Janus activated kinase
kDa	Kilodalton
K_D	Dissociation constant
KLRG1	Killer cell lectin-like receptor subfamily G member 1

KO	Knock out
KRAB	Krüppel associated box
LAG-3	Lymphocyte-activation gene 3
LAP	Surface latency associated peptide of TGFβ
LAT	Linker of activated T cells
Lck	Lymphocyte-specific protein tyrosine kinase
LFA-1	Lymphocyte-function-associated antigen 1
M	Molar
mAb	Monoclonal antibody
MAPK	Mitogen-activated protein kinases
Mcl-1	Induced myeloid leukemia cell differentiation protein
MFI	Mean fluorescent intensity
MHC	Major histocompatibility complex
MEPE	Mean equivalent soluble PE molecules
mTECs	Medullary Thymic epithelial cells
mTOR	Mammalian target of rapamycin
NFAT	Nuclear factor of activated T-cells
NFκB	Nuclear factor kappa-light-chain-enhancer of activated B cells
NK	Natural killer
NRP-1	Neuropilin 1
PAGE	Polyacrylamide gel electrophoresis
PBS	Phosphate buffered saline
PB	Pacific blue
PD-1	Programmed cell death protein 1
PE	Phycoerithrine
PE-Cy7	Phycoerythrin-cyanine dye 7
PerCp	Peridinin Chlorophyll protein
PFA	Paraformaldehyde
PI	Proliferation index
PI3K	Phosphatidylinositol 3-kinase
PKC	Protein kinase C
PLCγ	Phosphoinositide phospholipase C gamma
pMHC	Peptide-major histocomatibiliy complex
PMA	Phorbol myrisate acetate
PPARγ	Peroxisome proliferator-activated receptor gamma

PTEN	Phosphate and tensin homolog
Rag	Recombinant activating gene
ROR	RAR-related orphan receptor
RPM	Revolutions per minute
RPMI	Roswell park memorial institute 1640 medium
RT	Room temperature
RUNX	Runt-related transcription factor
SA	Streptavidin
SD	Standard deviation
SDS	Sodium dodecyl sulfate
SEM	Standard error of the mean
SLP-76	Lymphocyte cytosolic protein 2
SP	Single positive
STAT	Signal transducer and activator of transcription
Tbet	T-box transcription factor
TCR	T cell receptor
TCRα	TCR alpha chain
TCRβ	TCR beta chain
Tconv	T conventional cell
TEMED	Tetramethylethylendiamin
TFH	T follicular helper cells
TFR	T follicular regulatory cells
TGF-β	Transforming growth factor beta
Tg	Transgenic
Th	T helper cells
TNFα	Tumor necrosis factor alpha
TNFR	Tumor necrosis factor receptor
Treg	T regulatory cell
TSDR	Treg-specific-de-methylated region
WT	Wild type
Zap-70	Zeta-chain-associated protein kinase 70

9 Appendix

9.1 Posters

9.1.1 WIRM 2014, Davos

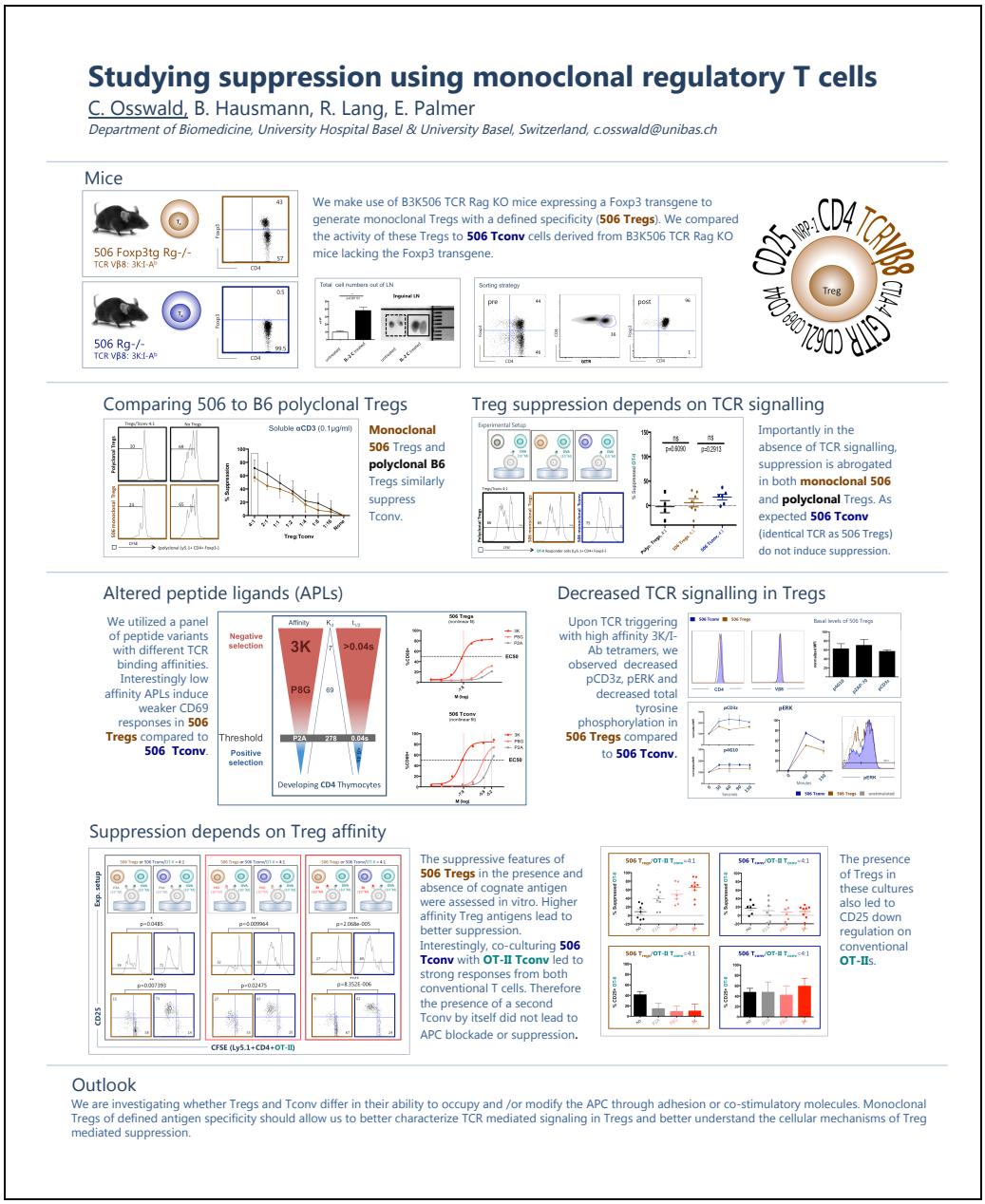

9.1.2 PhD Retreat 2013

Affinity Threshold for T cell tolerance depends on co-receptor/Lck coupling

C. Osswald, C. King, O. Stepanek, V. Galati, B. Hausmann, D. Naeher and E. Palmer
Department of Biomedicine and Nephrology, University Hospital Basel

Background

1. T cell selection

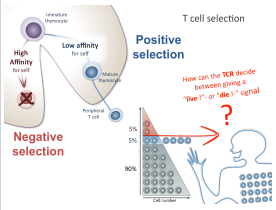

Thymic negative selection results in the depletion of autoimmune T cells expressing TCRs with high affinity for self-antigens. It is therefore considered a key mechanism in the induction of tolerance.

2. What is affinity?

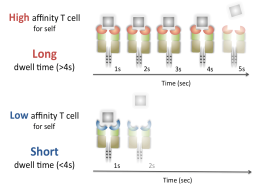

A ligand dissociation constant (K_D) of 6uM and a half-life of ≈ 2 seconds define the affinity threshold for a class I MHC restricted double positive (DP) thymocyte to succumb to negative selection in the thymus.

3. Threshold for thymocytes

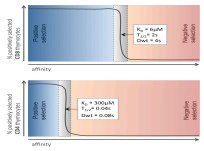

For class II restricted TCRs this threshold is much lower (K_D≈300 uM, $t_{1/2}$≈0.04 seconds) and leads to negative selection in response to much lower affinity self antigen.

Why does the threshold for CD4 and CD8 Thymocytes vary?

Methods

4. Signaling machinery

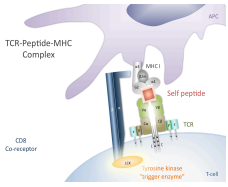

Peptide-MHC driven TCR signaling initiates with co-receptor bound Lck phosphorylating ITAMs within the TCR/CD3 complex. However, every co-receptor carries Lck indicating that only some collisions between a TCR and a co-receptor are capable of triggering TCR signaling. Therefore not all co-receptor TCR collisions are productive.

5. LCK measurement

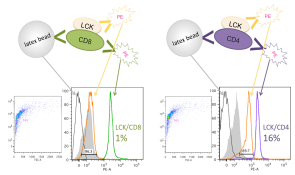

Using a method where multiprotein complexes are analyzed via immunoprecipitation and quantitative flow cytometry (IP-FCM), we determined the percentage of CD4 and CD8 co-receptors carrying an LCK molecule in various thymocyte and peripheral T cell populations.

Results

6. In vivo model

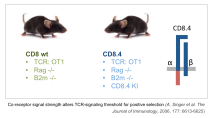

OT-1 TCR transgenic mice were bred to a CD8.4 co-receptor chimera knock-in strain where thymocytes express a co-receptor consisting of the extracellular CD8α chain and the intracellular CD4 tail carrying Lck. 9.8% of CD8.4 molecules are loaded with Lck in DP thymocytes from these mice.

7. The threshold

Organ	Co-receptor	Threshold for activation (K_D)	Threshold Affinity ($1/K_D$)	% LCK coupled to co-receptor
Thymus	CD8	6μM	167'000 L/mol	1%
Thymus	CD8.4	≈40μM	25'000 L/mol	10%
Thymus	CD4	≈300μM	3300 L/mol	16%

The threshold affinity for negative selection inversely correlates with the LCK /co-receptor coupling.

8. CD8.4 lowers the threshold

(fetal thymic organ cultures)

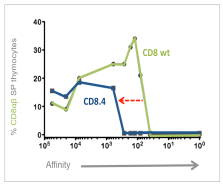

Conclusion **–The affinity threshold for CD4 and CD8 co-receptors depends on the probability that a peptide-MHC-TCR complex will collide with a co-receptor carrying Lck. Here we show that as the co-receptor/Lck coupling ratio increases, the affinity threshold for negative selection is lowered.**

9.3 Publication

9.3.1 Coreceptor Scanning by the T Cell Receptor Provides a Mechanism for T Cell Tolerance.

Ondrej Stepanek, Arvind S. Prabhakar, Celine Osswald, Carolyn G. King, Anna Bulek, Dieter Naeher, Marina Beaufils-Hugot, Michael L. Abanto, Virginie Galati, Barbara Hausmann, Rosemarie Lang, David K. Cole, Eric S. Huseby, Andrew K. Sewell, Arup K. Chakraborty, and Ed Palmer

Cell, 2014

Cell

Coreceptor Scanning by the T Cell Receptor Provides a Mechanism for T Cell Tolerance

Ondrej Stepanek,[1,*] Arvind S. Prabhakar,[2] Celine Osswald,[1] Carolyn G. King,[1] Anna Bulek,[3] Dieter Naeher,[1] Marina Beaufils-Hugot,[1] Michael L. Abanto,[1] Virginie Galati,[1] Barbara Hausmann,[1] Rosemarie Lang,[1] David K. Cole,[3] Eric S. Huseby,[4] Andrew K. Sewell,[3] Arup K. Chakraborty,[2,5,6,7] and Ed Palmer[1,7,*]

[1]Departments of Biomedicine and Nephrology, University Hospital Basel and University of Basel, 4031 Basel, Switzerland
[2]Department of Chemical Engineering, Massachusetts Institute of Technology, Cambridge, MA 02139, USA
[3]Institute of Infection and Immunity, Cardiff University School of Medicine, Cardiff CF14 4XN, UK
[4]Department of Pathology, University of Massachusetts Medical School, Worcester, MA 01655, USA
[5]Institute for Medical Engineering and Science, Departments of Physics, Chemistry, and Biological Engineering, Massachusetts Institute of Technology, Cambridge, MA 02139, USA
[6]Ragon Institute of MGH, MIT, and Harvard, 400 Technology Square, Cambridge, MA 02139, USA
[7]Co-senior author
*Correspondence: ondrej.stepanek@unibas.ch (O.S.), ed.palmer@unibas.ch (E.P.)
http://dx.doi.org/10.1016/j.cell.2014.08.042

SUMMARY

In the thymus, high-affinity, self-reactive thymocytes are eliminated from the pool of developing T cells, generating central tolerance. Here, we investigate how developing T cells measure self-antigen affinity. We show that very few CD4 or CD8 coreceptor molecules are coupled with the signal-initiating kinase, Lck. To initiate signaling, an antigen-engaged T cell receptor (TCR) scans multiple coreceptor molecules to find one that is coupled to Lck; this is the first and rate-limiting step in a kinetic proofreading chain of events that eventually leads to TCR triggering and negative selection. MHCII-restricted TCRs require a shorter antigen dwell time (0.2 s) to initiate negative selection compared to MHCI-restricted TCRs (0.9 s) because more CD4 coreceptors are Lck-loaded compared to CD8. We generated a model (Lck come&stay/signal duration) that accurately predicts the observed differences in antigen dwell-time thresholds used by MHCI- and MHCII-restricted thymocytes to initiate negative selection and generate self-tolerance.

INTRODUCTION

T cells regulate adaptive immune responses to pathogens and tumors but can also drive autoimmune diseases. The T cell antigen receptor (TCR) on conventional αβT cells recognizes peptide fragments bound to class I or class II major histocompatibility complexes (pMHCI or pMHCII). Each developing T cell expresses a unique TCR and generation of a self-MHC restricted and self-tolerant T cell repertoire results from a multistep selection process in the thymus. Thymocytes expressing a TCR weakly reactive to the host's self-antigens receive a maturation signal to generate the functional T cell repertoire in the periphery (positive selection). In contrast, thymocytes with strongly self-reactive TCRs receive a death signal (negative selection). A failure to prevent strongly self-reactive T cells from entering the peripheral T cell pool is one of the main causes of autoimmune diseases (Yin et al., 2013). How thymocytes discriminate between positive- and negative-selecting antigens in the thymus is incompletely understood. Another open question is how a thymocyte balances the high sensitivity required to recognize just a few molecules of strong antigens (Ebert et al., 2008; Peterson et al., 1999) with the selectivity needed to discriminate between positive- and negative-selecting antigens even at relatively high densities (Daniels et al., 2006; Naeher et al., 2007).

Engagement of a TCR by its cognate ligand leads to phosphorylation of TCR-associated ITAM-containing TCRζ and CD3 chains by a Src family kinase, Lck (Straus and Weiss, 1992). Antigen discrimination might already occur at this step, because positive selecting antigens poorly induce phosphorylation of TCRζ chain (Kersh et al., 1998). Doubly phosphorylated ITAMs recruit ZAP70, a kinase that is subsequently activated by a second round of Lck-mediated phosphorylation (Straus and Weiss, 1993). ZAP70 relays the signal downstream by phosphorylating LAT and SLP76 (Smith-Garvin et al., 2009).

The CD4 and CD8 coreceptors bind to MHCII and MHCI, respectively. It has been suggested that the principal role of coreceptors is to enhance TCR signaling by delivering Lck to an engaged TCR (Artyomov et al., 2010; Veillette et al., 1988). CD8 additionally stabilizes TCR-pMHC interaction (Stone et al., 2009). Although signaling can be induced by very strong agonists or anti-TCR antibodies in the absence of coreceptors (van der Merwe and Dushek, 2011), CD4 or CD8 are required for signaling induced by most ligands (Kerry et al., 2003; Vidal et al., 1999). Moreover, coreceptors are vitally important for selecting T cells that recognize pMHCI and pMHCII antigens (Van Laethem et al., 2013). Along these lines, increasing Lck coupling

to CD8 enhances the efficiency of positive selection of MHCI-restricted thymocytes (Erman et al., 2006).

The strength of a self-antigen-TCR interaction dictates whether a developing thymocyte undergoes negative selection (Daniels et al., 2006; Hogquist et al., 1994; Williams et al., 1999). The main parameters describing the interaction between a TCR and its ligand are association rate (k_{on}), dissociation rate (k_{off}), and equilibrium dissociation constant (K_D). Whereas k_{off} determines the median dwell time of the antigen-TCR interaction ($\tau_{1/2} = \ln 2/k_{off}$), k_{on} (that is concentration-dependent) determines the rate of TCR-pMHC complex formation. K_D (= k_{off}/k_{on}) indicates the concentration-dependent occupancy of the TCR under equilibrium conditions. Although there are conflicting data whether k_{on}, k_{off}, K_D, or aggregate dwell time better describes the biological response induced by particular antigens, k_{off} predicts the magnitude of TCR responsiveness in most studies (Bridgeman et al., 2012; Govern et al., 2010; Huang et al., 2010; Kersh et al., 1998; Tian et al., 2007). Moreover, mathematical modeling and experiments with TCR-induced IFNγ production showed that biological potency correlated with an antigen's K_D, but that maximal response was determined by its k_{off} (Dushek et al., 2011).

T cells expressing a monoclonal TCR together with a set of altered peptide ligands (APL) are commonly used to address the issue of antigen discrimination by TCRs. OT-I is a murine TCR recognizing MHCI (H2-K^b) loaded with OVA peptide (SIINFEKL) or OVA-derived APLs. We previously showed that transgenic OT-I thymocytes discriminate between positive- and negative-selecting APLs in a manner that was largely dependent on antigen affinity and less dependent on a ligand concentration (Daniels et al., 2006). Two other MHCI-restricted TCRs could similarly discriminate between negative- and positive-selecting ligands. Threshold antigens were estimated to have on-cell K_D ~6 μM and $\tau_{1/2}$ ~1 s (Naeher et al., 2007; Palmer and Naeher, 2009). Moreover, negative, but not positive, selectors provoked a sufficiently strong response in mature CD8 OT-I T cells to induce autoimmunity in an experimental model of type I diabetes (King et al., 2012). These results indicate that T lineage cells sense an intrinsic binding parameter of their antigens. One plausible explanation includes the ability of a TCR to measure the duration of TCR-pMHC interactions (antigen dwell time), as suggested by a kinetic proofreading model of TCR triggering (McKeithan, 1995). However, the mechanism used by the TCR to sense antigen dwell time is largely unknown.

In this study, we show that an antigen-engaged TCR scans multiple coreceptors to find one that is coupled to Lck; this is the first and rate-limiting step in signal initiation. Based on experimental data and mathematical modeling, we propose a mechanism of TCR signaling (Lck come&stay/signal duration), where the kinetics of Lck delivery by coreceptors underlies a kinetic proofreading process that establishes a dwell-time threshold for negative selection.

RESULTS

Dwell-Time Threshold for Negative Selection by pMHCI versus pMHCII Ligands

To identify positive- and negative-selecting ligands for MHCII-restricted TCRs, we analyzed the development of I-A^b- restricted, peptide-specific B3K506 and B3K508 TCR transgenic Rag1$^{-/-}$ thymocytes exposed to a variety of APLs with known affinities (Huseby et al., 2005, 2006). Using the frequency of CD4 single positive (SP) cells as an indicator of negative selection in B3K508 fetal thymic organ cultures (FTOCs), we identified ligands behaving as negative selectors (3K, P5R, and P2A), one partial negative selector (threshold selector) (P-1A), and two ligands unable to negatively select (P3A, P-1K) (Figures 1A and 1B). Interestingly, negative- and positive-selecting ligands also affected the development of the CD8 SP compartment. Previous work showed that developing MHCII-restricted thymocytes undergoing negative selection generate a population of CD8αα innate-like T cells, while the same cells undergoing positive selection paradoxically select a minor population of CD8αβ SP cells (Yamagata et al., 2004). Similarly, in B3K508 FTOCs, only negative-selecting ligands generated a population of CD8αα SP cells, while CD8αβ SP thymocytes were present in FTOCs exposed to threshold and positive-selecting ligands (Figure S1A available online). Nevertheless, negative selection can be followed by the disappearance of the CD4 SP population. We also identified negative and threshold selectors using FTOCs from B3K506 Rag1$^{-/-}$ mice (Figure 1C). Threshold selectors for B3K508 and B3K506 thymocytes exhibited similar K_D values (263 μM and 319 μM, respectively) (Huseby et al., 2006), indicating that MHCII-restricted TCRs use a fixed affinity threshold (K_D ~300 μM) for negative selection.

To compare the affinities of threshold antigens mediating MHCI- and MHCII-restricted negative selection, we determined the affinities of several antigens for MHC-I restricted OT-I TCR using surface plasmon resonance (SPR) (Figures 1D and S1B–S1D). The threshold selector for OT-I thymocytes (K^b-T4) had a K_D value of 444 μM (Figure 1D) (Daniels et al., 2006). Taken together, results from our FTOC and SPR experiments argue that MHCI- and MHCII-restricted TCRs use a similar ligand affinity threshold to initiate negative selection. However, SPR affinity measurements neglect the roles of CD4 and CD8 coreceptors that bind to pMHCII and pMHCI antigens, respectively. Importantly, CD8, but not CD4, stabilizes the TCR-pMHC complex and prolongs a ligand's dwell time on the cell surface (Huppa et al., 2010; Naeher et al., 2007; Stone et al., 2009).

To directly determine the length of TCR-pMHC interactions in the presence of coreceptors, we measured the dwell times of Qdot-labeled-pMHC monomers on their respective peripheral T cells or double positive (DP) thymocytes by direct observation using single molecule microscopy (Movies S1 and S2). The observed dwell times could be fitted to a one-phase exponential decay curve (Figure 1E). For OT-I, an MHCI-restricted TCR, the $\tau_{1/2}$ of the various APLs on mature T cells range from 1 s to 16 s and the $\tau_{1/2}$ correlates well with antigenic potency (Daniels et al., 2006). The $\tau_{1/2}$ of the threshold selector, K^b-T4, is 1.3 s. Interestingly, the $\tau_{1/2}$s of strong negative selectors for the B3K506 (3K) and B3K508 (P1-A) MHCII-restricted TCRs are 1.3 s and 1.4 s, respectively.

We could not directly measure the dwell-time distribution of pMHCII threshold ligands, due to the speed of image acquisition. To estimate the $\tau_{1/2}$ for an MHCII-restricted threshold selector, we made some additional measurements.

We determined the $\tau_{1/2}$s of several ligands binding to their respective DP thymocytes (Figures 1E, panels 2 and 8, and

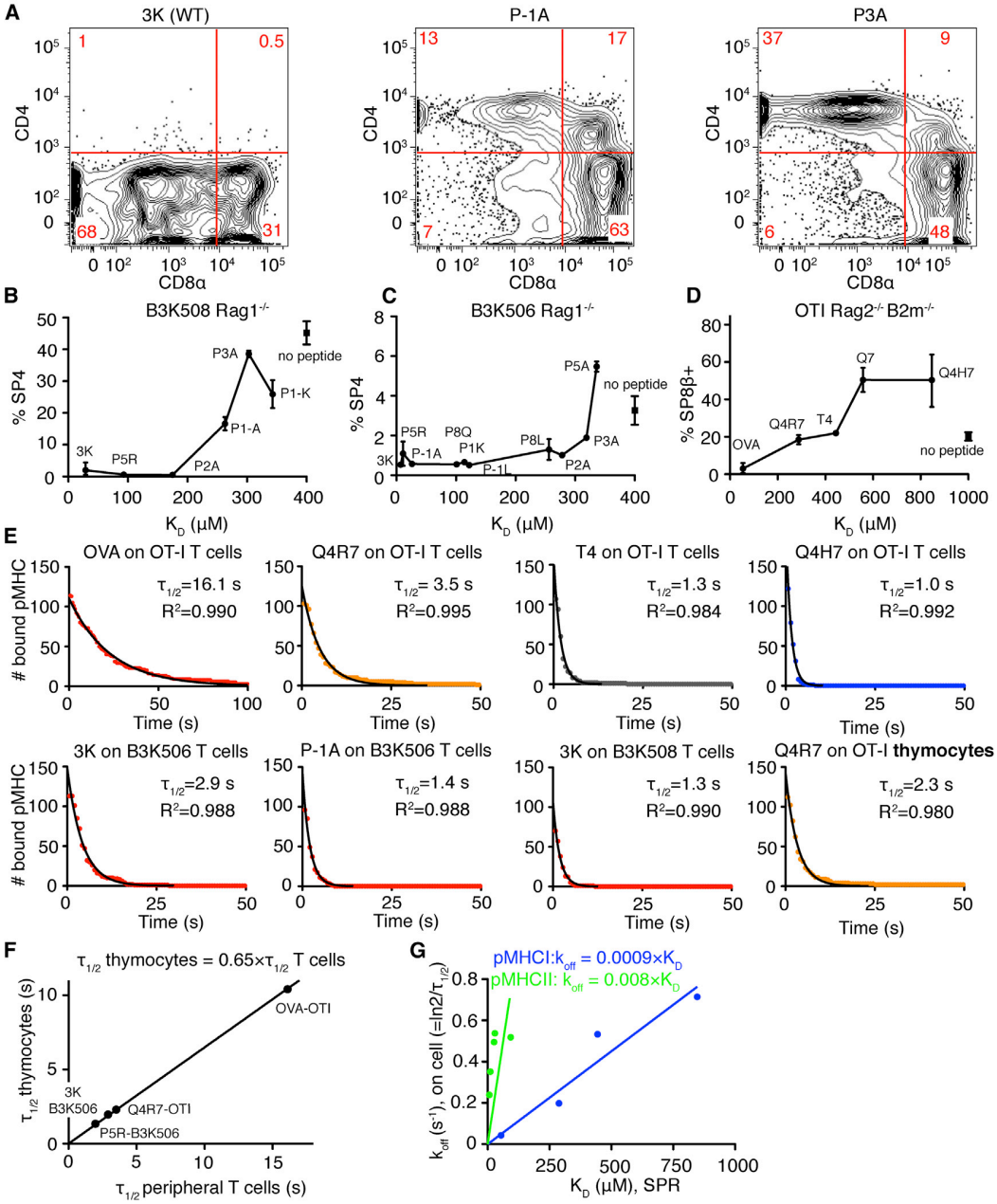

Figure 1. Thresholds for Negative Selection by pMHCII and pMHCI Ligands Show Similar SPR Affinities but Different On-Cell Dwell Times

(A–D) Fetal thymi from B3K508 Rag1$^{-/-}$ (A and B), B3K506 Rag1$^{-/-}$ (C), and OTI Rag2$^{-/-}$ β2 m$^{-/-}$ mice (D) were cultured with different APLs (20 μM) for 7 days and stained for CD4 and CD8. (A) Effects of 3K, P1-A, and P3A on the B3K508 Rag1$^{-/-}$ thymocyte development. Each panel is a representative plot from two thymi. (B–D) Percentage of CD4 or CD8β single positive cells versus K_D of APLs. Mean ± range, n = 2–5. Square symbol shows percentage of single positive cells without peptide (mean ± SEM, n = 5–11).

(E) Distribution of dwell times of pMHCI and pMHCII ligands on TCR transgenic CD4 or CD8 peripheral T cells, or preselection DP thymocytes. Data were fitted using one phase exponential decay curve.

(F) $\tau_{1/2}$ on preselection thymocytes versus $\tau_{1/2}$ on peripheral cells were plotted and fitted using linear regression with a fixed [0;0] point.

(G) k_{off}, calculated from on-cell $\tau_{1/2}$ on peripheral T cells versus K_D determined by SPR was plotted for pMHCI and pMHCII ligands and fitted with a linear regression with fixed [0;0] point.

See also Figure S1 and Table S1.

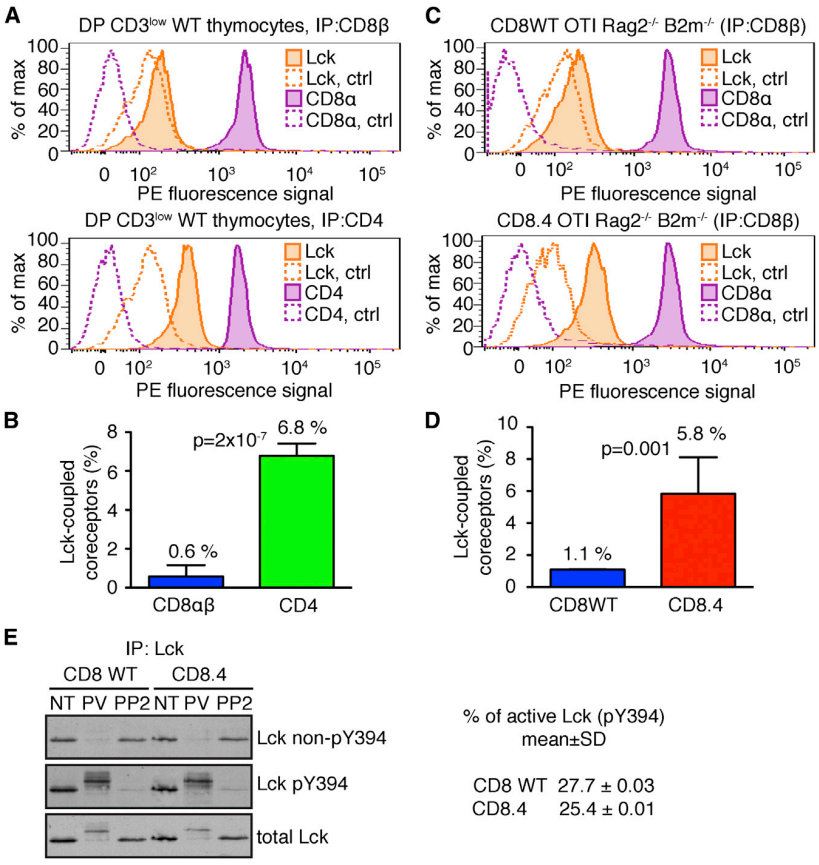

Figure 2. Quantitative Determination of Lck Coupling to CD4, CD8, and CD8.4 Coreceptors

Cell lysates were incubated with beads coated with antibodies to CD4, CD8β, or isotype controls. Beads were probed with PE-conjugated antibodies to Lck, CD8α, or CD4 and analyzed by flow cytometry.

(A–D) Sorted DP CD3low thymocytes from WT mice were analyzed (A and B). Thymocytes from CD8WT and CD8.4 OTI Rag2$^{-/-}$β2 m$^{-/-}$ mice were analyzed (C and D). Representative histograms (A and C) and aggregate data (B and D) (mean ± SD, n = 3–5) are shown. The p values were calculated using Student's t test (two-tailed, unequal variance). See also Figure S2.

(E) Lck was immunoprecipitated from lysates from nontreated (NT), pervanadate (PV), or 20 μM PP2-treated CD8WT and CD8.4 OTI Rag2$^{-/-}$ β2 m$^{-/-}$ thymocytes. Phosphorylation of Lck was analyzed by western blotting using simultaneous staining with Abs specific for phosphorylated or nonphosphorylated Y394. The membrane was reprobed with Ab to total Lck. Percentage of phosphorylated Lck molecules in resting CD8WT or CD8.4 DP thymocytes was calculated. CD8WT: n = 4; CD8.4: n = 5.

1F). The $\tau_{1/2}$s on DP thymocytes and peripheral T cells are in good agreement but the $\tau_{1/2}$s of a ligand binding to a thymocyte is approximately one-third shorter (Figure 1F). As peripheral T cells have substantially more TCR, the calculated $\tau_{1/2}$s on these cells may be slightly extended due to occasional rebinding to a second TCR. In any event, the threshold $\tau_{1/2}$s for negative selection of MHCI restricted thymocytes is ~0.9 s (Table S1).

We also observed that the on-cell k_{off} and SPR K_D are highly correlated, indicating that differences in K_D could be largely explained by differences in k_{off} (Figure 1G). Therefore, the extrapolated $\tau_{1/2}$ on thymocytes for pMHCII threshold antigens (K_D ~300 μM) is ~0.2 s (Table S1).

Thus, MHCI-restricted thymocytes use a longer dwell-time threshold for negative selection than MHCII-restricted thymocytes (0.9 versus 0.2 s). This raises the question, why MHCII-restricted thymocytes initiate negative selection with a shorter dwell time.

Extent of Coreceptor-Lck Coupling Determines the Threshold for Negative Selection

CD4 binds Lck better than CD8 (Wiest et al., 1993), which could explain the shorter dwell-time threshold for MHCII- versus MHCI-restricted thymocytes. We measured the CD4-Lck and CD8-Lck coupling ratios in polyclonal preselection DP thymocytes (B6) using immunoprecipitation followed by quantitative flow cytometric analysis (FC-IP). While only 0.6% of CD8αβ coreceptors bound Lck, 6.8% of CD4 molecules were Lck coupled (Figures 2A, 2B, and S2A). The CD4-Lck coupling in B3K508 and B3K506 preselection DP thymocytes was similar to that seen in polyclonal DPs from B6 mice (Figure S2B).

To further study the impact of coreceptor-Lck coupling on negative selection, we used homozygous CD8.4 knock-in mice (Erman et al., 2006), which are unable to express endogenous CD8α, and express instead only the chimeric CD8.4α chain, which consists of the extracellular part of CD8α and a cytoplasmic CD4 tail, which binds Lck. In OT-I DP thymocytes expressing CD8WT or CD8.4, coreceptor-Lck coupling is 1.1% and 5.8%, respectively (Figures 2C and 2D). It was important to know the percentage of coreceptors coupled with catalytically active Lck. For this reason, we used pair of antibodies recognizing active (pY394) and nonactive (non-pY394) Lck, respectively (Nika et al., 2010). This analysis indicated that the percentage of active Lck in the preselection DP thymocytes is 25%–28% (Figure 2E). Because the majority of Lck molecules are coreceptor-coupled (Van Laethem et al., 2007), the fraction of CD4 and CD8 coreceptors loaded with catalytically active Lck in DP thymocytes is 1.8% and 0.16%, respectively. Thus, the majority of coreceptors in DP thymocytes cannot initiate a TCR signal.

Expression of the CD8.4 coreceptor had no impact on the developmental arrest at the DP stage or surface TCR levels in the OT-I DP thymocytes (Figure S2C). Moreover, CD8.4 does not significantly affect antigen binding because K^b-Q4R7 binds to CD8WT and CD8.4 OT-I DP thymocytes with a similar $\tau_{1/2}$

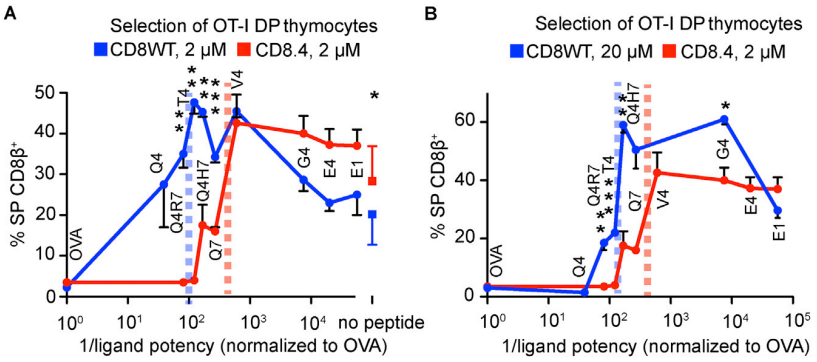

Figure 3. Enhanced Lck Coupling Lowers the Threshold for Negative Selection

Fetal thymi from CD8WT and CD8.4 OT-I Rag2$^{-/-}$β2 m$^{-/-}$ mice were exposed to OVA-derived APLs at the indicated concentrations Percentage of CD8β+ single positive cells versus 1/potency of the ligands (Daniels et al., 2006) is shown (mean ± SEM, n = 2–7). The squares show percentage of single positive cells generated with no peptide (mean ± SD, n = 11–12). The threshold for negative selection is marked by dashed vertical lines. Student's t test (two-tailed, unequal variance): *p < 0.05, **p < 0.01, *** < 0.001.
See also Table S1.

(Figures 1E and S2D). Despite these similarities, the threshold for negative selection was strikingly reduced in CD8.4 thymocytes, converting threshold and partial negative selectors (T4, Q4R7) into pure negative selectors and some positive selectors (Q4H7, Q7) into threshold selectors (Figure 3A). The effect of increasing CD8-Lck coupling cannot be mimicked by increasing the antigen concentration in CD8WT OT-I FTOCs (Figure 3B). Ten-fold higher concentrations (20 μM) of the APLs in CD8WT OT-I FTOCs do not generate the same degree of negative selection as 2 μM peptides used in CD8.4 OT-I FTOCs. Therefore, the increased Lck coupling to the CD8.4 coreceptor leads to a shorter dwell-time threshold for negative selection that is largely concentration insensitive. The impact of Lck-coupling on the development of thymocytes is summarized in Table S1.

Increased CD8-Lck Coupling Enhances Proximal Signaling and Cellular Responses

We further focused on the role of Lck coupling in the initiation of TCR signaling by analyzing the response of CD8WT and CD8.4 OT-I DP thymocytes to stimulation with various K^b-peptide tetramers (strong negative selector, K^b-OVA; just above threshold selector, K^b-Q4R7; positive selector, K^b-Q4H7). In CD8WT OT-I DP thymocytes, ligand-induced phosphorylation was modest for TCRζ and ZAP70 but downstream signaling proteins LAT, SLP76, VAV, and Erk1 exhibited more extensive phosphorylation upon stimulation (Figures 4A–4G and S3A–S3C). The data indicate an amplification step between ZAP70 activation and LAT phosphorylation. Importantly, CD8.4 thymocytes exhibited enhanced phosphorylation of TCRζ, ZAP70, LAT, SLP76, VAV, and Erk1 following TCR stimulation (Figures 4A–4G and S3A–S3C). The CD8.4 coreceptor increased overall TCR proximal signaling by 1.4, 3.7, and 5.8 following stimulation with K^b-OVA, K^b-Q4R7, and K^b-Q4H7, respectively (Figure S3D). Enhanced coreceptor-Lck coupling augments the proximal TCR signaling especially for lower affinity ligands.

Tetramer-stimulated CD8.4 thymocytes exhibited substantially increased calcium influx compared to CD8WT thymocytes (Figure 4H). In fact, CD8.4 thymocytes stimulated with below threshold K^b-Q4H7 tetramers exhibited a comparable level of calcium signaling as CD8WT thymocytes stimulated with high-affinity K^b-OVA tetramers, indicating a substantial shift in the signaling threshold induced by the chimeric coreceptor (compare purple and red curves in Figure 4H, upper left panel).

To address the role of CD8-Lck coupling in response to a broader range of APLs, CD8WT and CD8.4 OTI DP thymocytes were stimulated with antigen presenting cells (APCs) loaded with various peptide variants. We monitored induced expression of CD69, an activation marker that is upregulated both upon positive and negative selection (Figure S4). While CD8WT and CD8.4 thymocytes responded similarly to the strongest peptide, OVA, CD8.4 thymocytes were more sensitive to weaker antigens (Figures 5A–5C). The impact of enhanced Lck delivery mediated by the CD8.4 coreceptor inversely correlated with potency of the ligand (Figure 5D), consistent with the effects of CD8.4 on proximal signaling (Figure S3D).

Frequency of Coreceptor-Lck Coupling Determines the Kinetics of Lck Delivery to the TCR

The overall experimental data implied that Lck delivery is a limiting factor in signal initiation and potentially sets the dwell-time threshold to initiate negative selection. To better understand why coreceptor-Lck coupling is so important in this process, we generated a mathematical model that calculates the probability of recruiting an Lck-coupled coreceptor to an established TCR:pMHC pair as a function of time, when the CD4, CD8, or CD8.4 coreceptor is involved. The model is based on a Markov chain that describes the behavior of coreceptor and TCR-pMHC in the plasma membrane. A TCR-pMHC can form a pair (close proximity) or a complex (binding) with an empty or Lck-coupled coreceptor (Figure 6A). Because Lck-coupled coreceptors are relatively rare, a TCR-pMHC usually has to scan a large number of empty coreceptors before encountering an Lck-coupled one. The average time to recruit an Lck-loaded coreceptor to the TCR-pMHC is determined by the rate of coreceptor:TCR-pMHC complex formation, the duration of empty coreceptor:TCR-MHC interaction, and importantly, the percentage of Lck-coupled coreceptors (see Extended Experimental Procedures). The parameters used to construct the model were based on our measurements or published data (Figures S5A–S5C; Table S2). The model shows that Lck delivery is very fast in case of TCR-pMHCII interactions (CD4), but substantially slower upon TCR-pMHCI engagement (CD8). CD8.4 shows faster Lck recruitment than CD8WT (Figure 6B). When only active (pY394) Lck delivery is considered, the delivery of the Lck is delayed but the hierarchy of the coreceptors is maintained (dashed line in Figure 6B). Importantly, the model predicts that the probability of Lck recruitment is

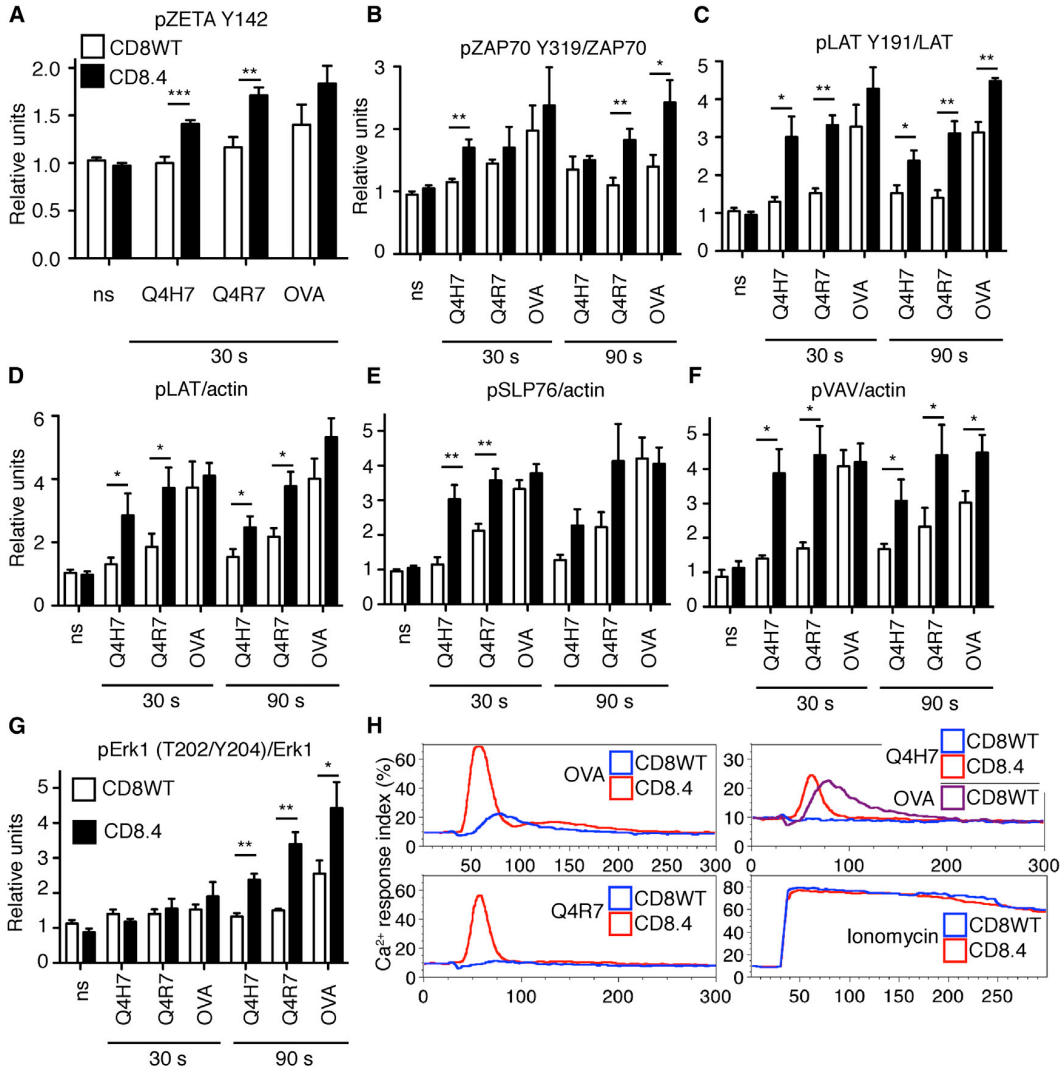

Figure 4. CD8.4 Enhances Proximal Signaling in OT-I Thymocytes

(A–G) Thymocytes from CD8WT or CD8.4 OT-I Rag2$^{-/-}$β2 m$^{-/-}$ mice were stimulated with 100 nM K^b-OVA, K^b-Q4R7, or K^b-Q4H7 tetramers or left unstimulated (ns). Results were normalized to the average of signal from unstimulated CD8WT or CD8.4 cells in each experiment. (A) Phosphorylation of TCRζ (Y142) was analyzed by flow cytometry on CD4+CD8+ population. Mean ± SEM, n = 6. (B, C, and G) Phosphorylation of LAT, ZAP70, and Erk was analyzed using phospho-specific Abs. Reprobing the membranes for total ZAP70, LAT, and Erk served as respective loading controls. (D–F) Phosphorylation of LAT, SLP76, and VAV in whole cell lysates was determined using anti-pTyr Ab and anti-actin Ab. as a loading control by western blotting. Mean ± SEM, n = 4. Statistical significance was tested using Student's t test (one-tailed, unequal variance): *p ≤ 0.05, **p < 0.01. See also Figure S3.

(H) CD8WT or CD8.4 OT-I DP thymocytes were loaded with Indo-1 and stimulated with 200 nM K^b-OVA, -Q4R7, or -Q4H7 tetramers or 1.5 μM ionomycine. Calcium mobilization was analyzed by flow cytometry. Ca^{2+} response index is shown (see Extended Experimental Procedures). A representative experiment from a total of three is shown.

highly dependent on the extent of coreceptor-Lck coupling (Figure 6C), underscoring its importance for setting the dwell-time threshold. Other parameters (number of CD8 molecules, diffusion coefficient of membrane anchored receptors, coreceptor-TCR interaction kinetics, and lattice spacing) play less important roles (Figure 6D).

To provide experimental evidence that a single TCR-pMHC complex serially engages large number of coreceptors, we carried out the following experiment. Qdot-labeled K^b-OVA or K^b-Q4R7 monomers were bound to OT-I DP thymocytes allowing the coengagement of the TCR and CD8 with the labeled antigen. After reaching equilibrium binding, the cells were diluted in presence or absence of an anti-CD8β mAb. Blocking the unengaged CD8 molecules accelerated the off-rate of pMHC dissociation (Figures S5E and S5F). This is consistent with the idea that during the life time of a pMHC-engaged TCR, there is significant

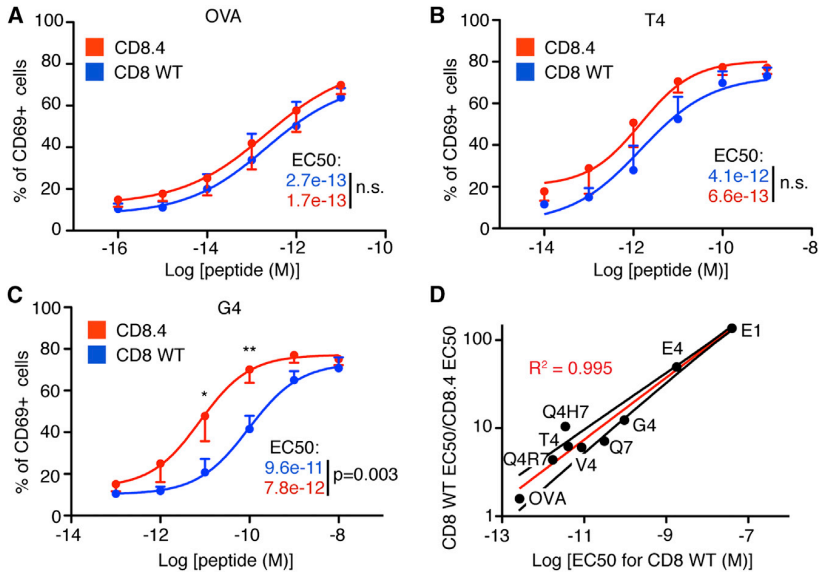

Figure 5. CD8.4 Preferentially Enhances Response to Weak Ligands

(A–C) Thymocytes from CD8WT and CD8.4 OT-I Rag2$^{-/-}$β2 m$^{-/-}$ mice were incubated with APCs loaded with varying concentrations of different peptides. After 24 hr, the percentage of CD69+ thymocytes was measured by flow cytometry. Response to OVA (A), T4 (B), and G4 (C) is shown. Mean ± SEM, n = 4. Statistical significance was tested using Student's t test (one-tailed, unequal variance): *p < 0.05, **p < 0.01.

(D) CD69 response of CD8WT and CD8.4 OT-I DP thymocytes to different antigens was examined and EC_{50} values were calculated. Ratio of EC_{50} CD8WT/EC_{50} CD8.4 was plotted versus EC_{50} CD8WT. Results show that CD8.4 thymocytes are preferentially more sensitive to weaker ligands, compared to CD8WT thymocytes. Red line shows the log-log line fit and the black lines represent 95% confidence intervals.

See also Figure S4.

turnover of CD8 molecules, which only transiently bind to the pMHC. This coreceptor exchange would allow the engaged TCR to eventually find an Lck coupled coreceptor if the pMHC engagement is sufficiently long.

Lck Delivery Is the Initial Step during Kinetic Proofreading

The Markov chain model explained the importance of the proportion of Lck-coupled coreceptors and coreceptor exchange in determining the speed of the signal initiation. We subsequently generated four different models that extended the Markov chain model by combining Lck delivery together with its kinase activity. Comparison of the models' predictions with the experimental data should indicate the actual molecular mechanism that initiates TCR triggering and sets the antigen dwell-time threshold for negative selection.

For all four models, we assumed that the recruited Lck has to minimally phosphorylate four tyrosines (two ITAM tyrosines and Y315 and Y319 in ZAP70) to obtain ZAP70 activation and signal propagation. The actual number of tyrosine phosphorylations is likely higher because phosphatase activity can counteract the Lck activity and Lck might phosphorylate tyrosines in separate ITAMs. Thus, we set five phosphorylations by an Lck molecule as a criterion for TCR triggering to make it more than the minimal number.

Our preferred model, "Lck come&stay/signal duration," combines the Lck recruitment calculated from the Markov chain model with the classical TCR kinetic proofreading model (McKeithan, 1995). In this model, we assumed the following scenario. A newly formed TCR-pMHC pair eventually interacts with a coreceptor coupled to active Lck (pLck). The coreceptor-pLck remains attached to the TCR-pMHC complex due to the interactions of Lck's SH2 domains with partially phosphorylated TCR (and/or ZAP70) and stabilization via the pMHC:coreceptor interaction (Jiang et al., 2011; Straus et al., 1996). Lck triggers TCR signaling by phosphorylating ITAM tyrosines and a subsequently recruited ZAP70. Active ZAP70 continuously generates downstream signals by phosphorylating LAT, SPL76, and other signaling molecules. When antigen disengages from the TCR, coreceptor-Lck is released as well, leading to a massive decrease in kinase activity. This shifts the kinase/phosphatase equilibrium toward phosphatase activity and sets the TCR and ZAP-70 back into a less phosphorylated state. "'Lck come&stay/signal duration" model assumes that the TCR-pMHC interaction has to last long enough to recruit and activate ZAP70. Once the ZAP70 is activated, further antigen occupancy of the already triggered TCR determines the strength of the TCR signal. The overall TCR signal induced in a thymocyte is determined by the number of triggered TCRs and the amount of time they remain occupied by pMHC subsequent to TCR triggering (Extended Experimental Procedures; Table S3). The model calculates total TCR signal as a function of number of antigen molecules available in the thymocyte/APC interface and their $\tau_{1/2}$ (Figures 7A and S6A). In contrast to a pure TCR occupancy model (Figure 7B) that predicts little discrimination between ligands with different dwell times, the "Lck come&stay/signal duration" model displays the kinetic proofreading principle. Our data clearly show that antigens with $\tau_{1/2}$ ~10 s (K^b-OVA) can negatively select at low concentrations; antigens with $\tau_{1/2}$ ~1–2 s (Kb-T4 and Kb-Q4R7) negatively select at higher concentrations; and antigens with $\tau_{1/2} \leq 0.6$ s (Kb-Q4H7) are incapable of negative selection even when present at very high concentrations in the synapse (i.e., 250 cognate pMHC, which is ~5%–10% of the pMHCI pool at the interface). The model assumes that as few as two to four triggered and occupied TCRs can initiate negative selection, which has previous experimental support (Ebert et al., 2008; Peterson et al., 1999).

The model predicts a shift of the dwell-time threshold for negative selection in CD8.4 cells (Figures 7A and 7C), which in good agreement with the experimental data (Figures 1 and 3; Table S1). Moreover, this model predicts that the shorter the $\tau_{1/2}$ of a TCR ligand is, the more pronounced is the difference between

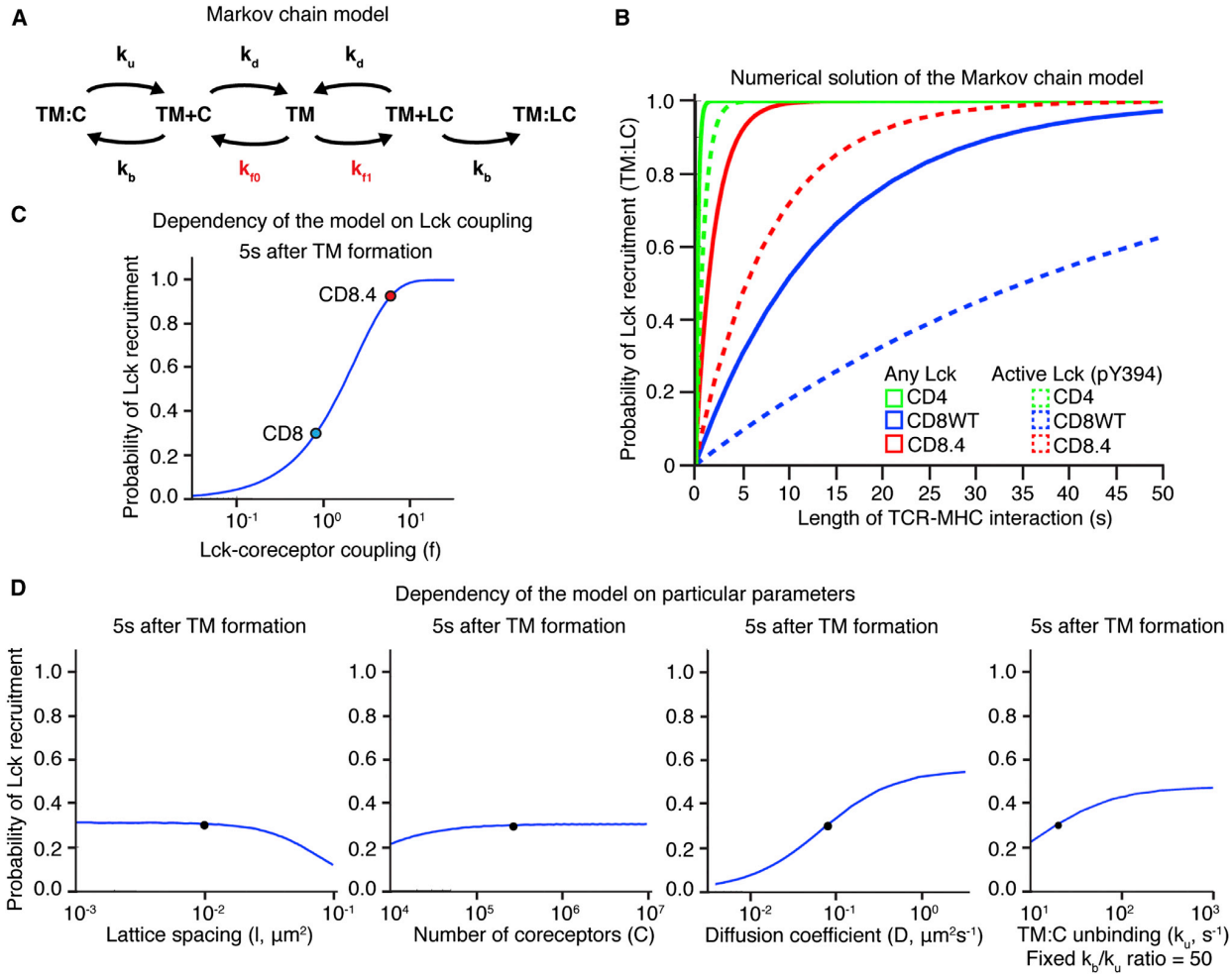

Figure 6. Markov Chain Model for Lck Delivery to the TCR-pMHC Pair

(A) Scheme of the Markov chain model describing kinetics of protein interactions in the plasma membrane. TM is a TCR-pMHC pair, C is an empty coreceptor, and LC is an Lck coupled coreceptor. TM+C and TM+LC represent coreceptor and TCR-pMHC pairs (in close proximity), TM:C and TM:LC represent coreceptor-TCR-pMHC complexes (binding). The complex of Lck-coupled coreceptor and TCR-pMHC (TM:LC) is an absorbing end state. K_D, k_b, k_u, k_{f0}, k_{f1} represent kinetic rates (Table S2). The rates that depend on the extent of coreceptor-Lck coupling are shown in red.

(B) Numerical solution of Markov chain model. The probability of TM:LC complex formation as a function of time was calculated for CD4 (pMHCII), CD8WT (pMHCI), and CD8.4 (pMHCI). Both the probability of recruitment of any Lck-coupled coreceptor (solid line) or a coreceptor coupled to active Lck (pY394) is shown (dashed line).

(C) Probability of TM:LC pair formation as a function of CD8-Lck coupling for MHCI ligand. The values for CD8WT (blue dot) and CD8.4 (red dot) are marked. Other parameters remained fixed.

(D) The probabilities of TM:LC formation as a function of lattice spacing, coreceptors number, CD8 and TCR diffusion coefficient and CD8:MHC unbinding k_u (when k_u/k_b ratio was fixed) for MHCI ligand and CD8 coreceptor. The original parameters are marked (black dot).

See also Extended Experimental Procedures, Figure S5, and Table S2.

CD8.4 and CD8WT signaling (Figure 7D). This is essentially in agreement with the experimental data (Figures 4 and 5). The "Lck come&stay/signal duration" model predicts the dwell-time thresholds used by polyclonal pMHCI- and pMHCII-restricted thymocytes (~1 s for MHCI and ~0.2 for MHCII antigens) (Figure 7E). The model also reveals that antigens with $\tau_{1/2}$ at or just above the dwell-time threshold must be presented at a relatively high copy number to induce negative selection (e.g., 50 molecules of pMHCI antigens with $\tau_{1/2}$ ~2 s). If such peri-threshold ligands are presented at low numbers in the thymus, but at higher levels in peripheral tissues, the generation of central self-tolerance may be defective.

The serial triggering (productive hit) model assumes that once a TCR is triggered, continued pMHC binding does not further increase the TCR signal (Dushek et al., 2011; Valitutti, 2012). We also constructed a combined "Lck come&stay/serial triggering" model that assumes that the total TCR signal is determined by the number of triggered TCRs. However, the "Lck

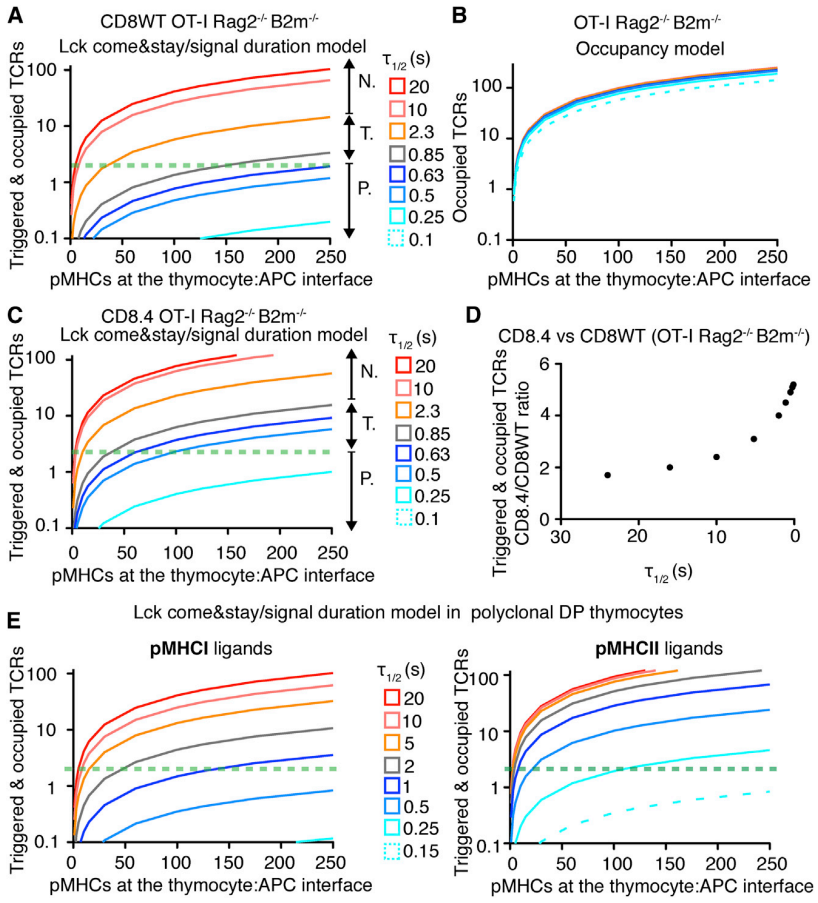

Figure 7. Model of Lck Recruitment Combined with Kinetic Proofreading Predicts Experimental Data

Graphs show TCR signal intensity as a function of number of cognate ligands at the thymocyte/APC interface for different ligands (k_{on} = 0.1 μm^2 s^{-1}, $\tau_{1/2}$ variable). Horizontal green dashed line shows the likely threshold when two TCRs are triggered and still occupied.

(A) "Lck come&stay/signal duration" model for CD8WT OT-I Rag2$^{-/-}$ β2 m$^{-/-}$ thymocytes. N, negative selectors; T, threshold ligands (partial negative selectors); P, positive selectors.

(B) Pure TCR occupancy model for OT-I Rag2$^{-/-}$ β2 m$^{-/-}$ thymocytes.

(C) "Lck come&stay/signal duration" model for CD8.4 OT-I Rag2$^{-/-}$ β2 m$^{-/-}$ thymocytes.

(D) Difference between CD8.4- and CD8WT-mediated TCR signaling (CD8.4/CD8WT ratio) in OT-I Rag2$^{-/-}$ β2 m$^{-/-}$ thymocytes versus $\tau_{1/2}$ of a TCR ligand, predicted by the "Lck come&stay/signal duration" model. Advantage of increased Lck coupling (CD8.4) is increasingly apparent at low $\tau_{1/2}$.

(E) Comparison of TCR responses induced by pMHCI and pMHCII ligands in polyclonal preselection DP thymocytes predicted by the Lck come&stay/signal duration model.

See also Extended Experimental Procedures, Figure S6, and Table S3.

come&stay/serial triggering" model does not predict the experimentally observed hierarchy of the ligands, arguing that serial triggering cannot explain the negative selection threshold (Figure S6B).

We also generated two additional models requiring multiple visits of Lck to trigger the TCR (Figure S6C). In these models, we assumed that Lck is not stabilized at the TCR-pMHC and phosphorylates only one tyrosine upon a single interaction between a coreceptor-Lck molecule and the TCR-pMHC. Thus, coreceptor-Lck has to be repeatedly recruited to the TCR-pMHC to trigger the TCR. These models predict very strong discrimination between ligands based on their $\tau_{1/2}$, but displays very low sensitivity to ligands, just over the dwell-time threshold; this is not compatible with our experimental data. Given the poor predictive power of these last three models, the "Lck come&stay/signal duration" model clearly provides the best explanation of our experimental data.

DISCUSSION

Here, we describe a mechanism that allows thymocytes to discriminate antigens of differing median dwell times and establish an antigen dwell-time threshold for negative selection. During the time that a TCR binds a pMHC antigen, the TCR-pMHC complex scans up to several hundreds of coreceptors to find one, which carries catalytically active Lck; subsequently this recruited kinase phosphorylates ITAMs and activating tyrosines on ZAP70. Finding an Lck-loaded coreceptor represents the first and rate-limiting step in signal initiation, because only a minority of coreceptor molecules are actually coupled to active Lck. MHCI-restricted TCRs require antigens with a $\tau_{1/2}$ >0.9 s to induce negative selection, while the negative selection threshold for MHCII-restricted TCRs is $\tau_{1/2}$ >0.2 s. A higher frequency of CD4 molecules are coupled to catalytically active Lck compared to CD8 (2% versus 0.2%); for this reason, MHCII-restricted receptors have a shorter dwell-time threshold.

Modeling studies revealed that the frequency of Lck-coupled coreceptors is a critical parameter in establishing the dwell-time threshold for negative selection. The decrease in the dwell-time threshold for negative selection seen in CD8.4 OT-I mice is a consequence of CD8.4's increased coupling to Lck, resulting in a faster arrival of a coreceptor-pLck complex to an antigen-occupied TCR. CD8.4 mediates an enhanced activation of proximal TCR signaling pathways and, similar to CD4, allows negative selection by antigens with short dwell times. It is not clear whether having a shorter dwell-time threshold for the deletion of MHCII-restricted thymocytes provides an intrinsic advantage or whether this is simply a consequence of the differences in Lck coupling exhibited by CD4 and CD8. Nevertheless, these differences illustrate the mechanism, where the dwell-time threshold is set by the median time required for the antigen engaged TCR to find an Lck-loaded coreceptor.

To directly estimate the dwell-time threshold, we attached monomeric pMHCs to Qdots and observed the binding of monomeric pMHC to antigen-specific T cells by single molecule microscopy. The $\tau_{1/2}$ for the OT-I threshold ligand (K^b-T4) was estimated to 0.9 s on thymocytes and 1.3 s on peripheral T cells, which corresponds well to the dwell-time threshold for H2-K^d-restricted T1 TCR (0.8–1.5 s), estimated by an on-cell photoaffinity labeling technique (Naeher et al., 2007; Palmer and Naeher, 2009). How well does $\tau_{1/2}$ measured with soluble ligand (3D) correspond to antigen binding at the thymocyte/APC interface? Although the $\tau_{1/2}$ was originally viewed as a biophysical parameter describing ligand-receptor interactions independent of their spatial context (Dustin et al., 2001), several studies report that k_{off} is accelerated in a planar configuration (2D) of T cell-APC contacts (Huang et al., 2010; Huppa et al., 2010). However, other studies showed that pMHC $\tau_{1/2}$ measured using 2D or 3D techniques are similar, consistent with the original view (O'Donoghue et al., 2013; Robert et al., 2012). Recently, pMHCI/TCR dwell times were analyzed under tensile force in a 2D setting (Liu et al., 2014). Interestingly, TCR interactions with potent ligands are stabilized when a moderate force (5–10 pN) is applied due to the formation of catch bonds. The authors suggest that a tensile force generated at the thymocyte/APC interface contribute to TCR specificity. However, their results show that both positive and negative selectors can form catch bonds, so the formation of a catch bond per se does not explain the negative selection threshold. Nevertheless, the catch bond phenomenon can be easily integrated with our "Lck come&stay/signal duration model" that provides the signaling mechanism underlying TCR triggering and discrimination between negative and positive ligands based on their dwell times.

Interestingly, $\tau_{1/2}$ measurements in their system corresponded well with our on-cell measurements. We determined that the $\tau_{1/2}$ of OT-I:K^b-OVA is ~10 s, while Zhu and coworkers (Liu et al. 2014) measured the $\tau_{1/2}$ for the same antigen as 0.8 s under 10 pN; the ~10-fold difference is expected because of the absence of CD8 engagement in their system (Naeher et al., 2007). However, it remains unclear why an application of a moderate tensile force is required in the 2D setting, but not in our on-cell 3D assay, to measure biologically relevant dwell times of TCR-antigen interactions.

We generated four mathematical models describing TCR signaling response in thymocytes, using a combination of our measurements and published data as input parameters. The k_{on} (Huppa et al., 2010) was sufficiently high that it hardly limited the formation of TCR-pMHC bonds in the thymocyte:APC contact area. Ligand concentration and $\tau_{1/2}$ had the largest impact on the quantity of TCR signals generated. To find the most relevant model, we compared the outcome of the models with our experimental data on TCR signaling in CD8WT and CD8.4 OT-I DP thymocytes. The "Lck come&stay/Signal duration" model, which best explains our experimental data, is based on the principle of kinetic proofreading (McKeithan, 1995), where Lck recruitment is the most proximal limiting step. The model assumes that transient CD4-MHCII or CD8-MHCI interactions allow the TCR-pMHC pair to scan multiple coreceptors via coreceptor exchange before finding a coreceptor carrying catalytically active Lck. Nika et al. (2010) demonstrated that 38% of Lck molecules are catalytically active in human CD4+ T cells and moreover Lck does not undergo further activation upon TCR stimulation. Murine preselection DP thymocytes have a slightly lower percentage of active Lck (25%–28%), implying that only ~0.16% of CD8 and ~1.8% of CD4 molecules are capable of initiating a TCR signal. Following the recruitment of catalytically active Lck, the kinase phosphorylates ITAM tyrosines in the CD3 complex and subsequently phosphorylates a recruited ZAP70 kinase. Coreceptor-Lck binding to TCR-pMHC is potentially stabilized via an interaction of Lck's SH2 domain with a phosphotyrosine in an ITAM or ZAP70 (Jiang et al., 2011; Straus et al., 1996). If the TCR-pMHC interaction lasts long enough to enable Lck-mediated phosphorylation of ZAP70, then ZAP70 generates downstream signals by phosphorylating LAT and SLP76 for the duration of the TCR-pMHC interaction. The longer the duration of antigen binding, the more downstream mediators are generated. Signaling is terminated when the pMHC and subsequently, the coreceptor-Lck disengage from TCR. A thymocyte surveys a single APC for several minutes (Ebert et al., 2008; Melichar et al., 2013); over this time span, the decision to initiate negative selection must be made.

We propose that positive- and negative-selecting ligands induce quantitatively different responses at the level of TCR activation (i.e., number of TCRs kept triggered) that is transformed to qualitatively different events in downstream signaling pathways. Our model is in line with the observation that positive- and negative-selecting ligands induce distinct patterns of Erk activation (Daniels et al., 2006). Previous mathematical modeling suggested that only negative-selecting ligands are able to induce extensive LAT phosphorylation and trigger a feed-forward loop resulting in the activation of SOS and activation of pErk at the plasma membrane (Prasad et al., 2009).

The TCR has the unusual property of being able to recognize antigens with a high degree of sensitivity and an ability to discriminate between closely related structural variants. As few as two to four strong ligands within the thymocyte-APC contact area are able to trigger a strong TCR response and induce negative selection (Ebert et al., 2008; Peterson et al., 1999). This sensitivity has been explained by the ability of one pMHC ligand to trigger several TCRs and amplify the signal. However, evidence for serial triggering is so far indirect (Valitutti, 2012). Moreover, a strict serial triggering model does not explain our experimental data, because it predicts that threshold ligands (K^b-T4) will engage and trigger similar number of TCRs as long dwelling ligands (K^b-OVA). Furthermore, serial triggering could not be detected during direct observation of TCR-pMHC interactions in situ (O'Donoghue et al., 2013). Along this line, we propose that very few strong ligands are able to keep a few TCRs continually engaged and triggered; this amplifies the TCR signal by continuous generation of intracellular signaling intermediates. Higher numbers of less potent, but above threshold ligands are required to induce the same effect, while below threshold ligands are essentially unable to trigger negative selection.

The two models, which employ the Lck multiple visit assumption, are relatively insensitive. These models predict that only antigens with very long dwell times or present at high concentrations can initiate a TCR signal. For this reason, we do not favor these models. We also observed that the serial triggering

strategy poorly discriminates between antigens with differing median dwell times. On the other hand, the signal duration mechanism allows the amount of TCR generated signal to reflect the actual dwell time. Thus, the "Lck come and stay/signal duration" mechanism allows for antigen recognition, which is both highly sensitive and discriminatory.

"Lck come and stay/signal duration" model uncovers molecular events constituting for a TCR kinetic proofreading mechanism. Highly specific recognition of negative-selecting ligands by a developing thymocyte is an analogy to a kinetic proofreading that provides specificity in DNA, protein, and amino acid-tRNA synthesis (Hopfield, 1974). These diverse molecular processes have a built in time delay between a substrate binding the enzyme and its conversion into a product molecule. A substrate molecule (nucleotide, amino acid, etc.) that binds the respective enzyme for a longer time is more likely to be the biologically "correct" molecular species. The TCR and coreceptor operate under a similar principle; a long-lasting antigen binding event is more likely to be converted into a (negative selection) signaling event.

Our experimental results and mathematical models explain how the TCR actually measures antigen affinity to initiate a negative selection signal. The kinetics of Lck delivery by coreceptors plays a crucial role in setting the antigen dwell-time threshold for negative selection. The kinetic proofreading mechanism suggested by our model implies that collisions between hundreds of coreceptor molecules and a small number of antigen bound TCRs allow the developing thymocyte to sense the antigen's median dwell time and initiate a critical cell fate decision (negative selection).

EXPERIMENTAL PROCEDURES

Mice

All adult mice were 6–12 weeks old and had a C57Bl/6 genetic background. OT-I Rag2$^{-/-}$, OT-I Rag2$^{-/-}$ β2 m$^{-/-}$, B3K508 Rag1$^{-/-}$, and B3K506 Rag1$^{-/-}$ mice were described previously (Daniels et al., 2006; Huseby et al., 2005).

CD8.4 OT-I Rag2$^{-/-}$ β2 m $^{-/-}$ strain was generated by crossing CD8.4 knock-in mouse (Erman et al., 2006) with OT-I Rag2$^{-/-}$ β2 m$^{-/-}$. Mice were bred in our colony (University Hospital Basel) in accordance with Cantonal and Federal laws of Switzerland. Animal protocols were approved by the Cantonal Veterinary Office of Baselstadt, Switzerland.

Surface Plasmon Resonance

SPR equilibrium binding analysis was performed using a BIAcore T100™ equipped with a CM5 sensor chip. SPR equilibrium analyses were carried out to determine the K_D values for OT-I:H2-K^b-APL interactions at 25°C. Approximately 300 response units of pMHC or TCR were coupled to the CM5 sensor chip surface. Analyte was injected at concentrations ranging from ten times above and ten times below the estimated K_D of the interaction.

Flow Cytometry

Live cells were stained with relevant Abs on ice. For intracellular staining, cells were fixed in 4% paraformaldehyde (15 min, room temperature [RT]), permeabilized by 90% methanol (30 min, on ice) and stained with indicated antibodies at RT. Determination of surface molecule number was performed using saturating concentrations of PE-conjugated Abs and calibration beads. Calcium mobilization was measured using Indo-1 probe and Calcium response index was calculated (see Extended Experimental Procedures).

Flow cytometry immunoprecipitation (FC-IP) was done as described previously (Schrum et al., 2007). Briefly, beads coated with anti-CD4 or anti-CD8α Abs were used to pull down CD4 or CD8. Subsequently, PE-conjugated anti-CD4, anti-CD8β, or anti-Lck Abs were used to quantify Lck/CD8 and Lck/CD4 coupling ratios.

Flow cytometry was carried out with a FACSCantoII (BD Bioscience). Cell sorting was performed using an Influx sorter (BD Bioscience). Data were analyzed using FlowJo software (TreeStar).

Determination of Lck Phosphorylation Status

Lck was immunoprecipitated from untreated, or PV- or PP2-treated thymocytes and analyzed by western blotting. Signals from Abs recognizing phosphorylated and nonphosphorylated Lck (Y394) were normalized to total Lck and the percentage of phosphorylated molecules was calculated as previously described (Stepanek et al., 2011).

On-Cell Dwell-Time Measurement

Qdot-pMHC monomers were added to T cells or thymocytes attached to poly-lysine-coated borosilicate glass. Binding of Qdot-pMHC monomers was observed using single molecule microscopy for 2.5 min and the duration of pMHC binding events was measured. The number of persisting binding events was plotted versus time and fitted with to a one phase exponential decay function. See also Extended Experimental Procedures.

FTOC

FTOCs were performed as described (Hogquist et al., 1994). Briefly, thymic lobes were excised from mice at a gestational age of day 15.5 and incubated in the presence of particular peptide and, in case of OT-I Rag2$^{-/-}$ β2 m$^{-/-}$ thymi, exogenous β2 m (5 μg/ml). After 7 days of culture, thymocytes were analyzed by flow cytometry.

Western Blotting

Samples for western blotting were heated in Laemmli sample buffer (2 min, 95°C), sonicated and analyzed by SDS-PAGE and western blotting, using AlexaFluor790- or AlexaFluor680-conjugated goat anti-mouse or anti-rabbit secondary antibodies (Jackson ImmunoResearch). Specific Ab signals were quantified using an Odyssey Infrared Imaging System (LI-COR Biosciences) and analyzed by ImageJ software (NIH).

Mathematical Model

The models are composites of Markov chain model describing behavior of surface molecules, equations describing TCR occupancy, and equations describing initial catalytic steps in TCR triggering. The models predict either a number of triggered TCRs within a time interval or a number of occupied and triggered TCRs in any given time point.

SUPPLEMENTAL INFORMATION

Supplemental Information includes Extended Experimental Procedures, six figures, three tables, and two movies and can be found with this article online at http://dx.doi.org/10.1016/j.cell.2014.08.042.

AUTHOR CONTRIBUTIONS

O.S., C.O., C.G.K., M.L.A., M.B., D.K.C., A.K.S., D.N., and E.P. designed experiments. O.S., C.G.K., C.O., M.L.A., B.H., V.G., M.B., A.B., D.K.C., A.K.S, E.P., D.N., and R.L. performed experiments and analyzed data. O.S., A.S.P., and A.K.C. generated the mathematical models. E.S.H. provided mice and generated MHCII monomers. O.S. and E.P. wrote the manuscript. All authors commented on the manuscript draft. A.K.C., E.S.H., A.K.S., and E.P. funded and supervised the study.

ACKNOWLEDGMENTS

We thank U. Schneider for animal husbandry and E. Traunecker and T. Krebs for cell sorting. This study was funded by grants to E.P. (310030-149972/1 and Synergia [SNF], Sybilla [EU FP7], and TerraIncognita [ERC]), A.K.C. (1-P01-AI091580 [NIH]), E.S.H. (R01-DK095077 [NIH]), and A.K.S. (BB/H001085/1 [BBSRC]). D.K.C. is a Wellcome Trust Career Development Fellow. A.K.S. is a Wellcome Trust Senior Investigator.

Received: April 17, 2014
Revised: July 14, 2014
Accepted: August 29, 2014
Published: October 2, 2014

REFERENCES

Artyomov, M.N., Lis, M., Devadas, S., Davis, M.M., and Chakraborty, A.K. (2010). CD4 and CD8 binding to MHC molecules primarily acts to enhance Lck delivery. Proc. Natl. Acad. Sci. USA *107*, 16916–16921.

Bridgeman, J.S., Sewell, A.K., Miles, J.J., Price, D.A., and Cole, D.K. (2012). Structural and biophysical determinants of αβ T-cell antigen recognition. Immunology *135*, 9–18.

Daniels, M.A., Teixeiro, E., Gill, J., Hausmann, B., Roubaty, D., Holmberg, K., Werlen, G., Holländer, G.A., Gascoigne, N.R., and Palmer, E. (2006). Thymic selection threshold defined by compartmentalization of Ras/MAPK signalling. Nature *444*, 724–729.

Dushek, O., Aleksic, M., Wheeler, R.J., Zhang, H., Cordoba, S.P., Peng, Y.C., Chen, J.L., Cerundolo, V., Dong, T., Coombs, D., and van der Merwe, P.A. (2011). Antigen potency and maximal efficacy reveal a mechanism of efficient T cell activation. Sci. Signal. *4*, ra39.

Dustin, M.L., Bromley, S.K., Davis, M.M., and Zhu, C. (2001). Identification of self through two-dimensional chemistry and synapses. Annu. Rev. Cell Dev. Biol. *17*, 133–157.

Ebert, P.J., Ehrlich, L.I., and Davis, M.M. (2008). Low ligand requirement for deletion and lack of synapses in positive selection enforce the gauntlet of thymic T cell maturation. Immunity *29*, 734–745.

Erman, B., Alag, A.S., Dahle, O., van Laethem, F., Sarafova, S.D., Guinter, T.I., Sharrow, S.O., Grinberg, A., Love, P.E., and Singer, A. (2006). Coreceptor signal strength regulates positive selection but does not determine CD4/CD8 lineage choice in a physiologic in vivo model. J. Immunol. *177*, 6613–6625.

Govern, C.C., Paczosa, M.K., Chakraborty, A.K., and Huseby, E.S. (2010). Fast on-rates allow short dwell time ligands to activate T cells. Proc. Natl. Acad. Sci. USA *107*, 8724–8729.

Hogquist, K.A., Jameson, S.C., Heath, W.R., Howard, J.L., Bevan, M.J., and Carbone, F.R. (1994). T cell receptor antagonist peptides induce positive selection. Cell *76*, 17–27.

Hopfield, J.J. (1974). Kinetic proofreading: a new mechanism for reducing errors in biosynthetic processes requiring high specificity. Proc. Natl. Acad. Sci. USA *71*, 4135–4139.

Huang, J., Zarnitsyna, V.I., Liu, B., Edwards, L.J., Jiang, N., Evavold, B.D., and Zhu, C. (2010). The kinetics of two-dimensional TCR and pMHC interactions determine T-cell responsiveness. Nature *464*, 932–936.

Huppa, J.B., Axmann, M., Mörtelmaier, M.A., Lillemeier, B.F., Newell, E.W., Brameshuber, M., Klein, L.O., Schütz, G.J., and Davis, M.M. (2010). TCR-peptide-MHC interactions in situ show accelerated kinetics and increased affinity. Nature *463*, 963–967.

Huseby, E.S., White, J., Crawford, F., Vass, T., Becker, D., Pinilla, C., Marrack, P., and Kappler, J.W. (2005). How the T cell repertoire becomes peptide and MHC specific. Cell *122*, 247–260.

Huseby, E.S., Crawford, F., White, J., Marrack, P., and Kappler, J.W. (2006). Interface-disrupting amino acids establish specificity between T cell receptors and complexes of major histocompatibility complex and peptide. Nat. Immunol. *7*, 1191–1199.

Jiang, N., Huang, J., Edwards, L.J., Liu, B., Zhang, Y., Beal, C.D., Evavold, B.D., and Zhu, C. (2011). Two-stage cooperative T cell receptor-peptide major histocompatibility complex-CD8 trimolecular interactions amplify antigen discrimination. Immunity *34*, 13–23.

Kerry, S.E., Buslepp, J., Cramer, L.A., Maile, R., Hensley, L.L., Nielsen, A.I., Kavathas, P., Vilen, B.J., Collins, E.J., and Frelinger, J.A. (2003). Interplay between TCR affinity and necessity of coreceptor ligation: high-affinity peptide-MHC/TCR interaction overcomes lack of CD8 engagement. J. Immunol. *171*, 4493–4503.

Kersh, G.J., Kersh, E.N., Fremont, D.H., and Allen, P.M. (1998). High- and low-potency ligands with similar affinities for the TCR: the importance of kinetics in TCR signaling. Immunity *9*, 817–826.

King, C.G., Koehli, S., Hausmann, B., Schmaler, M., Zehn, D., and Palmer, E. (2012). T cell affinity regulates asymmetric division, effector cell differentiation, and tissue pathology. Immunity *37*, 709–720.

Liu, B., Chen, W., Evavold, B.D., and Zhu, C. (2014). Accumulation of dynamic catch bonds between TCR and agonist peptide-MHC triggers T cell signaling. Cell *157*, 357–368.

McKeithan, T.W. (1995). Kinetic proofreading in T-cell receptor signal transduction. Proc. Natl. Acad. Sci. USA *92*, 5042–5046.

Melichar, H.J., Ross, J.O., Herzmark, P., Hogquist, K.A., and Robey, E.A. (2013). Distinct temporal patterns of T cell receptor signaling during positive versus negative selection in situ. Sci. Signal. *6*, ra92.

Naeher, D., Daniels, M.A., Hausmann, B., Guillaume, P., Luescher, I., and Palmer, E. (2007). A constant affinity threshold for T cell tolerance. J. Exp. Med. *204*, 2553–2559.

Nika, K., Soldani, C., Salek, M., Paster, W., Gray, A., Etzensperger, R., Fugger, L., Polzella, P., Cerundolo, V., Dushek, O., et al. (2010). Constitutively active Lck kinase in T cells drives antigen receptor signal transduction. Immunity *32*, 766–777.

O'Donoghue, G.P., Pielak, R.M., Smoligovets, A.A., Lin, J.J., and Groves, J.T. (2013). Direct single molecule measurement of TCR triggering by agonist pMHC in living primary T cells. eLife *2*, e00778.

Palmer, E., and Naeher, D. (2009). Affinity threshold for thymic selection through a T-cell receptor-co-receptor zipper. Nat. Rev. Immunol. *9*, 207–213.

Peterson, D.A., DiPaolo, R.J., Kanagawa, O., and Unanue, E.R. (1999). Cutting edge: negative selection of immature thymocytes by a few peptide-MHC complexes: differential sensitivity of immature and mature T cells. J. Immunol. *162*, 3117–3120.

Prasad, A., Zikherman, J., Das, J., Roose, J.P., Weiss, A., and Chakraborty, A.K. (2009). Origin of the sharp boundary that discriminates positive and negative selection of thymocytes. Proc. Natl. Acad. Sci. USA *106*, 528–533.

Robert, P., Aleksic, M., Dushek, O., Cerundolo, V., Bongrand, P., and van der Merwe, P.A. (2012). Kinetics and mechanics of two-dimensional interactions between T cell receptors and different activating ligands. Biophys. J. *102*, 248–257.

Schrum, A.G., Gil, D., Dopfer, E.P., Wiest, D.L., Turka, L.A., Schamel, W.W., and Palmer, E. (2007). High-sensitivity detection and quantitative analysis of native protein-protein interactions and multiprotein complexes by flow cytometry. Sci. STKE *2007*, pl2.

Smith-Garvin, J.E., Koretzky, G.A., and Jordan, M.S. (2009). T cell activation. Annu. Rev. Immunol. *27*, 591–619.

Stepanek, O., Kalina, T., Draber, P., Skopcova, T., Svojgr, K., Angelisova, P., Horejsi, V., Weiss, A., and Brdicka, T. (2011). Regulation of Src family kinases involved in T cell receptor signaling by protein-tyrosine phosphatase CD148. J. Biol. Chem. *286*, 22101–22112.

Stone, J.D., Chervin, A.S., and Kranz, D.M. (2009). T-cell receptor binding affinities and kinetics: impact on T-cell activity and specificity. Immunology *126*, 165–176.

Straus, D.B., and Weiss, A. (1992). Genetic evidence for the involvement of the lck tyrosine kinase in signal transduction through the T cell antigen receptor. Cell *70*, 585–593.

Straus, D.B., and Weiss, A. (1993). The CD3 chains of the T cell antigen receptor associate with the ZAP-70 tyrosine kinase and are tyrosine phosphorylated after receptor stimulation. J. Exp. Med. *178*, 1523–1530.

Straus, D.B., Chan, A.C., Patai, B., and Weiss, A. (1996). SH2 domain function is essential for the role of the Lck tyrosine kinase in T cell receptor signal transduction. J. Biol. Chem. *271*, 9976–9981.

Tian, S., Maile, R., Collins, E.J., and Frelinger, J.A. (2007). CD8+ T cell activation is governed by TCR-peptide/MHC affinity, not dissociation rate. J. Immunol. *179*, 2952–2960.

Valitutti, S. (2012). The Serial Engagement Model 17 Years After: From TCR Triggering to Immunotherapy. Front. Immunol. *3*, 272.

van der Merwe, P.A., and Dushek, O. (2011). Mechanisms for T cell receptor triggering. Nat. Rev. Immunol. *11*, 47–55.

Van Laethem, F., Sarafova, S.D., Park, J.H., Tai, X., Pobezinsky, L., Guinter, T.I., Adoro, S., Adams, A., Sharrow, S.O., Feigenbaum, L., and Singer, A. (2007). Deletion of CD4 and CD8 coreceptors permits generation of alphabetaT cells that recognize antigens independently of the MHC. Immunity *27*, 735–750.

Van Laethem, F., Tikhonova, A.N., Pobezinsky, L.A., Tai, X., Kimura, M.Y., Le Saout, C., Guinter, T.I., Adams, A., Sharrow, S.O., Bernhardt, G., et al. (2013). Lck availability during thymic selection determines the recognition specificity of the T cell repertoire. Cell *154*, 1326–1341.

Veillette, A., Bookman, M.A., Horak, E.M., and Bolen, J.B. (1988). The CD4 and CD8 T cell surface antigens are associated with the internal membrane tyrosine-protein kinase p56lck. Cell *55*, 301–308.

Vidal, K., Daniel, C., Hill, M., Littman, D.R., and Allen, P.M. (1999). Differential requirements for CD4 in TCR-ligand interactions. J. Immunol. *163*, 4811–4818.

Wiest, D.L., Yuan, L., Jefferson, J., Benveniste, P., Tsokos, M., Klausner, R.D., Glimcher, L.H., Samelson, L.E., and Singer, A. (1993). Regulation of T cell receptor expression in immature CD4+CD8+ thymocytes by p56lck tyrosine kinase: basis for differential signaling by CD4 and CD8 in immature thymocytes expressing both coreceptor molecules. J. Exp. Med. *178*, 1701–1712.

Williams, C.B., Engle, D.L., Kersh, G.J., Michael White, J., and Allen, P.M. (1999). A kinetic threshold between negative and positive selection based on the longevity of the T cell receptor-ligand complex. J. Exp. Med. *189*, 1531–1544.

Yamagata, T., Mathis, D., and Benoist, C. (2004). Self-reactivity in thymic double-positive cells commits cells to a CD8 alpha alpha lineage with characteristics of innate immune cells. Nat. Immunol. *5*, 597–605.

Yin, L., Dai, S., Clayton, G., Gao, W., Wang, Y., Kappler, J., and Marrack, P. (2013). Recognition of self and altered self by T cells in autoimmunity and allergy. Protein Cell *4*, 8–16.

Supplemental Information

EXTENDED EXPERIMENTAL PROCEDURES

Antibodies and Peptides

Antibodies to following antigens were used: Lck (clone 3A5), VAV (rabbit polyclonal), SLP76 (rabbit polyclonal, all Santa Cruz Biotechnology); Erk1/2 (clone L34F12), ZAP70 (clone L1E5), Erk1/2 pT202/pY204 (clone D13.14.4E), ZAP70 pY319 (rabbit), Src family pY416 (rabbit), Src family non-pY416 (mouse, clone 7G9, all Cell Signaling); TCRζ pY142 (clone K25-407.69) (all BD Biosciences); LAT pY191 (rabbit polyclonal), pTyrosine (clone 4G10, both Merck Millipore); actin (rabbit polyclonal, Sigma-Aldrich); CD3ε (clone 145-2C11), CD8α (clone 53-6.7), CD8β (clone 53-5.8), CD4 (clones RM4-5 and H129.19), TCRβ (clone H57-597), TCR-Vα2 (clone B20.1), CD69 (clone H1.2F3) (all BD PharMingen). For flow cytometry, antibodies were conjugated to various fluorescent dyes by the manufacturer.

Determination of Surface Molecule Numbers

Saturating concentrations of PE–conjugated antibodies were determined (40 μg/ml for CD3ε, CD8α and 10 μg/ml for CD4). 25,000 cells were stained in 25 μl of staining buffer (PBS/2% FCS) for 40 min on ice, washed, and analyzed along with PE calibration beads (RCP-30-5A, Spherotech Inc., Lake Forest, IL, USA) by flow cytometry. A calibration curve was generated based on the fluorescence signal from calibration beads to transform the geometric mean of fluorescence intensity (after subtraction of background signal from antibody stained peripheral B cells) into mean equivalent of PE intensity (MEPE) values. The actual number of surface molecules was calculated by adjusting the MEPE values to the PE/antibody ratio (determined by absorbance at 560 nm using soluble PE as a standard). Number of antigens captured by one molecule of antibody was assumed to be 2 (Davis et al., 1998), except for TCR, where the results were further corrected for the presence of 2 CD3ε molecules per TCR/CD3 complex.

Flow Cytometric Immunoprecipitation Assay

10^6 cells were lysed in 50 μl lysis buffer (1% NP-40, 10 mM Tris pH 7.4, 140 mM NaCl, 2 mM EDTA, Protease Inhibitor Cocktail (Sigma-Aldrich)) for 30 min on ice. 75,000 CML beads (Invitrogen) coupled to anti-CD4 (clone RM4.4), anti-CD8β (clone 53-5.8), or anti-MHCI (clone Y3.8) antibodies, as described previously (Schrum et al., 2007), were added to the lysate and incubated for 3 hr at 4°C. Beads were washed 3x in lysis buffer and stained with different PE-conjugated antibodies to CD4 (clone H129.19), CD8α (clone 53-6.7), or Lck (clone 3A5) at saturating concentrations (40 min, on ice) and analyzed by flow cytometry. The geometric mean fluorescence intensities (gMFI) were taken as the measure of the antibody binding. The CD8, CD8.4 or CD4-Lck coupling ratio was calculated as Lck signal to CD8 or CD4 signal (after subtracting respective background signal measured from control anti-MHCI beads) and adjusted for the PE/antibody ratio.

Calcium Mobilization

Cells (10^7/ml in RPMI/10%FCS) were loaded with 0.5 μM Indo-1 (Invitrogen) for 30 min at 37°C. Calcium mobilization was measured as a ratio of Indo-1 fluorescence intensities elicited by emission wavelengths at 400–500 nm and 500–560 nm (excitation 355 nm). Baseline Ca^{2+} mobilization was determined for 30 s after which, cells were stimulated by addition of 2 × concentrated activators (tetramers or ionomycin in RPMI/10%FCS). Measurements were continued for 5 min. Calcium response index (Stepanek et al., 2011) was calculated as the percentage of cells with an intracelluar calcium level, higher than the 90^{th} percentile found in resting cells during a 10 s time interval prior to stimulation.

Mice

B3K506 Rag1$^{-/-}$ I-A$^{-/-}$ and B3K508 Rag1$^{-/-}$ I-A$^{-/-}$ mice were generated by breeding B3K506 Rag1$^{-/-}$ and B3K508 Rag1$^{-/-}$ with I-A$^{-/-}$ mice.

Cells

The OT-I hybridoma line expressing CD8β-YFP and TCRζ-CFP (Mallaun et al., 2008), and T2-K^b cells (a gift from T. Potter) were cultivated in RPMI/10% FBS, 100 U/ml penicillin, 100 μg/ml streptomycin, and 50 μM 2-mercapthoethanol.

Cell Stimulation

DP thymocytes (2 × 10^8 mil/ml) were preincubated in RPMI (10 min, 37°C) and stimulated by adding an equal volume of 200 nM tetramers in RPMI. At indicated time points, cells were either fixed in formaldehyde (intracellular staining) or lysed in 2x SDS PAGE sample buffer (western blotting).

CD69 Upregulation Assay

T2-Kb cells were pre-incubated with varying amounts of peptide for 2 hr before addition of thymocytes. Final concentrations were 6 × 10^5 T2Kb cells, 10^6 thymocytes, and indicated concentration of peptide in 250 μl of RPMI/10% FCS. Thymocytes were examined by flow cytometry 24 hr later, using antibodies to CD69, CD4, CD8α, and Vα2 TCR. The EC_{50} values for CD69 upregulation were calculated using nonlinear regression curve (y = a+(b-a)/(1+10^((log(EC_{50})-x) × H))). Aggregate data showing CD8WT/CD8.4 EC_{50} versus CD8WT EC_{50} dependency were fitted with log-log line regression (y = 10^(a × log(x)+b)).

Determination of Lck Phosphorylation Status

Preselection OT-I thymocytes were either treated with 20 μM PP2 (Calbiochem) or 1 mM pervanadate for 10 min or left untreated. Cells were lysed in a lysis buffer (1% dodecylmaltoside, 1 mM Pefabloc, 5 mM iodoacetamide, 1mM sodium orthovanadate, 100 mM NaCl, 50 mM NaF, 10% glycerol v/v, and 20 mM Tris, pH 7.5) and incubated for 30 min on ice. Nuclei and debris were removed by centrifugation, and the resulting lysate was subjected to immunoprecipitation with anti-Lck antibody (2 μg/ml) followed by incubation with Protein G Sepharose (GE Healthcare). Immunoprecipitates were eluted with SDS-PAGE sample buffer and subjected to immunoblotting. Src family pY416 and Src family non-pY416 antibodies were used for the detection of the phosphorylation state of Lck Y394. Signals from phospho and non-phospho specific antibodies were normalized to total Lck signal. The percentage of phosphorylated Lck in untreated cells (P) was calculated using equation:

$$P = \frac{\frac{b_2}{b_1} - 1}{\frac{b_2}{b_1} - \frac{a_2}{a_1}}$$

where *b* and *a* are signal intensities from non-phospho and phospho specific antibodies, respectively (Stepanek et al., 2011). The terms 1 and 2 represent untreated and treated conditions, respectively. Percentage of phosphorylated Lck was independently calculated using either PP2 or PV-treated cells and averaged to obtain a single value for each independent experiment.

Generation of Expression Plasmids

The OT-I TCR α and β chains, H2-K^b heavy chain and human β2 m chain were generated by PCR mutagenesis (Stratagene) and PCR cloning. Three versions of the OT-I TCR were generated. One with a leucine zipper attached to the C terminus, one with a biotinylation site on the alpha chain C terminus, and one incorporating human constant domains with an artificial inter chain disulphide to produce the soluble TCR. These molecules contained residues 1–207 and 1–247 of TCRα and β, respectively (Boulter et al., 2003; Garboczi et al., 1996). H2-K^b heavy chain (residues 1–248) (α1, α2 and α3 domains), tagged with a biotinylation sequence, and human β2 m (residues 1–100) were also cloned and used to generate pMHCI complexes. The TCR α and β chains, the H2-K^b α chain and human β2 m sequences were inserted into separate pGMT7 expression plasmids under the control of the T7 promoter (Garboczi et al., 1996).

Protein Expression, Refolding, Purification

Competent Rosetta DE3 *E.coli* cells were used to produce the TCR α and β chains, H2-K^b heavy chain and human β2 m in the form of inclusion bodies following induction with 0.5 mM IPTG as described previously (Cole et al., 2006, 2008; Garboczi et al., 1996). Biotinylated pMHCI was prepared as previously described (Wyer et al., 1999).

MHC Tetramer and Monomer-Qdot Assembly

K^b-peptide and I-A^b-peptide tetramers were generated by incubating biotinylated pMHC monomers with streptavidin (Jackson Immunoresearch) or PE-streptavidin (Invitrogen) at a 4:1 ratio on ice. Streptavidin was separately added to pMHC-monomers in two aliquots. Qdot-labeled pMHC monomers were generated by mixing biotinylated pMHC monomers with Qdot605-streptavidin conjugates (Invitrogen) at a 0.5:1 ratio for 20 min at 26°C. Free biotin binding sites were subsequently blocked with an excess of free biotin.

Surface Plasmon Resonance

SPR equilibrium binding analysis was performed using a BIAcore T100™ equipped with a CM5 sensor chip as previously reported (Cole et al., 2007; Gostick et al., 2007; Wyer et al., 1999). Experiments were conducted with H2-K^b variants immobilised on the chip surface. Two OT-I TCR constructs, one with a leucine zipper attached to the C terminus and one implementing a human constant domain with an artificial inter chain disulphide, were used in different experiments. SPR equilibrium analyses were carried out to determine the K_D values for OT-I:H2-K^b-APL interactions at 25°C in multiple experiments (representative data shown). In all experiments, approximately 300 response units of pMHC or TCR were coupled to the CM5 sensor chip surface. Analyte was injected at concentrations ranging from 10 times above and 10 times below the known K_D of the interaction (where possible) at 45 μl/min. K_D values were calculated assuming 1:1 Langmuir binding ($AB = B^*AB_{MAX}/(K_D + B)$) and data were analyzed using a global fit algorithm (BIAevaluation™ 3.1). A blank flow cell and irrelevant HLA-A*0201-ALWGPDPAAA, or HLA-B*3501-VPLRPMTY monomers were used as negative controls on flow cell 1. The SPR measurements for B3K506 and B3K508 TCRs were carried out previously at 25°C (Huseby et al., 2006).

Single Molecule Microscopy

LabTek chambers (Thermo Scientific) were precoated with poly-l-lysine at 37°C overnight. 1–2 × 10^6 lymph node T cells or thymocytes were stained with anti-CD45.2-AlexaFluor488 antibody, washed and resuspended in 200 μl of RPMI (without phenol red)/5% FCS and added to the chamber. Cells were allowed to attach to the surface for at least 30 min. A Nikon A1 microscope equipped with 100 × magnifying objective (1.49Na), ORCA2 CCD camera (Hamatsu Photonics), and Visiview software (Visitron systems) were used to acquire images using 50 ms exposure time. One frame consisted of 14 Z-steps with a track radius of 0.65 μm collected over 0.7 s.

3D movies were analyzed using Imaris software (Bitplane). The measurements of the Qdot-pMHC dwell times on the cell surface were done manually, excluding first three and last three frames of each movie. Only binding events, which began and ended during the time of the movie and lasted at least 2 frames, were analyzed. The number of persisting binding events was ploted versus time and fitted with to a one phase exponential decay function: $Y = Y_{max} \times e^{-\ln 2 \times X/\tau 1/2}$.

Statistical Analysis

Curve fitting and statistical analysis was performed using Prism version 5.0d (GraphPad Software) and Excel for Mac 2011 version 14.3.9 (Microsoft).

Markov Chain Model

To model the interactions between an engaged TCR (TCR-pMHC) and CD4 or CD8 coreceptors in the membrane, we generated a Markov chain model (Figure 6A). The interactions of CD4 and CD8 with Lck seem to be very strong, because the majority of Lck molecules in thymocytes are bound to CD4 or CD8 coreceptors (Van Laethem et al., 2007; Van Laethem et al., 2013). In contrast, the CD4 or CD8 interactions with MHCII or MHCI, respectively, are rather weak and transient (Gao and Jakobsen, 2000; Wyer et al., 1999). For our model, we assumed that the CD4- and CD8-Lck interactions are stable and there is negligible Lck turnover among the coreceptors within the time scale of interest (<30 s). In this context, DP thymocytes contain a small fraction of Lck-coupled coreceptors and a larger pool of empty coreceptors, devoid of Lck (Figure 2). We neglected the role of coreceptor-free Lck in TCR triggering for two reasons, because it comprises less than 1/3 of total Lck in thymocytes (Van Laethem et al., 2007). Moreover, a significant part of the coreceptor-free pool is not anchored in the plasma membrane and cannot easily contribute to TCR signaling. (Zimmermann et al., 2010). While a free Lck molecule within the cytoplasm might occasionally collide with a TCR, this occurs in a random orientation and presumably has a only a small chance to phosphorylate CD3 and ZAP70. In contrast, coreceptor-bound Lck is recruited to the TCR complex in a more constrained position under the plasma membrane. In this regard, it has been postulated that orientation of a coreceptor-bound Lck is constrained to optimize phosphorylation of CD3 chains (Li et al., 2013). This gives an advantage to coreceptor-bound Lck.

The model predicts that the TCR-pMHC (TM) pair typically scans multiple coreceptor molecules before it encounters one coupled with Lck.

The parameters for the Markov chain models are listed in Table S2. For the case of calculations, we considered that there is just one TCR-pMHC pair and a proportional number of coreceptors (= C/A, ca. 3500 in case of CD8) on a 1 μm × 1 μm patch of membrane. The average distance between the TCR-pMHC and a coreceptor molecule is:

$$r = \frac{1}{\sqrt{\pi \times C/A}} \quad \text{(Equation 1)}$$

The average time for a TM to form a pair (close proximity) with a coreceptor is:

$$\tau = \frac{r^2}{D} \quad \text{(Equation 2)}$$

Thus, the k_{f0} and k_{f1} finding rates for forming a pair with a coreceptor loaded with (active) Lck (TM+LC) or with a coreceptor devoid of (active) Lck (TM+C), respectively, are:

$$k_{f0} = \frac{1}{\tau_0} = \frac{(1-f)\pi CD}{A} \quad \text{(Equation 3)}$$

$$k_{f1} = \frac{1}{\tau_1} = \frac{f\pi CD}{A} \quad \text{(Equation 4)}$$

We assumed a lattice spacing of l = 0.01 μm, meaning that when a coreceptor and TCR-pMHC are in the same lattice site, they can either diffuse apart or bind with rates k_d and k_b, respectively. The diffusion coefficient was scaled to a "hopping rate" k_d, that describes the movement of molecules in the lattice grid:

$$k_d = \frac{D}{l^2} \quad \text{(Equation 5)}$$

The initial state of the Markov chain is a free TCR-pMHC (TM) and the formation of coreceptor-Lck:TCR-pMHC complex was set as an absorbing end state. A set of 5 ordinary differential equations describe the evolution of probabilities of the various states of the model with time (see also Figure 6A):

$$\frac{dP_{TM:C}}{dt} = -k_u P_{TM:C} + k_b P_{TM+C} \quad \text{(Equation 6)}$$

$$\frac{dP_{TM+C}}{dt} = k_u P_{TM:C} - (k_d + k_b) P_{TM+C} + k_{f0} P_{TM} \quad \text{(Equation 7)}$$

$$\frac{dP_{TM}}{dt} = k_d (P_{TM+C} + P_{TM+LC}) - (k_{f0} + k_{f1}) P_{TM} \quad \text{(Equation 8)}$$

$$\frac{dP_{TM+LC}}{dt} = k_{f1} P_{TM} - (k_d + k_b) P_{TM+LC} \quad \text{(Equation 9)}$$

$$\frac{dP_{TM:LC}}{dt} = k_b P_{TM+LC} \quad \text{(Equation 10)}$$

These equations were numerically solved (f = 0.014, for other parameters see Table S2 - CD8), showing that the TCR/pMHC mainly exists as a TM+C pair or eventually in the absorbing LC:TM state shortly after the initial time of TCR-pMHC binding (Figure S5D).

One of the most difficult parameters to estimate was k_u, the off-rate of coreceptor:MHC interaction. For CD8, we took the SPR data from human CD8αα interaction with HLA-2 (Wyer et al., 1999). The authors determined the dissociation rate to be $\geq$ 18 s^{-1}. Because other studies measured a higher CD8:MHCI affinity in the mouse system (indicating slower off-rate) we used k_u = 20 s^{-1} (close to the lower value) in the model. The affinity of CD4:MHCII interaction is lower than the affinity CD8-MHCI interaction, but association and dissociation rates of CD4:MHC binding and unbinding are above the detection limit of SPR (Gao and Jakobsen, 2000; van der Merwe and Davis, 2003; Xiong et al., 2001). We assumed a similar on-rate for both coreceptors (Artyomov et al., 2010), but a 10-fold higher off-rate for CD4-MHCII (200 s^{-1}). We experimentally determined the number of CD4, CD8, and TCR molecules on preselection DP thymocytes (Figures S5A and S5B) and diffusion coefficients for CD8 (0.085 μm^2 s^{-1}) and TCR (0.13 μm^2 s^{-1}) in a hybridoma cell line (Figure S5C). Others reported slightly lower diffusion coefficient for TCR (ca. 0.05–0.06 μm^2 s^{-1}) in primary T cells (Dushek et al., 2008). Based on our and previously published data, we assumed a diffusion coefficient of 0.08 μm^2 s^{-1} for both TCR and CD8. Remaining parameters were taken from the relevant literature or estimated (Table S2) (Altan-Bonnet and Germain, 2005; Artyomov et al., 2010).

Equations describing the Markov state model were solved using MATLAB (MathWorks). We also tested some results of the Markov state model with fully stochastic solutions of the Master equations (data not shown) using a numerical implementation of the Gillespie method, called Stochastic Simulation Compiler (Lis et al., 2009). The probabilities of Lck delivery to the TCR as a function of time were generated for CD4 (MHCII), CD8 (MHCI), and CD8.4 (MHCI) coreceptors using numerical solution of the Markov chain model (Figure 6B).

Approximate Analytical Solution of the Reduced Markov Chain Model

To obtain an approximate analytical solution, we simplified the Markov chain model. Because we saw that the TM+C and TM+LC pairs are very infrequent and short-lived (Figure S5D) and approximately constant during the simulation (not shown), we made a pseudo-steady state assumption and set Equations 7 and 9 to 0. The free TM state is very short-lived, because it rapidly encounters a coreceptor. Thus, we assumed that the initial state of the model is TM:C ($P_{TM:C}(0) = 1$; $P_{TM:LC}(0) = 0$) and extended the pseudo-steady state to the free state (TM) as well. The simplified model consisted of the following equations (Equations 11, 12, 13, 14, and 15):

$$\frac{dP_{TM:C}}{dt} = -k_u P_{TM:C} + k_b P_{TM+C} \quad \text{(Equation 11)}$$

$$\frac{dP_{TM+C}}{dt} = k_u P_{TM:C} - (k_d + k_b) P_{TM+C} + k_{f0} P_{TM} = 0 \quad \text{(Equation 12)}$$

$$\frac{dP_{TM}}{dt} = k_d (P_{TM+C} + P_{TM+LC}) - (k_{f0} + k_{f1}) P_{TM} = 0 \quad \text{(Equation 13)}$$

$$\frac{dP_{TM+LC}}{dt} = k_{f1} P_{TM} - (k_d + k_b) P_{TM+LC} = 0 \quad \text{(Equation 14)}$$

$$\frac{dP_{TM:LC}}{dt} = k_b P_{TM+LC} \quad \text{(Equation 15)}$$

The analytical solution of the reduced model is:

$$P_{TM:C}(t) = e^{-\lambda t};\ P_{TM:LC}(t) = 1 - e^{-\lambda t} \quad \text{(Equation 16)}$$

Where λ is the rate of TCR-pMHC:Lck collision mediated by coreceptors.

$$\lambda = \frac{k_d k_{f1} k_u}{(k_b + k_d)(k_{f0} + k_{f1})} = \frac{f D k_u}{D + l^2 k_b} \quad \text{(Equation 17)}$$

The approximate analytical solution showed very similar results to the numerical solution of the full model (not shown).

TCR Occupancy Model

The TCR occupancy model assumes that the number of TCRs occupied by pMHC ligands determines the signal generated in a T cell or thymocyte. The magnitude of the response (R) can be calculated as:

$$R = TCR_{oc} = \frac{\frac{L}{A} + \frac{T}{A} + \frac{ln2}{k_{on} \times \tau_{1/2}} - \sqrt{\left(\frac{L}{A} + \frac{T}{A} + \frac{ln2}{k_{on} \times \tau_{1/2}}\right)^2 - \frac{4LT}{A^2}}}{2} \times A \quad \text{(Equation 18)}$$

where TCR_{oc} is the number of occupied TCRs in an equilibrium, k_{on} is 2D on-rate of the ligand (Huppa et al., 2010), L and T are numbers of ligands and TCRs, respectively, in the T cell/APC interface, and $\tau_{1/2}$ is the half dwell time of the TCR-pMHC interaction. We estimated the contact area between the thymocyte and APC to be one third of the total thymocyte surface.

"Lck Come&Stay/Signal Duration Model"

This model postulates that a TCR signal begins once a TCR-pMHC pair binds a coreceptor loaded with (active) Lck and the Lck-mediated phosphorylation results in recruitment and phosphorylation of ZAP70. The recruited coreceptor-Lck complex stays catalytically active for the duration of TCR-pMHC binding and generates additional down-stream signals by maintaining the ZAP70 in the active state. To calculate the TCR response in this scenario, we combined the Lck recruitment rate with the model of kinetic proofreading (McKeithan, 1995), that takes into account the Lck catalytic rate and the number of Lck-mediated phosphorylations required for ZAP70 recruitment and activation:

$$R = TCR_{oc} \times \frac{\lambda}{\lambda + k_{off}} \times \left(\frac{k_p}{k_p + k_{off}}\right)^n \quad \text{(Equation 19)}$$

where k_{off} is off-rate of the ligand (= $ln2/\tau_{1/2}$), k_p is the Lck catalytic rate, and n is the number of Lck-mediated phosphorylations of TCRζ and ZAP70 required to trigger the TCR (i.e., activate TCR-bound ZAP70). The magnitude of the induced TCR response (R) is determined by the number of triggered and still occupied TCRs at (pseudo)equilibrium. When accounting for TCR occupancy, the equation expands to:

$$R = \frac{\frac{L}{A} + \frac{T}{A} + \frac{ln2}{k_{on} \times \tau_{1/2}} - \sqrt{\left(\frac{L}{A} + \frac{T}{A} + \frac{ln2}{k_{on} \times \tau_{1/2}}\right)^2 - \frac{4LT}{A^2}}}{2} \times A \times \frac{\lambda}{\lambda + k_{off}} \times \left(\frac{k_p}{k_p + k_{off}}\right)^n \quad \text{(Equation 20)}$$

Because positive selectors do not induce a true synapse formation, the decision to proceed toward negative selection must be made before the synapse is formed (Ebert et al., 2008; Melichar et al., 2013). For this reason, the 'Lck come&stay/signal duration' model does not assume any significant accumulation of TCRs (nor pMHC) in the thymocyte-APC interface. The parameters are summarized in Table S3 (Huppa et al., 2010; Ramer et al., 1991).

Since it was previously shown in two independent reports that negative selection can be induced when 2–3 high-affinity antigen molecules are present at the thymocyte/APC interface (Ebert et al., 2008; Peterson et al., 1999), we used this experimental observation as an assumption in our model; i.e., to initiate negative election, $\geq$ 2–3 TCRs must be continuously activated up to the point of generating catalytically active ZAP70 within 5 min. The 5min interval was taken from the observations of Robey et al., who showed that in the absence of cognate antigen, thymocytes interact with an APC for an average of ~5 min (Melichar et al., 2013).

"Lck Come&Stay/Serial Triggering Model"

This model differs from the 'Lck come&stay/signal duration model' by assuming that once a TCR has been triggered by Lck-mediated activation of ZAP70, there is no further increase in the amount of TCR signal generated by continued ligand occupancy. Thus, short dwelling ligands benefit because they can trigger additional TCRs or have more attempts to trigger at least one TCR, while long dwelling ligands are arrested on TCRs that have already been fully triggered. In this model, the magnitude of the induced TCR response (R)

is expressed as a number of TCRs triggered during a time interval (length of a thymocyte-APC interaction before a decision is made) and can be calculated as:

$$R = \frac{\frac{L}{A}+\frac{T}{A}+\frac{ln2}{k_{on}\times\tau_{1/2}} - \sqrt{\left(\frac{L}{A}+\frac{T}{A}+\frac{ln2}{k_{on}\times\tau_{1/2}}\right)^2 - \frac{4LT}{A^2}}}{2} \times A \times \frac{\lambda}{\lambda+k_{off}} \times \left(\frac{k_p}{k_p+k_{off}}\right)^n \times t \times k_{off} \quad \text{(Equation 21)}$$

Model of Multiple Lck Visits

This model postulates that repetitive Lck visits are required for TCR triggering. We assumed that an Lck-coupled coreceptor remains at the TCR/pMHC complex just long enough to enable a single phosphorylation of the TCRζ or a recruited ZAP70 molecule. Thus, accumulation of n Lck visits within the dwell time of TCR/pMHC engagement would eventually lead to the TCR triggering. This model can be combined with the signal duration model, where the magnitude of the induced TCR response (R) is expressed as a number of triggered and occupied TCRs in equilibrium:

$$R = \frac{\frac{L}{A}+\frac{T}{A}+\frac{ln2}{k_{on}\times\tau_{1/2}} - \sqrt{\left(\frac{L}{A}+\frac{T}{A}+\frac{ln2}{k_{on}\times\tau_{1/2}}\right)^2 - \frac{4LT}{A^2}}}{2} \times A \times \left(\frac{\lambda}{\lambda+k_{off}}\right)^n \quad \text{(Equation 22)}$$

or with the serial triggering model, where the magnitude of the induced TCR response (R) is expressed as a number of TCRs triggered during a time interval:

$$R = \frac{\frac{L}{A}+\frac{T}{A}+\frac{ln2}{k_{on}\times\tau_{1/2}} - \sqrt{\left(\frac{L}{A}+\frac{T}{A}+\frac{ln2}{k_{on}\times\tau_{1/2}}\right)^2 - \frac{4LT}{A^2}}}{2} \times A \times \left(\frac{\lambda}{\lambda+k_{off}}\right)^n \times t \times k_{off} \quad \text{(Equation 23)}$$

SUPPLEMENTAL REFERENCES

Alam, S.M., Davies, G.M., Lin, C.M., Zal, T., Nasholds, W., Jameson, S.C., Hogquist, K.A., Gascoigne, N.R., and Travers, P.J. (1999). Qualitative and quantitative differences in T cell receptor binding of agonist and antagonist ligands. Immunity *10*, 227–237.

Altan-Bonnet, G., and Germain, R.N. (2005). Modeling T cell antigen discrimination based on feedback control of digital ERK responses. PLoS Biol. *3*, e356.

Boulter, J.M., Glick, M., Todorov, P.T., Baston, E., Sami, M., Rizkallah, P., and Jakobsen, B.K. (2003). Stable, soluble T-cell receptor molecules for crystallization and therapeutics. Protein Eng. *16*, 707–711.

Cole, D.K., Rizkallah, P.J., Gao, F., Watson, N.I., Boulter, J.M., Bell, J.I., Sami, M., Gao, G.F., and Jakobsen, B.K. (2006). Crystal structure of HLA-A*2402 complexed with a telomerase peptide. Eur. J. Immunol. *36*, 170–179.

Cole, D.K., Rizkallah, P.J., Boulter, J.M., Sami, M., Vuidepot, A.L., Glick, M., Gao, F., Bell, J.I., Jakobsen, B.K., and Gao, G.F. (2007). Computational design and crystal structure of an enhanced affinity mutant human CD8 alphaalpha coreceptor. Proteins *67*, 65–74.

Cole, D.K., Dunn, S.M., Sami, M., Boulter, J.M., Jakobsen, B.K., and Sewell, A.K. (2008). T cell receptor engagement of peptide-major histocompatibility complex class I does not modify CD8 binding. Mol. Immunol. *45*, 2700–2709.

Davis, K.A., Abrams, B., Iyer, S.B., Hoffman, R.A., and Bishop, J.E. (1998). Determination of CD4 antigen density on cells: role of antibody valency, avidity, clones, and conjugation. Cytometry *33*, 197–205.

Dushek, O., Mueller, S., Soubies, S., Depoil, D., Caramalho, I., Coombs, D., and Valitutti, S. (2008). Effects of intracellular calcium and actin cytoskeleton on TCR mobility measured by fluorescence recovery. PLoS ONE *3*, e3913.

Gao, G.F., and Jakobsen, B.K. (2000). Molecular interactions of coreceptor CD8 and MHC class I: the molecular basis for functional coordination with the T-cell receptor. Immunol. Today *21*, 630–636.

Garboczi, D.N., Ghosh, P., Utz, U., Fan, Q.R., Biddison, W.E., and Wiley, D.C. (1996). Structure of the complex between human T-cell receptor, viral peptide and HLA-A2. Nature *384*, 134–141.

Gostick, E., Cole, D.K., Hutchinson, S.L., Wooldridge, L., Tafuro, S., Laugel, B., Lissina, A., Oxenius, A., Boulter, J.M., Price, D.A., and Sewell, A.K. (2007). Functional and biophysical characterization of an HLA-A*6801-restricted HIV-specific T cell receptor. Eur. J. Immunol. *37*, 479–486.

Li, Y., Yin, Y., and Mariuzza, R.A. (2013). Structural and biophysical insights into the role of CD4 and CD8 in T cell activation. Front. Immunol. *4*, 206.

Lis, M., Artyomov, M.N., Devadas, S., and Chakraborty, A.K. (2009). Efficient stochastic simulation of reaction-diffusion processes via direct compilation. Bioinformatics *25*, 2289–2291.

Mallaun, M., Naeher, D., Daniels, M.A., Yachi, P.P., Hausmann, B., Luescher, I.F., Gascoigne, N.R., and Palmer, E. (2008). The T cell receptor's alpha-chain connecting peptide motif promotes close approximation of the CD8 coreceptor allowing efficient signal initiation. J. Immunol. *180*, 8211–8221.

Ramer, S.E., Winkler, D.G., Carrera, A., Roberts, T.M., and Walsh, C.T. (1991). Purification and initial characterization of the lymphoid-cell protein-tyrosine kinase p56lck from a baculovirus expression system. Proc. Natl. Acad. Sci. USA *88*, 6254–6258.

Rosette, C., Werlen, G., Daniels, M.A., Holman, P.O., Alam, S.M., Travers, P.J., Gascoigne, N.R., Palmer, E., and Jameson, S.C. (2001). The impact of duration versus extent of TCR occupancy on T cell activation: a revision of the kinetic proofreading model. Immunity *15*, 59–70.

van der Merwe, P.A., and Davis, S.J. (2003). Molecular interactions mediating T cell antigen recognition. Annu. Rev. Immunol. *21*, 659–684.

Wyer, J.R., Willcox, B.E., Gao, G.F., Gerth, U.C., Davis, S.J., Bell, J.I., van der Merwe, P.A., and Jakobsen, B.K. (1999). T cell receptor and coreceptor CD8 alphaalpha bind peptide-MHC independently and with distinct kinetics. Immunity *10*, 219–225.

Xiong, Y., Kern, P., Chang, H., and Reinherz, E. (2001). T Cell Receptor Binding to a pMHCII Ligand Is Kinetically Distinct from and Independent of CD4. J. Biol. Chem. *276*, 5659–5667.

Zimmermann, L., Paster, W., Weghuber, J., Eckerstorfer, P., Stockinger, H., and Schütz, G.J. (2010). Direct observation and quantitative analysis of Lck exchange between plasma membrane and cytosol in living T cells. J. Biol. Chem. *285*, 6063–6070.

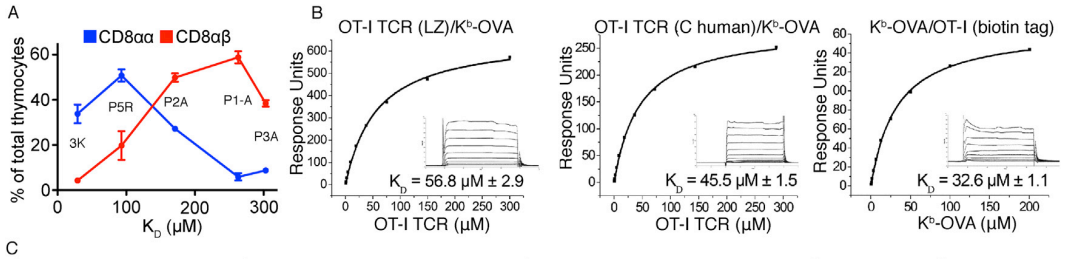

C

Analyte injected over immobilised ligand	OT-I TCR Leucine zipper at C-terminus		OT-I TCR C human interchain artificial disulphide		Kᵇ-OVA, prep 2
Ligand immobilised onto chip surface	Kᵇ-OVA, prep1	Kᵇ-OVA, prep 2	Kᵇ-OVA, prep1	Kᵇ-OVA, prep 2	OT-I TCR (biotin tag)
Exp 1 BIA 3000	46.1 μM ± 3	39.0 μM ± 6	66.3 μM ± 5	46.6 μM ± 6	ND
Exp 2 BIA T100	38.9 μM ± 2	55.4 μM ± 1	45.5 μM ± 2	61.4 μM ± 2	ND
Exp 3 BIA T100	56.8 μM ± 3	50.5 μM ± 3	ND	ND	32.6 μM ± 1

D

	Peptide	OVA	Q4R7	T4	Q7	Q4H7	V4	G4	R4	E4
Exp1	K_D (μM)	50.5 ± 2.7	268.3 ± 31.1	578.4 ± 38.9	628.0 ± 42.8	834.7 ± 56.6	>1mM	>1mM	ND	NB
Exp2	K_D (μM)	56.8 ± 2.9	307.4 ± 12.3	310 .1 ± 51.5	488.4 ± 35.3	858.8 ± 118.6	ND	ND	>1mM	ND
Mean	K_D (μM)	54	288	444	558	847	>1mM	>1mM	>1mM	NB

Figure S1. SPR Affinity Measurements, Related to Figure 1

(A) Relative frequency of CD8αα and CD8αβ thymocytes in B3K508 FTOCs (see Figure 1A). Mean ± range, n = 2. CD8αα cells appeared under conditions of negative selection and thus, probably represent a nonconventional innate-like T cell lineage (Yamagata et al., 2004). In contrast, a population of CD8αβ SPs were generated in FTOCs exposed to positive selecting ligands; these cells are either immature single positive thymocytes, a transitional stage between double negative and double positive cells or a population of thymocytes undergoing an atypical positive selection fate; this has been previously described for thymocytes expressing another MHCII-restricted TCR, 5C.C7 (Yamagata et al., 2004).

(B and C) Ten serial dilutions of OT-I TCR were measured in multiple experiments using different TCR constructs and experimental setups. Representative data from these experiments are plotted and the mean K_D ± SD was calculated. To calculate background binding, OT-I TCR, or H2-K^b–OVA was also injected over a negative control sample that was subtracted from the experimental data. (Left panel) OT-I TCR with a leucine zipper at the C terminus binding to immobilized H2-K^b–OVA. (Middle panel) OT-I TCR with a human C terminus binding to immobilized H2-K^b–OVA. (Right panel) H2-K^b–OVA binding to biotin tagged immobilized OT-I TCR. Two different preparations of H2-K^b-OVA from two different labs gave similar results (EP and AKS).

(D) Ten serial dilutions of OT-I TCR with C-terminal leucine zipper were measured in multiple experiments using different K^b-OVA peptide variants. Mean K_D values ± SD were calculated and are indicated in the table. NB, not binding. ND, not determined. Our SPR affinity measurements of the interaction between OT-I TCR and K^b-OVA or K^b-OVA-derived APLs showed much higher K_D values and a more pronounced difference between strong and weak ligands than previously published SPR data on the same TCR (Alam et al., 1999; Rosette et al., 2001). While Alam et al. (1999) determined the K_D of OT-I/H-2K^b-OVA and OT-I/H-2K^b-E1 (very weak ligand) to be 6 μM and 20 μM, respectively, our measurements showed K_D ~50 μM for K^b-OVA and > 1 mM for ligands even more potent than K^b-E1. We measured two different H-2K^b-OVA preparations produced in two labs and two different OT-I TCR constructs that were heterodimerized using a non-native disulphide bond or a leucine zipper. In different experiments, the soluble TCRs were used as analyte or bait ligand. All experiments produced similar results. As the previous report showed an unexpected decrease in binding dynamics at higher temperature, these data might have been influenced by protein aggregation. The measurements determined in this work correspond more closely with the distribution of antigen potencies of the various OT-I ligands (Daniels et al., 2006). As the previously published data have been frequently used for modeling of the TCR response and for arguing against the relevance of SPR measurements in studying TCR-pMHC interactions, the affinities measured here may resolve some of the discrepancies in the literature.

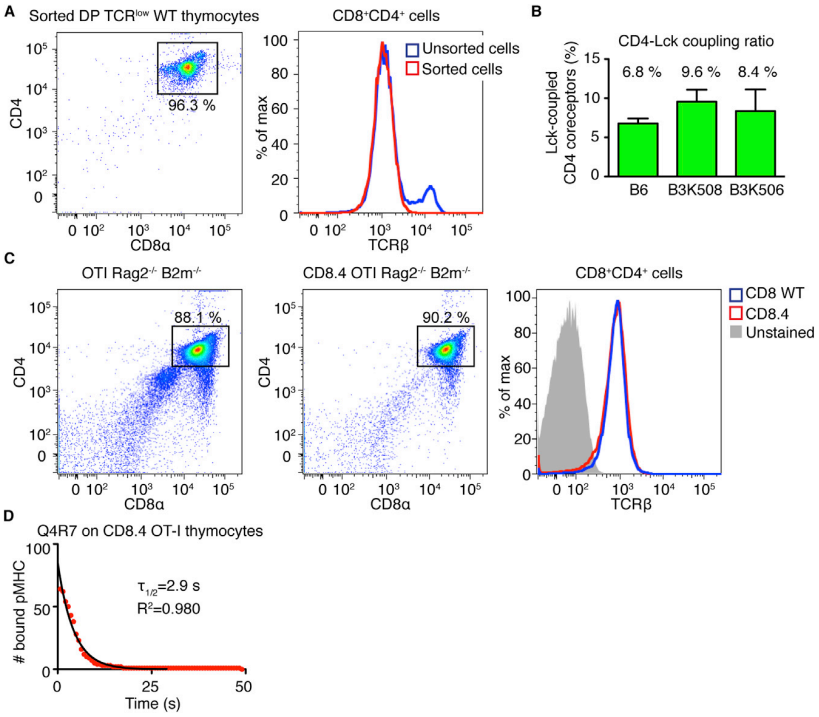

Figure S2. Determining Coreceptor-Lck Coupling, Related to Figure 2

(A) Sorted preselection CD3^{low} DP thymocytes from B6 mice were analyzed for CD4, CD8α, and TCRβ expression levels. Purity of DP thymocytes (left panel) and TCR levels on sorted DP thymocytes compared to unsorted thymocytes (right panel) are shown.

(B) Mean percentage ± SD of Lck-coupled CD4 molecules in B3K506 Rag1$^{-/-}$ I-A$^{-/-}$, B3K508 Rag1$^{-/-}$ I-A$^{-/-}$, and sorted polyclonal DP TCR^{low} thymocytes is shown (n = 2–5).

(C) CD8WT and CD8.4 OT-I DP thymocytes were stained with antibodies to CD4, CD8α, and TCRβ. Percentage of DP thymocytes (left panel) and TCR levels on pre-selection DP thymocytes (right panel) are shown.

(D) On cell dwell times of Q4R7 monomer on CD8.4 OT-I DP thymocytes were measured by single molecule microscopy and fitted using a one phase exponential decay curve; $\tau_{1/2}$ and R-square values are shown. $\tau_{1/2}$ on CD8WT (Figure 1E) and CD8.4 OT-I DP thymocytes are similar.

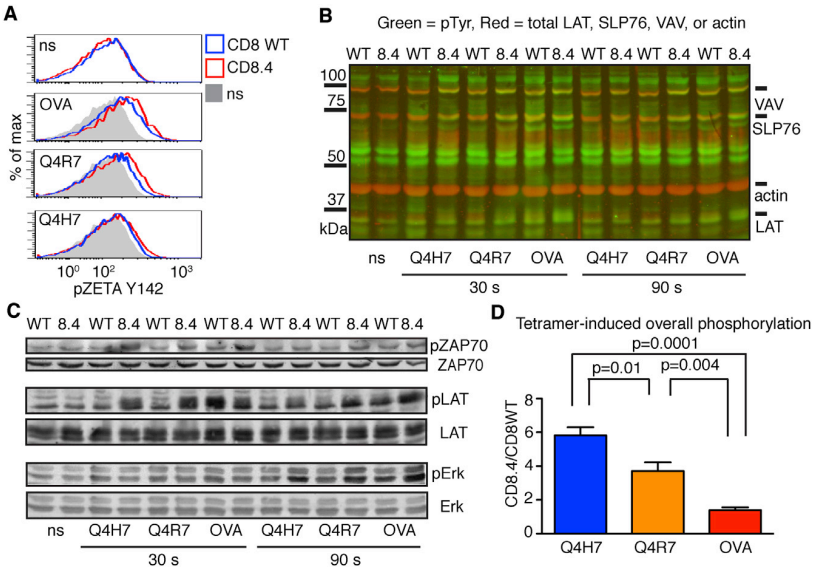

Figure S3. CD8.4 Enhances Proximal Signaling in OTI Thymocytes, Related to Figure 4

Thymocytes from CD8WT and CD8.4 OTI Rag2$^{-/-}$β2 m$^{-/-}$ mice were stimulated with 100 nM K^{b}-OVA, K^{b}-Q4R7, or K^{b}-Q4H7 tetramers or left unstimulated (ns).

(A) Zeta chain phosphorylation was analyzed by flow cytometry. A representative experiment from a total of 6 is shown.

(B) Total phosphorylation of VAV, SLP76, and LAT was analyzed by probing whole cell lysates with mouse anti-pTyr antibody (green) and rabbit antibodies to VAV, SLP76, LAT, and actin (red) by western blotting. A representative experiment from a total of 4 is shown.

(C) The phosphorylation of specific phosphorylation site was analyzed by probing whole cell lysates with antibodies to LAT pY191, ZAP70 pY319, and Erk pT202/Y204 by western blotting. Total ZAP70, LAT, and Erk served as the respective loading controls. A representative experiment from a total of 4 is shown.

(D) Tetramer induced increase of Erk1 (at 90 s), ZAP70, LAT, VAV, and SLP76 (at 30 s) phosphorylation was calculated by subtracting normalized basal level of phosphorylation from the values induced following tetramer stimulation (Figure 4B–4G). For each phosphoprotein, the average ratio of the induced phosphorylation (determined from 4 experiments) observed in CD8.4 and CD8 WT thymocytes was calculated (CD8.4/CD8WT). To obtain a broader view of the differences in early signaling intermediates, the ratios for the induction of the various phosphoproteins were pooled; from these pooled values, the mean and SEM were plotted. Statistical significance was tested using Student's t test (2 tailed, unequal variance).

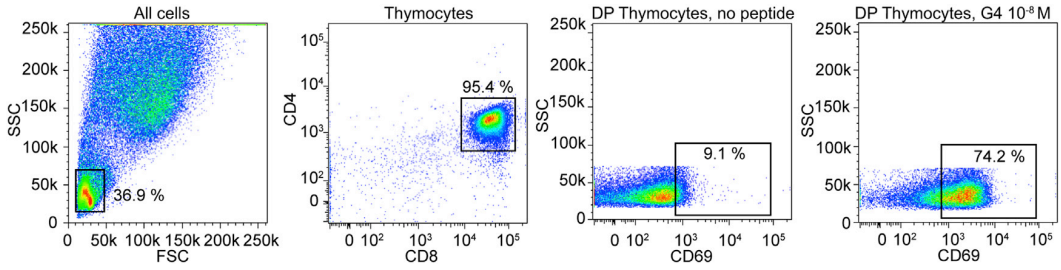

Figure S4. Gating Strategy, Related to Figure 5

CD8WT and CD8.4 OT-I Rag2$^{-/-}$ β2 m$^{-/-}$ thymocytes were incubated with peptide loaded APCs (T2-K^{b} cells) for 24 hr and stained with antibodies to CD4, CD8, and CD69. DP thymocytes were gated using FSC^{low}SSC^{low}/CD4^{+}CD8^{+}. Individual gates are shown.

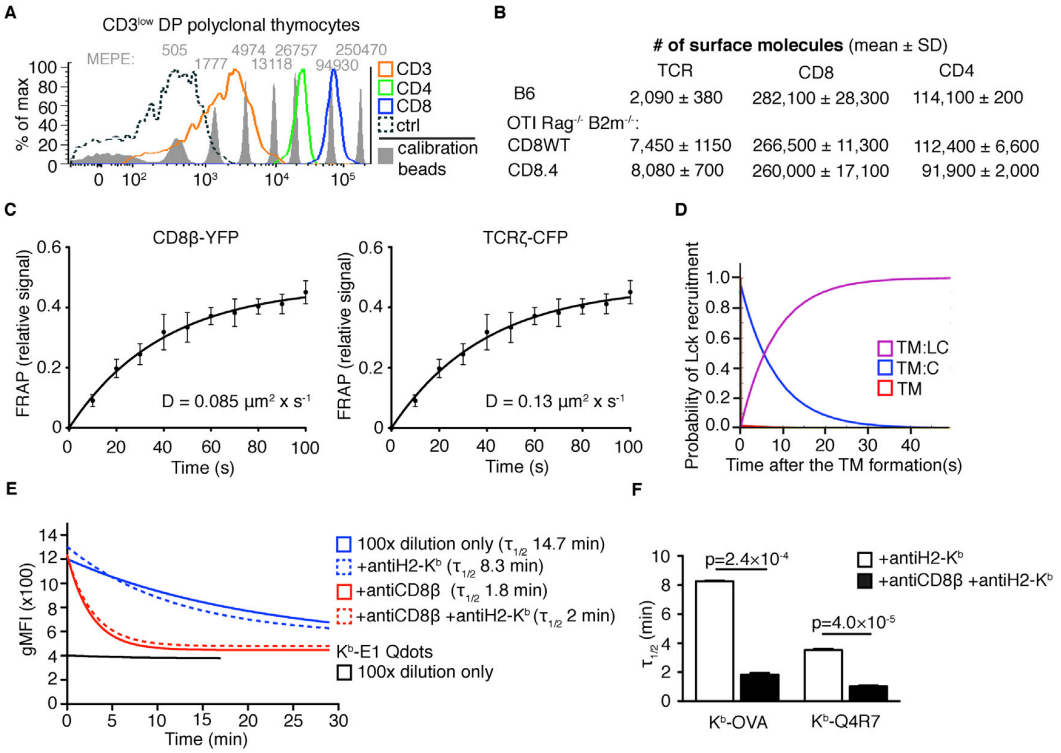

Figure S5. Parameters Relevant to Coreceptor Exchange, Related to Figure 6

(A) Sorted preselection polyclonal TCRβ^{low} DP thymocytes and control cells (peripheral B cells) were stained with saturating concentration of PE-conjugated antibodies to CD4, CD8α, or CD3 and analyzed by flow cytometry together with PE calibration beads. Fluorescence signals from stained thymocytes, negative control (representative negative control for CD3 staining) and calibration beads are shown. The number of mean equivalent soluble PE molecules (MEPE) is indicated for each peak of the PE calibration beads.

(B) Quantification of the number of TCR, CD8, and CD4 molecules per cell (mean number ± SD from 3 experiments) expressed on polyclonal sorted preselection DP thymocytes (B6) as well as CD8WT and CD8.4 OT-I Rag2$^{-/-}$ β2 m$^{-/-}$ thymocytes.

(C) Fluorescence recovery after photobleaching (FRAP) CD8β-YFP and TCRζ-CFP in OT-I hybridoma cell line was performed using an Olympus IX81 inverted microscope. Mean normalized fluorescence recovery ± SD (n = 6 for CD8β, n = 7 for TCRζ). The points were fitted with an exponential equation y = a × (1-e^(-K × x)). Calculated diffusion coefficients are shown.

(D) Probability of various states in the Markov chain model. TM (free TCR-pMHC), TM:C (TCR-pMHC complexed with an Lck-free coreceptor), and TM:LC (TCR-pMHC complexed with an Lck-bound coreceptor) states are shown. The states TM+C and TM+LC (TCR-pMHC in a close proximity of an Lck-free or Lck-bound coreceptor, respectively) are very rare (under the resolution of the y axis).

(E) OT-I preselection thymocytes were incubated with 100 nM monomeric K^b-OVA Qdots or K^b-E1 Qdots in PBS/5% FCS at 4°C for 2 hr to establish binding equilibrium. Subsequently, the cells were diluted 100x with the staining buffer with or without antiCD8β (clone 53.5.8, Biolegend) and/or antiH2-K^b (clone Y3) antibodies (10 μg/ml). The antiH2-K^b antibody was used to prevent antigen rebinding. The decrease of Qdot fluorescence intensity was monitored by flow cytometry at 0°C in real time. K^b-E1 Qdots monomers that have undetectable binding to OT-I TCR were used to determine baseline fluorescence signal. Blocking free CD8 rapidly accelerated the release of antigen from the thymocytes, providing experimental evidence for the cycling of coreceptors at the TCR-pMHC complex, as assumed by our Markov chain model. In contrast, preventing of rebinding of monomers to the thymocytes using anti-H2-K^b antibody had only a modest effect (compare solid and dashed lines). This showed that the effects of CD8 blocking cannot be explained by inhibition of new thymocyte-pMHC interactions due to antigen rebinding. Data were fitted with a one phase exponential decay function.

(F) Quantifying the effect of CD8 blocking on the dissociation of prebound K^b-OVA and K^b-Q4R7 monomers from OT-I T cells. Mean ± SEM n = 2–5. Statistical significance was tested using Student's t test (unequal variance, 2 tailed).

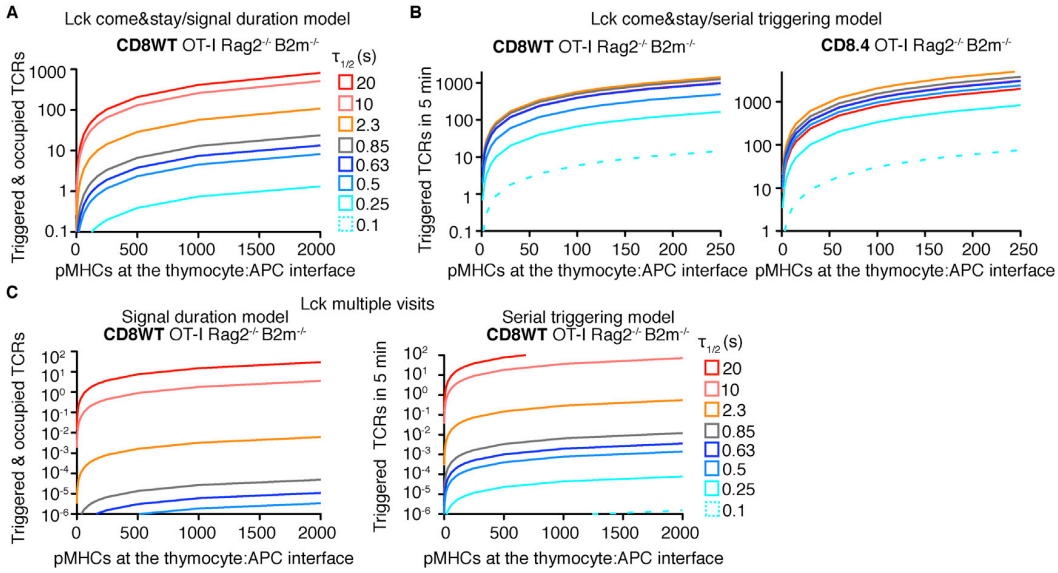

Figure S6. Four Models of TCR Triggering, Related to Figure 7

Graphs show the TCR signal intensity as a function of number of cognate ligands at the thymocyte/APC interface for different ligands (k_{on} = 0.1 $\mu m^2 s^{-1}$, $\tau_{1/2}$ varied).
(A) 'Lck come&stay/signal duration model' as in Figure 7A with x axis scaled up to show the effect of increasing antigen concentration to non-physiological levels.
(B) 'Lck come&stay/serial triggering model' for CD8WT OT-I Rag2$^{-/-}$ β2 m$^{-/-}$ and CD8.4 OT-I Rag2$^{-/-}$ β2 m$^{-/-}$ thymocytes.
(C) 'Multiple Lck visits/signal duration model' and 'Multiple Lck visits/serial triggering model' for CD8WT OT-I Rag2$^{-/-}$ β2 m$^{-/-}$ thymocytes.
See Extended Experimental Procedures.